Title
The Role of SQLE in Head and Neck Squamous Cell Carcinoma

Author
Liu, Yujiao

Publication Date
2021

Peer reviewed|Thesis/dissertation

UNIVERSITY OF CALIFORNIA

Los Angeles

The Role of SQLE in Head and Neck Squamous Cell Carcinoma

A thesis submitted in partial satisfaction

of the requirements for the degree Master of Science

in Oral Biology

by

Yujiao Liu

2021

ABSTRACT OF THE THESIS

The Role of SQLE in Head and Neck Squamous Cell Carcinoma

by

Yujiao Liu

Master of Science in Oral Biology

University of California, Los Angeles, 2021

Professor Shen Hu, Chair

Background: Head and neck cancer (HNC) is the sixth most common cancer globally, and it is an aggressive malignancy with high morbidity and mortality [1-3]. Every year, 650,000 people are diagnosed with, and about 350,000 people die from, head and neck cancer [3]. Currently, 40,000 new cases and 12,460 deaths are reported in the United States annually [4]. Therefore, it is important to investigate the underlying molecular mechanisms of head and neck carcinogenesis to save the lives of HNC patients.

Squalene epoxidase (also called squalene monooxygenase, SQLE, or SM) is an enzyme that uses NADPH and molecular oxygen to oxidize squalene to 2,3-oxidosqualene (squalene epoxide). Squalene epoxidase catalyzes the first oxygenation step in sterol biosynthesis and is

thought to be one of the rate-limiting enzymes in this pathway. In cancer biology, SQLE is involved in human esophageal squamous cell carcinoma, lung squamous cell carcinoma, breast cancer, and leukemia [5-8]. SQLE has also recently been linked to nasopharyngeal cancer, but no study to date has described the role of SQLE in HNSCC [9]. Based on our TCGA and GEO database analysis, SQLE was found to be overexpressed in HNSCC tissues when compared to adjacent normal tissues ($P < 0.0001$). Besides, a significantly worse overall survival rate was observed in the HNSCC patients with high SQLE gene expression than those with low SQLE gene expression ($P = 0.001$). Thus, we hypothesize that SQLE may play an important role in HNSCC, and it is important to investigate the cellular and molecular mechanisms of SQLE in HNSCC.

Objectives: This study aims to identify the role and regulatory mechanisms of SQLE in HNSCC. Considering the oncogenicity of SQLE in other types of cancers, a link between SQLE and HNSCC is worthy of further research.

Methods: Phenotypic studies were conducted in two HNSCC cell lines (UMSCC1 and UMSCC23) with knockdown of SQLE. Western blotting was used to quantify protein expression levels. MTT, cell colony formation, EdU, migration, and invasion assays were utilized to assess the phenotype of cancer cells. RNA sequencing was used to analyze the global gene expression in cancer cells.

Results: Based on the statistical analysis of existing TCGA and GEO datasets, we found that SQLE may play an important role in HNSCC. Therefore, we aimed to study the function of SQLE in HNSCC cell lines by knocking down the SQLE gene and assessing the altered phenotypes of the cancer cells. Knockdown of SQLE in UMSCC1 and UMSCC23 cells led to

significantly decreased proliferation, migration, and invasion potential. Considering that PD-L1, EGF, and FGF are therapeutically important in HNSCC, we also investigated their relationships with SQLE. However, the expression level of PD-L1 did not change after SQLE knockdown. Neither EGF nor FGF altered the expression of SQLE in HNSCC. In order to find potential downstream targets of SQLE, we performed RNA sequencing analysis of UMSCC1 cells with SQLE knockdown. In total, 2,994 genes were differentially expressed following SQLE knockdown, including 1,527 up-regulated and 1,467 down-regulated genes. Signaling pathways were found to be significantly altered by SQLE knockdowns, such as MAPK/ERK signaling, mTOR signaling, and cell cycle pathways.

Conclusions: This study has demonstrated that SQLE plays a vital role in HNSCC progression by promoting cancer cell growth, migration, and invasion. RNA sequencing analysis indicates that SQLE may participate in the regulation of HNSCC through interacting with multiple critical regulatory pathways. These findings suggest that SQLE may be an essential target for clinical applications in HNSCC.

The thesis of Yujiao Liu is approved.

Diana V. Messadi

Yong Kim

Shen Hu, Committee Chair

University of California, Los Angeles

2021

TABLE OF CONTENTS

Abstract ii

Table of Contents vi

List of Figures vii

Introduction 1

Materials and Methods 7

Results 15

Discussion 26

Conclusion 29

Figures 31

References 74

LIST OF FIGURES

Figure 1 31

Figure 2 32

Figure 3 33

Figure 4 34

Figure 5 35

Figure 6 36

Figure 7 38

Figure 8 39

Figure 9 40

Figure 10 41

Figure 11 42

Figure 12 43

Figure 13 44

Figure 14 45

Figure 15 46

Figure 16 47

Figure 17 48

Figure 18 49

Figure 19 50

Figure 20 51

Figure 21 52

Figure 22 53

Figure 23 54

Figure 24 55
Figure 25 56
Figure 26 57
Figure 27 58
Figure 28 59
Figure 29 60
Figure 30 61
Figure 31 62
Figure 32 63
Figure 33 64
Figure 34 65
Figure 35 66
Figure 36 67
Figure 37 68
Figure 38 69
Figure 39 70
Figure 40 71
Figure 41 72
Figure 42 73

INTRODUCTION

Head and neck cancer (HNC) is the sixth most common cancer globally with high morbidity and mortality [1-3]. Every year, 650,000 people are diagnosed with, and about 350,000 people die from, head and neck cancer [3]. HNC encompasses a great number of the malignancies of the upper aerodigestive tract, including oral cavity, nasal cavity, pharynx, larynx, and sinuses [2, 3]. Most of these epithelial malignancies are head and neck squamous cell carcinoma (HNSCC) [3]. Around 40,000 new cases and 12,460 deaths are reported in the United States annually [10]. The major etiologic factors of HNSCC include tobacco, alcohol, betel nut, and now human papillomavirus (HPV), which has been identified as the key risk factor for HPV-related oropharyngeal cancer [1, 11]. Even though treatments have made significant progress in the past few decades, including surgery, radiation therapy, and chemotherapy with epidermal growth factor receptor (EGRF) inhibitor and immune-checkpoint inhibitors (ICI), nearly half of the HNC patients will relapse, and 5-year survival is a dismal 35%-45% [1, 12]. Therefore, new diagnostics and treatment approaches are needed to improve the survival rates of HNC patients.

Squalene epoxidase (SQLE, *a.k.a.*, squalene monooxygenase) is a 574-amino acid protein encoded by the SQLE gene, which is located at the chromosome 8q24.13 and spans approximately 23.8 kilobase pairs [13]. It was first discovered in rat liver microsomes in 1969 [14]. In humans, SQLE is highly expressed in the liver, neural tissue, gut, and skin, but non-cholesterogemic tissues lack SQLE expression [15]. SQLE is located in the endoplasmic reticulum, as most of the cholesterogenic enzymes [16]. The enzyme is a member of the flavoprotein monooxygenase family, which catalyzes a variety of oxidative reactions [17].

There are two rate-limiting enzymes in the cholesterol biosynthesis pathway, 3-hydroxy-

3-methylglutaryl-CoA reductase (HMGCR) and SQLE. HMGCR catalyzes the conversion of HMG-CoA to mevalonate. Statins can inhibit this process. Epidemiologists have reported that statins may inhibit the progression of certain types of cancers [18]. SQLE, the second rate-limiting enzyme, oxidizes squalene to 2,3(S)-monooxidosqualene (squalene epoxide), which is further converted to lanosterol by the lanosterol synthase (Figure 1). This pathway finally leads to the production of cholesterol. Besides, in the shunt pathway, SQLE functions to provide a second epoxide for the synthesis of 2, 3(S), 22(S), 23-dioxidosqualene, and gives rise to the production of 24(S), 25-epoxycholesterol in the end [13]. Researchers have found that excess cholesterol accelerates the degradation of SQLE via the ubiquitin-proteasome system, which further controls cholesterol synthesis. This feedback regulation depends on the first 100 amino acids of SQLE in the N-terminal of SQLE structure (SM N100), and it is regulated by the E3 ubiquitin ligase membrane-associated RING-CH protein 6 (MARCH 6) [19]. On the other hand, SQLE mRNA expression is upregulated when cholesterol level is low. This responsiveness is due to the activation of the SQLE promoter by sterol regulatory element binding proteins (SREBPs), which are usually activated under low sterol conditions and inhibited by elevated cholesterol [1, 20].

SQLE protein contains both regulatory and catalytic domains (Figure 2A). The N-terminal region represents the regulatory domain, which takes up the first 100 amino acids of SQLE, but it is only found in vertebrates instead of lower organisms [19]. This domain is embedded into the ER membrane *via* the re-entrant loop and followed by the weakly membrane-associated amphipathic helix, enabling the degradation of cholesterol *via* conformational change with excessive cholesterol [13]. Although the three-dimension structure of the regulatory domain

has not been determined so far, the importance of its role in sensing cholesterol cannot be ignored. In addition, the structure of the human SQLE catalytic domain was first discovered by using X-ray crystallography (Figure 2B). It exhibits a split structure that FAD and substrate-binding domains are interspersed within the primary structure, followed by a helical membrane-binding domain near the C-terminus. Flavin adenine dinucleotide (FAD) is a redox-active coenzyme associated with various proteins, which is involved with several enzymatic reactions in metabolism. Molecular docking experiment on the unliganded SQLE•FAD structure has revealed that most amino acid residues in the squalene binding pocket overlap with amino acids involved with inhibitor binding [21].

The primary substrate of SQLE is squalene, which was initially obtained from shark liver oil (hence its name, as Squalus is a genus of sharks). Squalene is a precursor for synthesizing of all plant and animal sterols, including cholesterol and steroid hormones in the human body [22]. Squalene in the human diet can be absorbed by the intestine and is detectable in human blood [23]. In addition to its role as the substrate of SQLE, squalene has gained more attention on its medical applications. Squalene may be conjugated to some drugs, such as paclitaxel, cytarabine, and gemcitabine. The formation of these lipid-drug conjugates has been proven to improve pharmacokinetics, decrease toxicity, and facilitate drug delivery of anticancer and antiviral agents [24]. Besides, squalene has been used in conjunction with surfactants in specific adjuvant formulations. An adjuvant using squalene is Seqirus' proprietary MF59, which is added to influenza vaccines to help enhance immune responses [25].

SQLE has been confirmed to be correlated with many diseases, such as neuropathy, cardiovascular diseases, and cancers [26-28]. Since the correlation between SQLE and cancer

has been recently studied [28], we will briefly summarize the findings below about the role of SQLE in human cancer. In 1981, a study in cholesterol biosynthesis in the human gastrointestinal tract showed that tumoral tissues had higher amounts of SQLE enzyme than normal mucosa in the terminal portion of the colon, despite no substantial variations in enzyme production [29]. In the recent study of hormone receptor-positive breast cancer, SQLE has been found to directly interact with CASIMO1 (cancer-associated small integral membrane open reading frame 1), which has been discovered to be essential for cancer cell survival. This interaction may eventually activate downstream ERK signaling [30]. This study contributes to the evidence linking SQLE upregulation to ERK activation in cancers such as hepatocellular carcinoma and lung squamous cell carcinoma [31, 32]. According to another report, upregulation of SQLE in non-alcoholic fatty liver disease-associated hepatocellular carcinoma facilitates the synthesis of cholesteryl esters, driving cancer aggressiveness. Besides, SQLE also promotes epigenetic silencing of PTEN, leading to the activation of the AKT-mTOR pathway and the development of hepatocellular carcinoma [33]. Elevated SQLE expression has also been linked to the development of lethal prostate cancer, the occurrence of colorectal cancer, and squamous lung cancer [34, 35]. An increasing body of evidence indicates a correlation between SQLE overexpression and poor prognosis in various tumors [28]. Meanwhile, some researchers suggest that using terbinafine to target SQLE may be a successful method for preventing and treating tumors, such as hepatocellular carcinoma and breast cancer [28, 33, 36].

While SQLE has been identified as a critical regulator of tumorigenesis, it is uncertain if it plays a role in HNSCC carcinogenesis. Therefore, we have investigated the expression level of SQLE in HNSCC and overall survival rate of the HNSCC patients with high SQLE gene

expression by statistical analyses of existing Gene Expression Omnibus (GEO) and The Cancer Genome Atlas (TCGA) datasets. GEO is an international public repository that archives and freely distributes microarray, next-generation sequencing, and other forms of high-throughput functional genomics data submitted by the research community [37]. We obtained data and the titles of samples for Gene Series Expression (GSE) data from GEO. TCGA is a public funded project that aims to catalogue and discover major cancer-causing genomic alterations to create a comprehensive "atlas" of cancer genomic profiles. So far, TCGA researchers have analyzed large cohorts of over 30 human tumors through large-scale genome sequencing and integrated multi-dimensional analyses [38]. In our analysis, compared to adjacent normal tissues, SQLE gene expression was significantly higher in HNSCC tissues ($P < 0.0001$) based on five independent datasets (GSE30784, GSE13601, GSE6631, GSE37991, and TCGA-HNSCC) (Figure 3). The expression of SQLE in other cancers was also investigated in this study. Compared to the normal controls, SQLE was significantly overexpressed in the following cancer types, including bladder urothelial carcinoma (BLCA), colon adenocarcinoma (COAD), esophageal carcinoma (ESCA), liver hepatocellular carcinoma (LIHC), lung squamous cell carcinoma (LUSC), rectum adenocarcinoma (READ), stomach adenocarcinoma (STAD), and uterine corpus endometrial carcinoma (UCEC) ($P < 0.0001$) (Figure 4). In addition, based on the TCGA datasets of HNSCC, a significantly worse overall survival rate was observed in the HNSCC patients with high SQLE gene expression than those with low SQLE gene expression ($P = 0.001$) (Figure 5). High SQLE expression was also significantly associated with worse long-term overall survival rates among the cancer patients with adrenocortical carcinoma (ACC), BRCA, cervical squamous cell carcinoma and endocervical adenocarcinoma (CESC), kidney renal papillary cell carcinoma

(KIRP), LIHC, lung adenocarcinoma (LUAD), mesothelioma (MESO), pancreatic adenocarcinoma (PAAD), sarcoma (SARC), thyroid carcinoma (THCA), and uveal melanoma (UVM) (Figure 6). Based on these results, we hypothesized that SQLE may play an important role in HNSCC, and it is important to investigate the cellular and molecular mechanism of SQLE in HNSCC.

MATERIALS AND METHODS

Cell culture

Human head and neck squamous cancer cell (HNSCC) lines, UMSCC1 and UMSCC23, were maintained in Dulbecco's modified eagle medium (DMEM) (Invitrogen, Carlsbad, CA, USA) containing 10% fetal bovine serum (FBS) and streptomycin (100 mg/ml) (Invitrogen, Carlsbad, CA, USA). UMSCC1 cells originated from the floor of the mouth, whereas UMSCC23 cells are aroused from the larynx. The cells were maintained at 37 ℃, 5% CO_2 in a humidified incubator and passaged or harvested at 95% confluency with trypsinization.

UMSCC1 or UMSCC23 cells were treated with epidermal growth factor (EGF) or fibroblast growth factor (FGF) to determine their effects on SQLE expression levels. Twenty-four hours following the passage to a 6-well plate, EGF or FGF (Gemini Bio, Sacramento, CA, USA) was added to separate wells of the plate to a final concentration of 10 ng/mL. The cells were incubated for two days and subsequently harvested for protein analysis.

siRNA knockdown of SQLE in HNSCC cells

UMSCC1 and UMSCC23 cells were maintained in 6-wells before transfection. After reaching 60% confluency, cells were treated with siRNA mixed with the lipofectamine RNAiMAX transfection reagent (Invitrogen, CA). Validated double-stranded siRNAs of SQLE and non-target control siRNAs (Sigma-Aldrich, MO) were used for the knockdown experiments. After 48 hours of incubation with siRNAs, cells were either collected for Western blot analysis or used for further phenotypic assays.

Western blotting

Protein samples were harvested in the RB buffer and separated with a 4-12% Bis-Tris

NuPAGE gel. The separated proteins were transferred onto a nitrocellulose membrane (NC) (Santa Cruz Biotech, CA) with a Tran-blot SD semi-dry transfer cell (Bio-Rad, CA), and the membrane was subsequently blocked with 5% non-fat milk for 60 minutes at room temperature. After blocking, the target proteins were incubated with anti-SQLE antibody (1:500, Cat# sc-271651, Santa Cruz Biotech, CA) and anti-GAPDH antibody (1:300, Cat# GT239, GeneTex, Irvine, CA) in the 4 ℃ cold room overnight with constant agitation. After incubated with the mouse secondary antibody (1:2000, GE Healthcare) for 1 h and washed with 1x TBST buffer three times, an enhanced chemiluminescence (ECL) kit (GE Healthcare) was utilized to detect the Western blot signal. The resultant bands were quantified by the ImageJ software, and the p value was calculated based on triplicate results.

Anti-PD-L1 antibody (1:1000, Cat#13684S, Cell Signaling Technology, Danvers, MA) was used to test the PD-L1 expression. The corresponding secondary antibody is rabbit antibody (1:10000, GE Healthcare). Other steps are the same as above.

MTT assay

The MTT (3-(4,5-dimethylthiazol-2-yl)-2,5-diphenyltetrazolium bromide) tetrazolium reduction assay was utilized to measure the proliferation of UMSCC1 and UMSCC23 cells following SQLE knockdown. After SQLE knockdown, cells were plated in a 96-well plate with 2000 cells/well and incubated for 24 hours to allow for attachment. Five wells were used for each sample at each time point. The outermost wells of the plates were filled with PBS to minimize evaporation. After the incubation, 20 µl of 5 mg/ml MTT was transferred to each well on day one and incubated for 4 hours. After 4 hours, the supernatant was carefully removed from each well at day 1, and 200 µL of DMSO (dimethyl sulfoxide) was added to dissolve the precipitate.

The absorbance was read at 570 nm. DMSO was removed from the plate and the empty wells were filled with 200 μL of PBS. This procedure from the addition of MTT reagent was repeated for five days in total, and the medium was changed for all remaining wells after absorbance measurement on days 2 and 4.

EdU assay

Cells were plated at 5×10^3 cells per well in a 24-well Falcon plate after SQLE knockdown. After 24 hours, half of the media was removed, and a 2X EdU solution was added to obtain a 1X EdU solution. After 2 hours incubation, cells were fixed with 3.7% (v/v) formaldehyde in PBS, washed with 3% (w/v) bovine serum albumin in PBS, and permeabilized with 0.5% Triton X-100 (v/v). Cells were then incubated with the Click-iT reaction cocktail (Alexa Fluor 555; Invitrogen), followed by DNA staining with Hoechst 33342 solution. The plates were imaged by a fluorescence microscope (ECHO, RVL-100-G). To quantify the number of EdU-positive cells, images were analyzed with ImageJ software.

Colony formation assay

The siRNA transfected and control cells were maintained in a 6-well plate with 3000 cells per well. Following 14 days' culture, cells were fixed and stained with crystal violet. Cell images were captured, and the numbers of cells were counted within the area of each well by the NIH Image J software.

Transwell migration assay

Transwells (Corning™ 3464, Corning, NY) were used for the migration assays. Following 24-hr starvation, siRNA-treated cells were collected and resuspended in the serum-free medium, and 1×10^5 cells were then loaded into the transwell inserts. Complete medium was

added to the lower chamber. After 24 h, the migrated cells were fixed with formaldehyde and stained with crystal violet. Four random areas for the migrated cells were counted, and an average number of cells in each area was plotted.

Matrigel invasion assay

The invasion assays were performed with the Matrigel-coated chambers (Corning™354480, Corning, NY). In a 24-well Falcon plate, the Matrigel chambers were first rehydrated for 2 hours with FBS-free medium in a humidified chamber. Complete medium was then added to the lower chambers, while 5.0×10^5 cells in FBS-free medium were seeded into the upper chamber. After 48 hours of incubation, all the medium was removed, the invaded cells were stained with a Diff-Quik stain kit and counted similarly as described in the migration assay.

RNA preparation

RNA was extracted from the cells with the Quick-RNA™ MiniPrep kit (Cat# R1054 & R1055, ZYMO RESEARCH, Irvine, CA) after successfully SQLE knockdown confirmed by Western blot. RNA degradation and contamination were monitored on 1% agarose gels. RNA purity was checked using the NanoPhotometer® spectrophotometer (IMPLEN, CA, USA). RNA integrity and quantitation were assessed using the RNA Nano 6000 Assay Kit of the Bioanalyzer 2100 system (Agilent Technologies, CA, USA).

Library preparation for transcriptome sequencing

A total amount of 1 μg RNA per sample was used as input material for the RNA sample preparations. Sequencing libraries were generated using NEBNext® UltraTM RNA Library Prep Kit for Illumina® (NEB, USA) following the manufacturer's recommendations, and index codes were added to attribute sequences to each sample. Briefly, mRNA was purified from total RNA

using poly-T oligo-attached magnetic beads. Fragmentation was carried out using divalent cations under elevated temperature in NEBNext First-Strand Synthesis Reaction Buffer (5X) or using sonication with Diagenode bioruptor Pico for breaking RNA strands. First-strand cDNA was synthesized using a random hexamer primer and M-MuLV Reverse Transcriptase (RNase H-). Second strand cDNA synthesis was subsequently performed using DNA Polymerase I and RNase H. Remaining overhangs were converted into blunt ends via exonuclease/polymerase activities. After adenylation of 3' ends of DNA fragments, NEBNext Adaptor with hairpin loop structure was ligated to prepare for hybridization. To select cDNA fragments of preferentially 150~200 bp in length, the library fragments were purified with the AMPure XP system (Beckman Coulter, Beverly, USA). Then 3 μl USER enzyme (NEB, USA) was used with size-selected, adaptor-ligated cDNA at 37 °C for 15 min followed by 5 min at 95 °C before PCR. Then PCR was performed with Phusion High-Fidelity DNA polymerase, Universal PCR primers, and Index (X) Primer. At last, PCR products were purified (AMPure XP system), and library quality was assessed on the Agilent Bioanalyzer 2100 system.

Clustering and sequencing

According to the manufacturer's instructions, the clustering of the index-coded samples was performed on a cBot Cluster Generation System using PE Cluster Kit cBot-HS (Illumina). After cluster generation, the library preparations were sequenced on an Illumina platform, and paired-end reads were generated.

Differential expression analysis

Differential expression analysis between the two groups was performed using the DESeq2 R package. DESeq2 provides statistical routines for determining differential expression

in digital gene expression data using a model based on the negative binomial distribution. The resulting P values were adjusted using Benjamin and Hochberg's approach for controlling the False Discovery Rate (FDR). Genes with an adjusted P value < 0.05 found by DESeq2 were assigned as differentially expressed.

Enrichment analysis

A common way for searching shared functions among genes is to incorporate the biological knowledge provided by biological ontologies. Gene Ontology (GO) annotates genes to biological processes, molecular functions, and cellular components in a directed acyclic graph structure, Kyoto Encyclopedia of Genes and Genomes (KEGG) annotates genes to pathways, Reactome annotates genes to pathways and reactions in human biology, Human Disease Ontology (DO) annotates genes to pathways and DisGeNET annotates genes to pathways.

GO enrichment analysis. GO is the abbreviation of Gene Ontology (http://www.geneontology.org/), which is a major bioinformatics classification system to unify the presentation of gene properties across all species. GO enrichment analysis of differentially expressed genes was implemented by the clusterProfiler R package. GO terms with corrected P value less than 0.05 were considered significantly enriched by differential expressed genes. KEGG Pathway enrichment analysis. KEGG is a database resource for understanding high-level functions and utilities of the biological system, such as the cell, the organism, and the ecosystem, from molecular-level information, especially large-scale molecular datasets generated by genome sequencing and other high-throughput experimental technologies (http://www.genome.jp/kegg/). We used R package clusterProfiler to test the statistical enrichment of differential expression genes in KEGG pathways. KEGG terms with adjusted P value less than 0.05 were considered

significant enrichment.

Reactome enrichment analysis. We used an R package called clusterProfiler for statistical Reactome enrichment of differential expression genes. Most importantly, clusterProfiler applies biological term classification and enrichment analyses to gene cluster comparison, helping to better understand higher-order functions of the biological system. In general, Reactome terms with adjusted P value less than 0.05 were considered significant enrichment.

DO enrichment analysis. The Human Disease Ontology (DO, http://www.disease-ontology.org) is a community driven standards-based ontology that provides the disease interface between data resources through ongoing support (term review and integration) of disease terminology needs, which is associated with human disease and gene function. We used an R package called clusterProfiler for statistical DO enrichment of differential expression genes. DO terms with adjusted P value less than 0.05 were considered significant enrichment.

DisGeNET enrichment analysis. The DisGeNET(https://www.disgenet.org) is a discovery platform containing one of the largest publicly available collections of genes and variants associated with human diseases. We used an R package called clusterProfiler for statistical DisGeNET enrichment of differential expression genes. DisGeNET terms with adjusted P value less than 0.05 were considered significant enrichment.

Statistical analysis

The t-test was used for statistical analysis with the GraphPad Prism (version 9.0, GraphPad Software Inc., CA), and P values < 0.05 were considered statistically significant. Error bars and standard deviations were measured and provided for each experiment. The data were presented as the mean ± standard deviation. The ImageJ software (NIH, Bethesda, MD, USA)

was utilized to quantify Western blots, migration, invasion, and colony formation assays.

RESULTS

siRNA knockdown of SQLE

In order to study the function of SQLE in HNSCC cell lines, we decided to knockdown SQLE and further assess phenotypes. Knockdown of SQLE was performed in UMSCC1 and UMSCC23 cell lines to evaluate phenotypic effects of SQLE down-regulation on cell proliferation, migration, and invasion. In each cell line, knockdown was confirmed by Western blot analysis (Figure 7A). Protein levels showed a reduction in both UMSCC1 and UMSCC23 cells when transfected with siSQLE (***, $P < 0.001$) (Figure 7B).

Knockdown of SQLE inhibits HNSCC cell proliferation

Cell proliferation is how quickly a cancer cell copies its DNA and divides into 2 cells. If the cancer cells are dividing more rapidly, it means the cancer is faster growing or more aggressive. The rate of cancer cell proliferation can be estimated by doing MTT assay, colony formation assay and EdU cell proliferation assay. In MTT assay, the proliferation rates of UMSCC1 and UMSCC23 cells were measured following SQLE knockdown for five days. The results illustrated an inhibited proliferative capacity of both cell lines when compared to their respective control groups. SQLE knockdown resulted in a significant decrease in cell proliferation in UMSCC1 cells and UMSCC23 cells (***, $P < 0.001$) (Figure 8). Besides, a significantly lower number of colonies were formed when SQLE was knocked down in UMSCC1 and UMSCC23 cells (**, $P < 0.01$, ***, $P < 0.001$) (Figure 9). In addition, the EdU cell proliferation assay was used to determine the impact of SQLE on the cell proliferation of UMSCC1 and UMSCC23 cells. A 2 hours' pulse of EdU was found to label more than half of the control cells, as expected for a rapidly dividing population, but it only labeled less than one-

fifth of the cells that were transfected with SQLE siRNA (Figures 10 and 11). The results indicate that the knockdown of SQLE significantly suppressed the proliferation rate of UMSCC1 and UMSCC23 cells (**, $P < 0.01$, ***, $P < 0.001$).

Knockdown of SQLE suppresses HNSCC cell migration

The study of cell migration in cancer research is of particular interest as the main cause of death in cancer patients is related to metastatic progression. In order for cancer to spread and disseminate throughout the body, cancer cells must migrate and invade through extracellular matrix (ECM), intravasate into blood circulation, attach to a distant site, and finally extravasate to form distant foci [39-42]. The transwell cell migration assay measures the chemotactic capability of cells toward a chemo-attractant [43]. In our study, transwell migration assays were performed to investigate the migration capacity of UMSCC1 and UMSCC23 cells following the siRNA knockdown of SQLE. When compared to the control groups, both UMSCC1 and UMSCC23 cells with SQLE knockdown had shown a significant reduction in migration capacity (***, $P < 0.001$) (Figures 12 and 13).

Knockdown of SQLE suppresses HNSCC cell invasion

Cell invasion is related to cell migration and defines the ability of cells to become motile and to navigate through the extracellular matrix within a tissue or to infiltrate neighboring tissues. Cancer cells that become invasive may disseminate to secondary sites and form metastases. The transwell cell invasion assay measures both cell chemotaxis and the invasion of cells through extracellular matrix, a process that is commonly found in cancer metastasis [43]. In our study, the invasion capabilities of UMSCC1 and UMSCC23 cells following siRNA knockdown of SQLE were evaluated by Matrigel invasion assay. After 48-h incubation, both

UMSCC1 and UMSCC23 cells with SQLE knockdown showed significantly reduced invasive capability versus the control cells (***, $P < 0.001$) (Figure 14 and 15).

Knockdown of SQLE shows no significant effect on PD-L1 expression

Expression of programmed death-ligand 1 (PD-L1) is frequently observed in HNSCC. Binding of PD-L1 to its receptor PD-1 on activated T cells inhibits anti-tumor immunity by counteracting T cell-activating signals [44]. Upregulation of PD-L1 may allow cancers to evade the host immune system. Compared with traditional therapies, the emerging PD-1/PD-L1 blockade immunotherapy exhibited more satisfactory curative effects and lower toxicity for patients with advanced HNSCC [45]. Therefore, we also want to investigate the relationship between PD-L1 and SQLE. However, western blot analysis showed that protein expression of PD-L1 was not significantly altered after SQLE knockdown in UMSCC1 and UMSCC23 cells (Figure 16). This result may indicate that SQLE is not involved in the regulation of PD-L1 expression.

EGF treatment does not alter the expression of SQLE in HNSCC cells

Epidermal growth factor (EGF) is a protein that stimulates cell growth and differentiation by binding to its receptor, EGFR. EGFR is expressed on normal human cells and also across a range of malignancies. Tumor EGFR expression correlates with poor prognosis and resistance to therapy. Therefore, EGFR has been recognized as an important therapeutic target in cancer [46]. Cetuximab, an EGF inhibitor, received authorization in 2004 from the European Medicines Agency (EMA) and in 2006 from the Food and Drug Association (FDA) for the treatment of patients with squamous cell cancer of the head and neck in combination with radiation therapy for locally advanced disease [47]. Considering the importance of EGF/EGFR pathway in

HNSCC, we performed western blot analysis to detect the expression of SQLE after treated with EGF. Western blot analysis showed that when treated with EGF, protein expression of SQLE was not significantly changed in UMSCC1 and UMSCC23 cells (Figure 17), indicating that EGF may not participate in the regulation of SQLE.

FGF treatment does not alter the expression of SQLE in HNSCC cells

Fibroblast growth factor receptors (FGFRs) are a family of tyrosine kinase receptors (RTKs). These receptors share the same canonical protein structure and their signaling axes are involved in cell proliferation, differentiation, tissue modeling and angiogenesis [48]. The FGF/FGFR signaling network is engaged in the progression of different human tumors by acting on both tumor and stromal cell compartments, thus affecting oncogenesis through different mechanisms, including cell signaling deregulation, angiogenesis and resistance to cancer therapies [49]. The FGF/FGFR signaling pathway is also frequently found in HNSCC. Targeted therapy with tyrosine kinase inhibitors (TKIs) or monoclonal antibodies against FGF receptors also represents a promising approach for the treatment of HNSCC [50]. Therefore, we decided to detect whether FGF would involve in SQLE regulation. However, our western blot analysis showed that when treated with FGF, protein expression of SQLE was not significantly changed in UMSCC1 and UMSCC23 cells (Figure 18), which indicates that FGF may not participate in the regulation of SQLE.

RNA sequencing analysis

Experimental design and approach

The primary goal of RNA-seq analysis is to discover genes that are differentially expressed and coregulated and deduce biological significance for future research. The ability to

interpret results is dependent on proper experimental design, the use of controls, and correct interpretation. This study uses two groups of UMSCC1 cells, including the SQLE knockdown group (KD_S) and control group (CTRL), and each group contains two replicates.

Determining intra- and intergroup sample variability

When evaluating variability among samples, the intergroup variability, depicting variations between experimental and control settings, should be greater than the intragroup variability, representing technical or biological variability.

Principal component analysis (PCA) is one approach to visualize the variation in a dataset. PCA is a statistical procedure, which uses an orthogonal transformation to convert a set of observations of possibly correlated variations into a set of values of linearly uncorrelated variations. The results are presented as a two-dimensional plot or a three-dimensional plot, describing the variation by principal components (PCs). PC1 describes the most variation within the data, PC2 describes the second most, and so forth. In the PCA 2D plot, PC1 accounts for 64.83% of the variance, and PC2 accounts for 22.48% (Figure 19A). In PCA 3D plot, PC1 accounts for 61.24% of the variance, PC2 accounts for 23.69%, and PC3 accounts for 15.07% (Figure 19B). These data demonstrated that the intergroup variability is greater than intragroup variability.

Another method for estimating intra- and intergroup variability is to measure distance as presented by correlation among samples. The Pearson's correlation expresses the linear relationship between two factors that accounts for variations in their mean and standard deviation. The closer the correlation coefficient is to 1, the more similar the expression pattern is. The Pearson's correlation analysis shows all the variation between samples with a correlation

value r > 0.9, indicating that all these samples belong to the same cell type (Figure 19C). However, the correlation value between the knockdown and control samples is smaller than the correlation value between two knockdown samples or two control samples, further suggesting that the intergroup variability is more evident than intragroup variability.

Identification of differentially expressed genes (DEGs) and visualization

Gene expression level analysis is the core task in RNA-seq experiments. In the process of differential expression analysis, FPKM was applied in calculating the relative gene expression levels, and remarkably DEGs were identified by a corrected padj <0.05 and |log2 fold change| > 0. FPKM stands for Fragments Per Kilobase of transcript per Million mapped reads. In RNA-Seq, the relative expression of a transcript is proportional to the number of cDNA fragments that originate from it.

The co-expression Venn diagram presents the number of uniquely expressed genes within each group, with the overlapping regions showing the number of genes that are co-expressed in two groups. In total, 613 genes and 477 genes were uniquely expressed in the SQLE knockdown group and control group. 11,437 genes were found co-expressed in both groups (Figure 20).

After SQLE knockdown, 2,994 genes were differentially expressed, including 1,527 upregulated and 1,467 downregulated genes (Figure 21). Besides, a volcano plot is used to infer the overall distribution of differentially expressed genes (Figure 22). It shows statistical significance (p value) versus magnitude of change (fold change) on the y and x axes. It is constructed by plotting the -log10 of the corrected p value on the y axis. The smaller the corrected p value is, the bigger -log10 (corrected p value) will be, meaning the difference is more significant. The x axis is the log2 of the fold change of genes. In a volcano plot, the most

upregulated genes are towards the right, the most downregulated genes are towards the left, and the most statistically significant genes are towards the top. As labeled in the figure, the top 5 upregulated genes are AHNAK2, MX1, MYL9, KRT17, and BNIP3. The top 5 downregulated genes are SQLE, EI24, GCLM, TFRC, and COMMD8.

Cluster analysis on differential expression indicates genes with similar expression patterns under various experimental conditions. By clustering genes with similar expression patterns, it is possible to predict unknown functions of previously characterized genes or unknown genes. Hierarchical clustering analysis is carried out of log2 (FPKM+1) of union differential expression genes within the SQLE knockdown and control groups (Figure 23). From the heat map of hierarchical clustering, we found that two SQLE knockdown samples were clustered together, and two control groups were clustered together. Besides, the hierarchical cluster also revealed four main clusters. Clusters I, II, III, and IV had 69 (2.3%), 6 (0.2%), 1,461 (48.8%), and 1,458 genes (48.7%), respectively (Figure 24). Genes in the four clusters showed different expression patterns. In clusters I and IV, high levels of expression were observed in knockdown groups. In clusters II and III, genes were more abundantly expressed in control groups. The top 5 significant genes in cluster I are AHNAK2, MX1, MYL9, BNIP3, and OAS2. The top 5 significant genes in cluster II are SQLE, EI24, GCLM, COMMD8, and SNRPD1. The top 5 significant genes in cluster III are TFRC, LRRC58, FBXO45, CASC4, and TMEM167A. Finally, the top 5 significant genes in cluster IV are KRT17, TPM4, KIAA0513, TIMP2, and STC2.

Functional Analysis

Through the enrichment analysis of the differential expressed genes, we can determine

which biological functions or pathways are significantly associated with differentially expressed genes. ClusterProfiler [51] software was used for enrichment analysis, including GO Enrichment, DO Enrichment, KEGG, Reactome Enrichment, and DisGeNET database Enrichment.

GO Enrichment Analysis. GO is the abbreviation of Gene Ontology, which is a major bioinformatics classification system to unify the presentation of gene properties across all species. GO terms with padj < 0.05 are significant enrichment. In GO enrichment analysis for all genes, ribonucleoprotein complex biogenesis (133 unigenes), actin cytoskeleton (128 unigenes), and protein serine/threonine kinase activity (116 unigenes) take up top-3 counts of unigenes (Figure 25). Besides, GO functional analysis indicated 2,994 unigenes in three major categories: molecular function (MF), biological process (BP), and cellular component (CC) (Figure 26). Among molecular functions, the most significant group was ATPase activity (109 unigenes), followed by cadherin binding (98 unigenes) and ubiquitin-like protein ligase binding (93 unigenes). For the category of biological process, the most significantly enriched group was the defense response to virus (72 unigenes) and response to type I interferon (38 unigenes). As to the cellular component category, the most dominant groups were chromosomal region (101 unigenes), cell-cell junction (113 unigenes), and actin cytoskeleton (128 unigenes).

To be more specific, upregulated genes and downregulated genes were analyzed separately. In the result of upregulated genes analysis, actin binding (83 unigenes), cellular response to type I interferon (29 unigenes), and actin cytoskeleton (104 unigenes) are the most significant groups in molecular function, biological process, and cellular component categories, respectively (Figure 27 and 28). As for the downregulated genes, catalytic activity, acting on RNA (79 unigenes), ribonucleoprotein complex biogenesis (118 unigenes), and chromosomal

region (86 unigenes) are the most significantly enriched groups in molecular function, biological process, and cellular component categories, respectively (Figure 29 and 30), which indicates that DNA replication, transcription, and translation may be decreased by SQLE knockdown.

DO Enrichment Analysis. The Human Disease Ontology (DO) is a community-driven standards-based ontology that provides the disease interface between data resources through ongoing support (term review and integration) of disease terminology needs, which is associated with human disease and gene function. DO terms with padj < 0.05 are significant enrichment. Germ cell cancer (101 genes) and embryonal cancer (93 genes) are the dominant cancer types in the analysis (Figure 31). However, there are no significantly enriched diseases when analyzing upregulated genes and downregulated genes separately.

KEGG Enrichment Analysis. The interactions of multiple genes may be involved in certain biological functions. KEGG (Kyoto Encyclopedia of Genes and Genomes) is a collection of manually curated databases containing resources on genomic, biological-pathway, and disease information [52]. Pathway enrichment analysis identifies significantly enriched metabolic pathways or signal transduction pathways associated with differentially expressed genes, comparing the whole genome background. KEGG terms with padj < 0.05 are significant enrichment. KEGG pathway analysis showed that the differentially expressed genes after SQLE knockdown were significantly enriched in several pathways, including cell cycle and DNA replication (Figure 32). In KEGG analysis of cell cycle, TGF-β and Cip1 are upregulated, both of which can arrest the cell cycle at the G1 stage to stop proliferation (Figure 33). On the other hand, MCM, ORC, and E2F1, 2, 3 are downregulated, which indicates the decrease of DNA synthesis.

To be more specific, some upregulated genes following SQLE knockdown were significantly enriched in some other pathways, such as MAPK/ERK signaling and mTOR signaling pathways (Figure 34). In the MAPK/ERK signaling pathway, TGFBR and HSP72 are downregulated (Figure 35), both of which have been linked to the development of some cancers [53]. In mTOR signaling pathway KEGG analysis, frizzled, the receptor in the Wnt signaling pathway, is downregulated, which might explain the inhibition of HNSCC by SQLE knockdown (Figure 36). This may be due to the role of Wnt signaling in the development of cancers [54]. In KEGG analysis for downregulated DEGs, spliceosome, DNA replication and cell cycle are the top 3 significant pathways (Figure 37), which further illustrates the reduction of mitosis in SQLE-knockdown HNSCC cells.

Reactome Enrichment Analysis. The Reactome is a database of reactions, pathways, and biological processes, which can be used to browse pathways and submit data to a suite of data analysis tools, containing curated annotations that cover a diverse set of topics in molecular and cellular biology. Reactome terms with padj < 0.05 are considered as significant enrichment. It is apparent that most of the pathways were related to different phases of the cell cycle and transitions between them, stimulus-based changes in gene expression, DNA damage repair, and DNA damage-induced programmed cell death (Figure 38). Genes involved in interferon alpha/beta signaling and interferon signaling are most significantly upregulated, and genes that participated in cell cycle and DNA replication are downregulated, both of which were in accordance with the results of the GO enrichment analysis (Figure 39 and 40).

DisGeNET Enrichment Analysis. The DisGeNET is a discovery platform containing one of the largest publicly available collections of genes and variants associated with human

diseases. DisGeNET terms with padj < 0.05 are significant enrichment. However, there is no significantly affected disease observed in this study.

Function Annotation of Oncogene. An oncogene is a potentially cancer-causing gene, which is typically mutated or expressed at a high level. Proto-oncogene as a normal gene, involved in cell development, cell division, and cell differentiation, turns into oncogene when sequence mutation happens. Generally, the expression of some specific oncogenes is upregulated in tumor or malignant cell lines. Studies on the differential expression of oncogenes help reveal the mechanism of disease development and cancer occurrence. By using the COSMIC database (Catalogue of Somatic Mutations in Cancer), 123 significant oncogenes are discovered following SQLE knockdown. Among the top 4 significant oncogenes, a head and neck cancer-associated oncogene, TGFBR2, was significantly decreased in the SQLE knockdown group, which indicates that TGFBR2 is positively associated with the oncogenicity of SQLE in head and neck cancer (Figure 41).

DISCUSSION

Based on our informatic analyses, SQLE expression was significantly overexpressed in HNSCC tissues compared with adjacent normal tissues. Furthermore, the overall survival rate of HNSCC patients with higher SQLE expression levels was significantly lower than that of patients with lower SQLE expression levels. Similar findings were observed in a number of other cancers, indicating that SQLE may be an important molecular target in HNSCC. In our studies, the knockdown of SQLE suppressed the proliferation, migration, and invasion of the two HNSCC cell lines, UMSCC1 and UMSCC23, indicating that SQLE may play an important role in the progression of HNSCC. RNA sequencing analysis showed that SQLE may participate in the regulation of head and neck tumors through interacting with many important regulatory pathways, such as cell cycle, MAPK signaling pathway, and mTOR signaling pathway.

It is well known that HNSCC carcinogenesis involves many molecular events, such as up-regulation of proto-oncogenes and down-regulation of tumor suppressor factors [55]. SQLE is the rate-limiting enzyme in cholesterol biosynthesis and considered to be the proto-oncogene [56]. Previous studies have provided clues for understanding the role of SQLE in cancer-related molecular mechanisms. In a hormone receptor-positive breast cancer study, overexpression of the CASIMO1 microprotein (cancer-associated small full-membrane open reading frame 1) was deemed necessary for cancer cell survival [30]. The tumor-promoting effect of CASIMO1 is achieved through the direct interaction and stabilization of SM (SQLE) thus stimulating downstream MAPK/ERK signaling pathway and cancer cell growth (Figure 42A). It has also been demonstrated in hepatocellular and lung squamous cell carcinoma that SQLE promoted the growth of cancer cells through activating MAPK/ERK signaling pathway [31, 32]. But no direct

link between SQLE and MAPK/ERK signaling pathway has been reported in HNSCC. Based on our findings in RNA sequencing analysis, proto-oncogenes involved in MAPK/ERK signaling pathway are downregulated following SQLE knockdown, such as TGFBR and HSP72 (Figure 35). Transforming growth factor-β (TGF-β) is a homo-dimeric protein known to be a multifunctional regulator in target cells and to serve a pivotal role in numerous types of cancer, including HNSCC [57]. Accumulating evidence suggested that deregulation of TGF-β signaling is of great importance in HNSCC and may be the result of defected TGF-β signaling [58-60].The effects of TGF-β signaling at a cellular level include the regulation of tumor cells and other stromal cells, as well as the possible mechanisms underlying the conversion from a tumor suppressor to a tumor promoter in HNSCC [61]. Some scientists reported that TGF-β signaling pathway serves as a tumor suppressor at an early stage, whereas it serves as a tumor promoter in transformed epithelial cells at a later stage[62]. However, the exact role of TGF-β in HNSCC is not completely understood. Therefore, the relationship between SQLE and TGF-β requires further investigation.

Another study found that upregulation of SQLE in nonalcoholic fatty liver-related hepatocellular carcinoma enhanced the synthesis of cholesteryl esters, which promotes cancer aggressiveness [33]. Increased SQLE activity leads to reactive oxygen species-induced silencing of PTEN and activation of oncogenic Akt signaling, a pathway in the mTOR signaling pathway (Figure 42B). In the mTOR signaling pathway (KEGG analysis of our result), frizzled (FZDs), serving as receptors in the Wnt signaling pathway, was found to be downregulated (Figure 36). Knockdown of FZDs may suppress the Wnt signaling pathway resulting in the reduction of cell growth, invasion, and metastasis of cancer cells [63]. Based on previous literature, FZDs are

highly expressed in cancer tissues and may serve as potentially valuable therapeutic targets [64]. Therefore, future studies are warranted to investigate the relationship between SQLE and FZDs.

Recent reports have also emphasized the role of lipid droplets (LDs) in adaptation to changes in SQLE activity, possibly accommodating excess squalene (Figure 42C). In breast cancer cells, the use of terbinafine to inhibit SM (SQLE) increases the formation of lipid droplets [30]. Meanwhile, the ability of neuroendocrine cell lines to adequately isolate squalene is a key determinant of their sensitivity to NB-598, a potent competitive inhibitor of squalene epoxidase [65]. Since lipid droplets are involved in aberrant cell proliferation and cancer aggressiveness [66], it is necessary to study the connection between SQLE and LDs' activities in HNSCC in the future.

High expression of SQLE has been associated with the pathogenesis of fatal prostate cancer [34], colorectal cancer [35], and the appearance and development of squamous lung cancer. Noteworthy, fungal SQLE inhibitor terbinafine dose-dependently reduced the number and viability of several cultured human malignant cells, thereby disrupting the cell cycle during the G0/G1 transition [36, 67-69]. In addition, a murine xenograft model study revealed that the tumor size decreased after intraperitoneal injection of terbinafine [67]. Based on the therapeutic effect of terbinafine on other cancers, the role of terbinafine as SQLE inhibitor may also provide positive therapeutic potential in HNSCC.

CONCLUSION

This study has preliminarily characterized the role of SQLE in HNSCC tumor growth and progression. The effect of SQLE on the proliferation, migration, and invasion of head and neck cancer cells was studied by the inhibition of SQLE through siRNA transfection. To determine the potential downstream targets of SQLE and related molecular mechanisms of SQLE's regulation, we also conducted RNA sequencing analysis of HNSCC cells with siSQLE knockdown and identified the differentially expressed genes.

Although the phenotypic effect of SQLE knockdown is recognized, the limitations of this study confine the full characterization of the existing mechanisms. Future studies are needed by overexpressing SQLE in HNSCC cells, which serve as rescue experiments of SQLE knockdown cells to further confirm the functional role of SQLE in promoting HNSCC progression. Based on the RNA sequencing analysis, both MAPK/ERK and mTOR signaling pathways were found to be significantly inhibited by SQLE downregulation. Specifically, TGFBR is downregulated after SQLE knockdown. Considering the paradoxical role of TGF-β in HNSCC, as a tumor suppressor in the early stages of oncogenesis or a potent tumor promoter in the epithelium at a later stage [70, 71], the relationship between SQLE and TGFBR warrants further investigation.

The clinical applicability of SQLE as a prognostic or therapeutic target for oral/head and neck cancer can be inferred from studies in other types of cancers and its role in cancer-related biological processes such as epithelial-mesenchymal transition (EMT). SQLE has been identified as a direct downstream target gene of miR-133b, a miRNA under-expressed in human esophageal squamous cell carcinoma (ESCC) [5]. The study demonstrated that ectogenic miR-133b expression followed by SQLE knockdown inhibits proliferation, metastasis, invasion, and

decreases the EMT of ESCC *in vitro*. Besides, the potential of SQLE as a prognostic target has been demonstrated in lung squamous cell carcinoma, breast cancer, and leukemia, and association with SQLE correlated to poor outcomes in prognosis as well as an increase in metastasis [6-8].

In summary, this study has uncovered a promoting role of SQLE in HNSCC development. SQLE could be used as a prognostic biomarker if further validated in large patient cohorts. However, further detailed studies are needed to investigate the relevant molecular pathways of SQLE in HNSCC. Whether SQLE can be used as a therapeutic target in HNSCC also warrants further studies in the future.

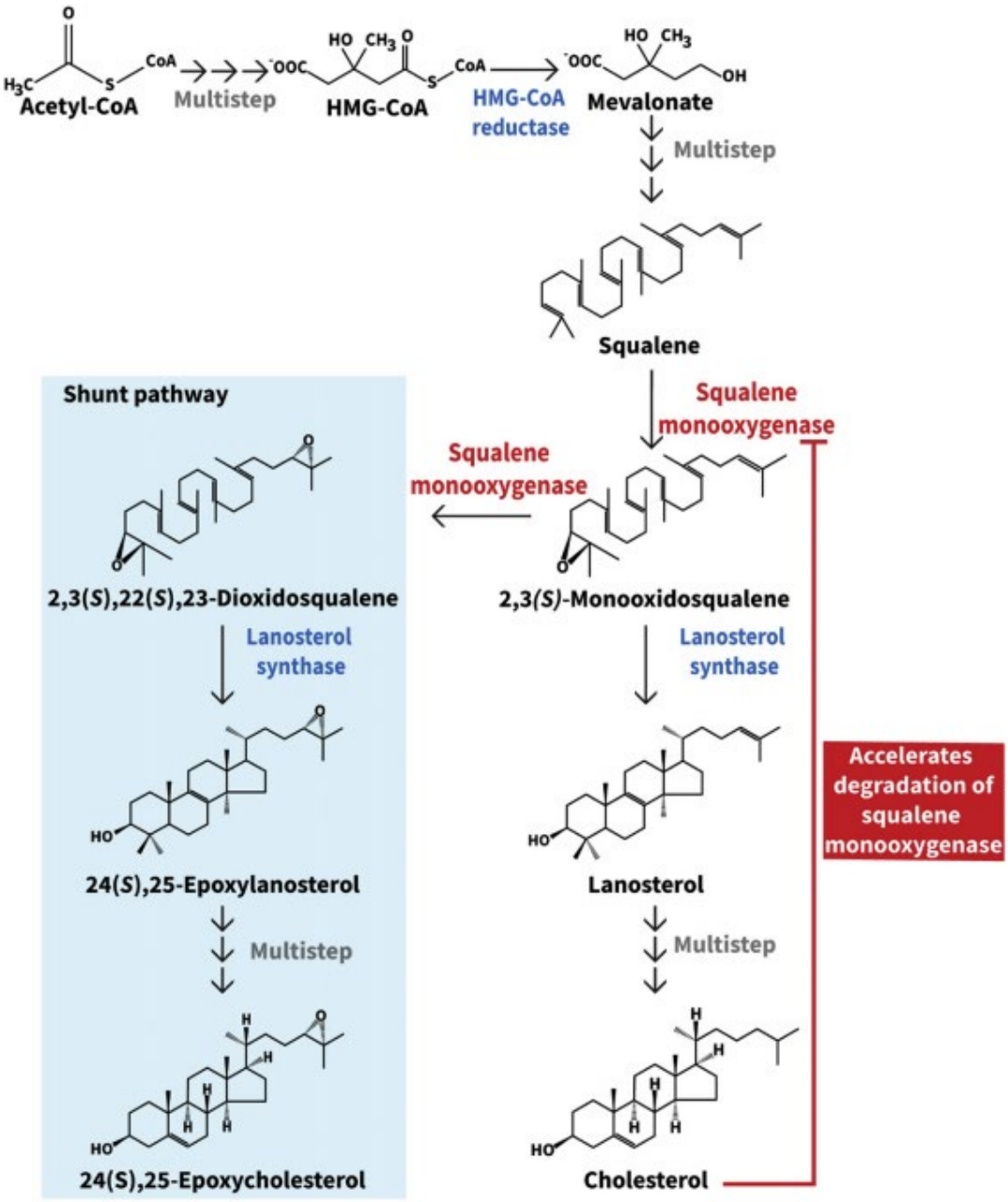

Figure 1. Squalene monooxygenase is the gateway enzyme to the shunt pathway, a branch of the mevalonate pathway [13].

A

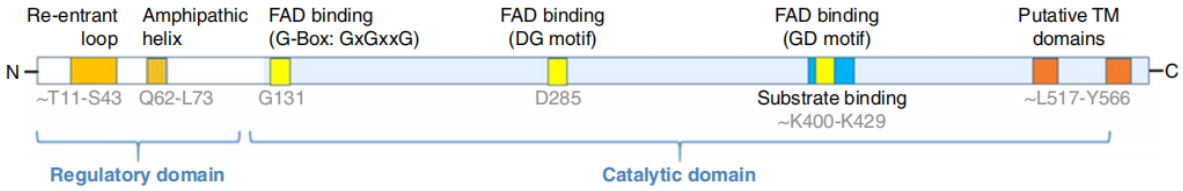

B

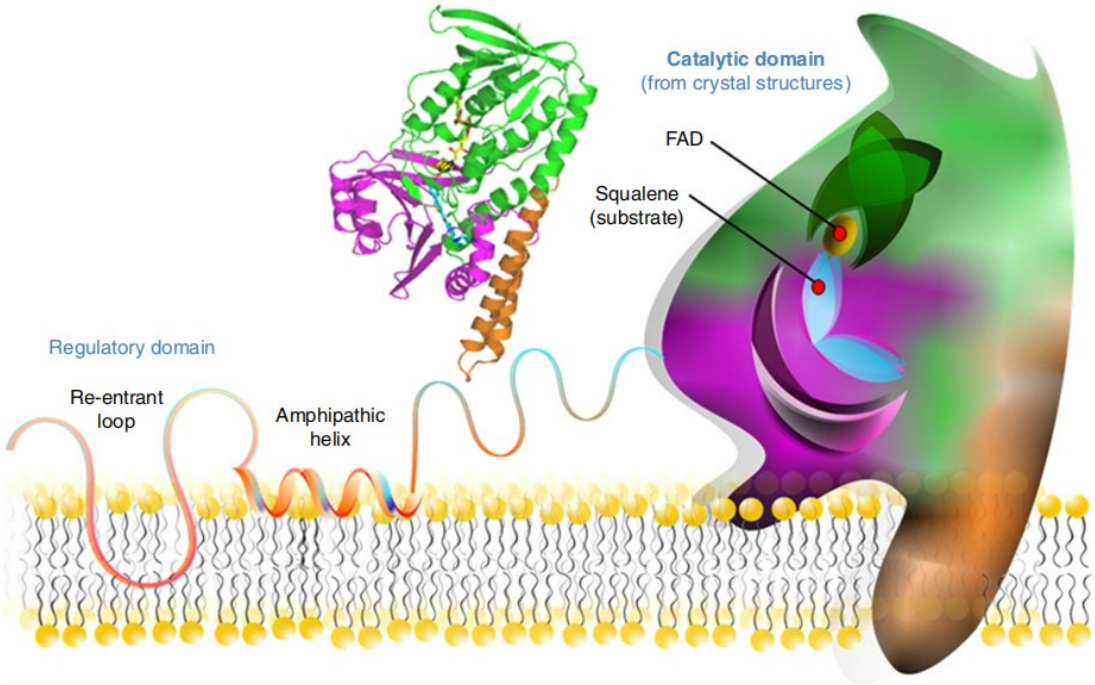

Figure 2. Structure of SQLE protein. **(A)** Linear view of SQLE protein with known structural features [16]. **(B)** Structure of the catalytic domain of human SQLE [16]. The FAD binding domain is shown in green, the substrate-binding domain in magenta, and the C-terminal membrane-associated helical domain in orange. FAD (yellow) and the inhibitor NB-598 (blue) are shown in stick representation.

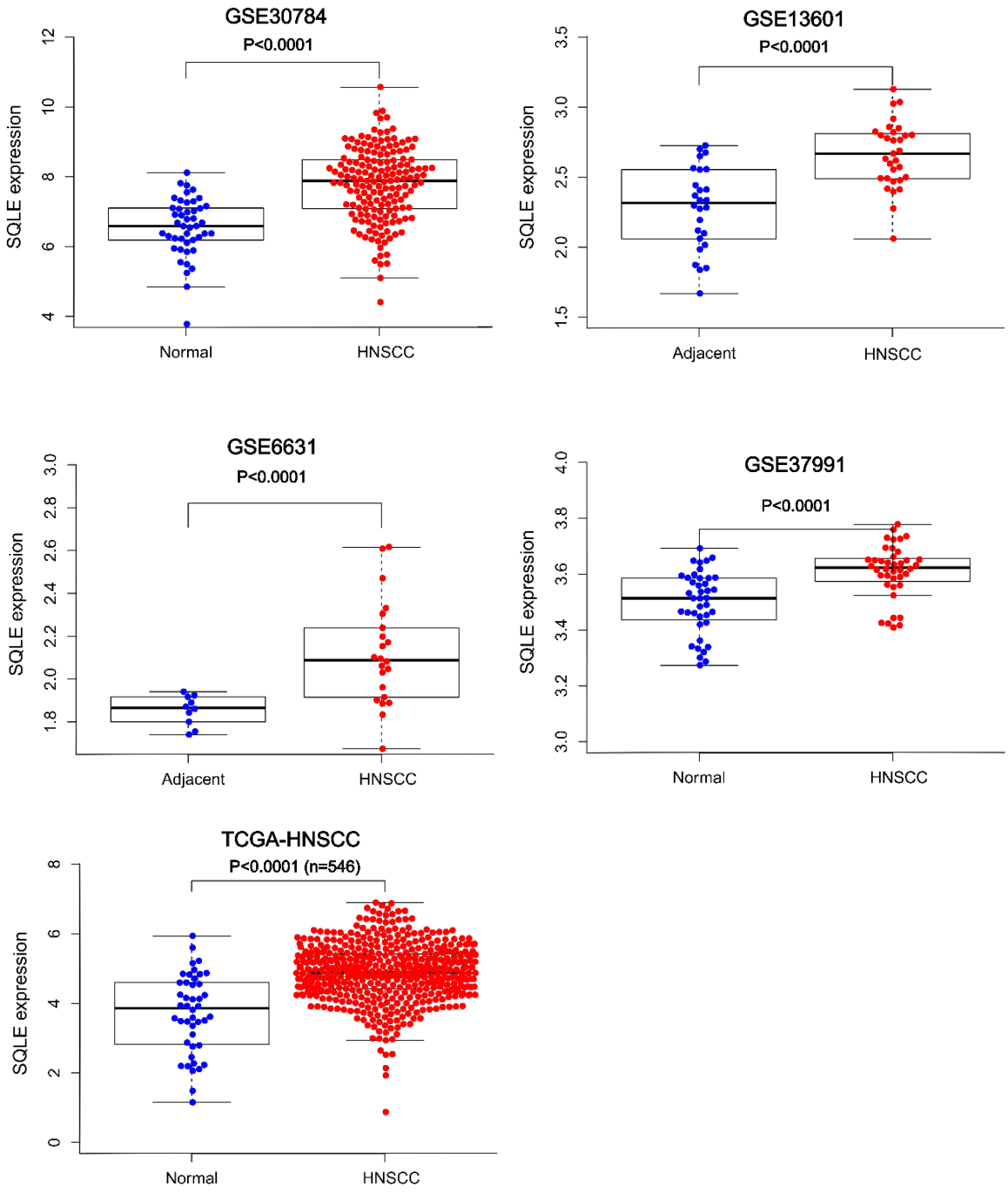

Figure 3. The gene expression level of SQLE is significantly higher in HNSCC tissues than adjacent normal tissues based on GSE and TCGA datasets ($P < 0.0001$).

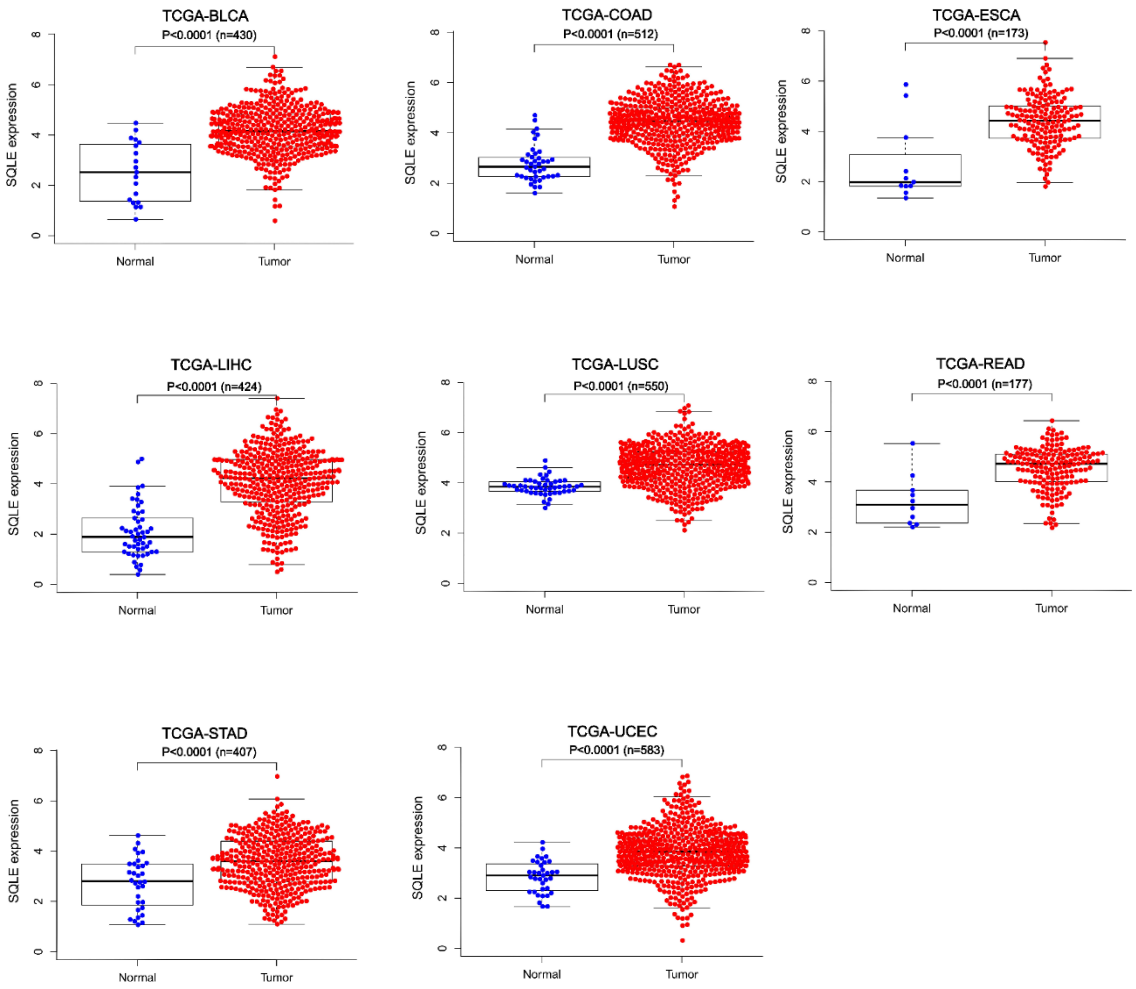

Figure 4. SQLE gene expression is significantly upregulated in many cancers, including bladder urothelial carcinoma (BLCA), colon adenocarcinoma (COAD), esophageal carcinoma (ESCA), liver hepatocellular carcinoma (LIHC), lung squamous cell carcinoma (LUSC), rectum adenocarcinoma (READ), stomach adenocarcinoma (STAD), and uterine corpus endometrial carcinoma (UCEC) ($P < 0.0001$).

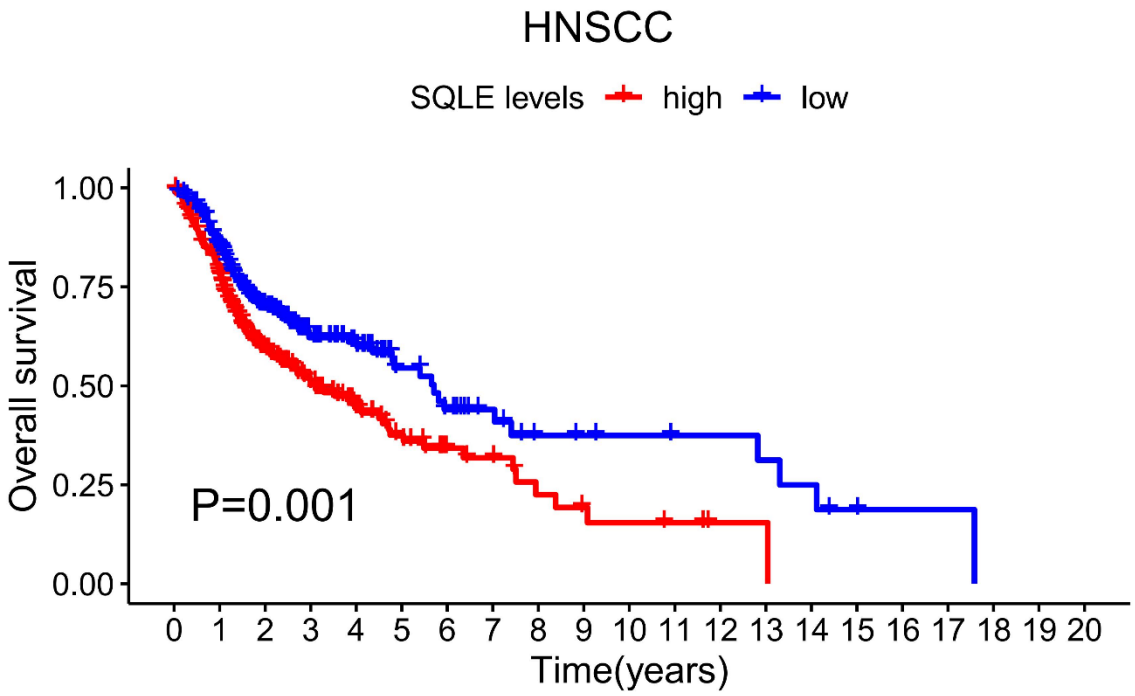

Figure 5. HNSCC patients with high SQLE gene expression show worse overall survival than those with low SQLE gene expression (P = 0.001).

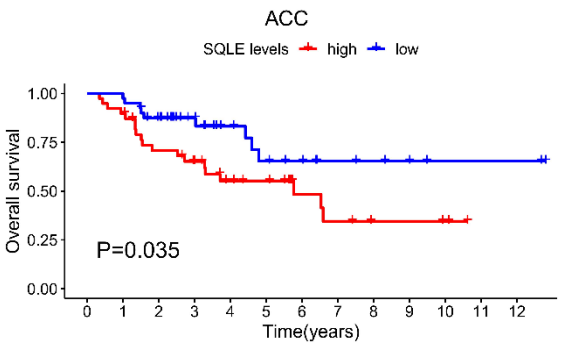
ACC
SQLE levels high low
Overall survival
1.00
0.75
0.50
0.25
0.00
P=0.035
0 1 2 3 4 5 6 7 8 9 10 11 12
Time(years)

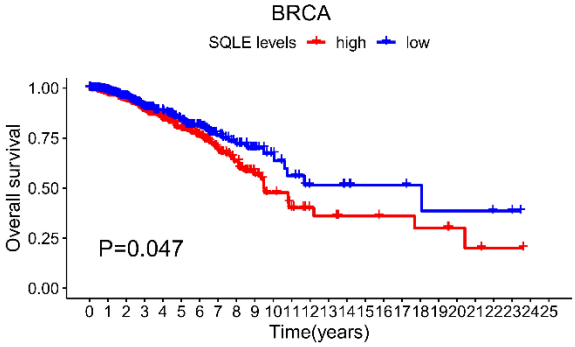
BRCA
SQLE levels high low
Overall survival
1.00
0.75
0.50
0.25
0.00
P=0.047
0 1 2 3 4 5 6 7 8 9 10 11 12 13 14 15 16 17 18 19 20 21 22 23 24 25
Time(years)

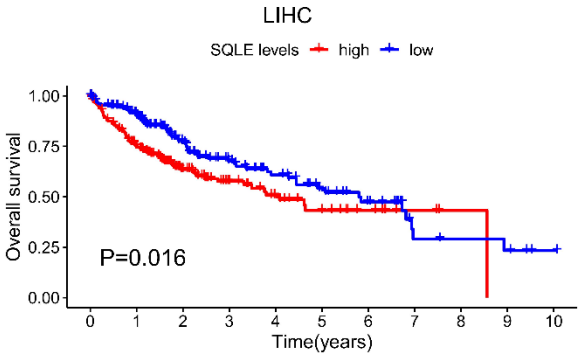
LIHC
SQLE levels high low
Overall survival
1.00
0.75
0.50
0.25
0.00
P=0.016
0 1 2 3 4 5 6 7 8 9 10
Time(years)

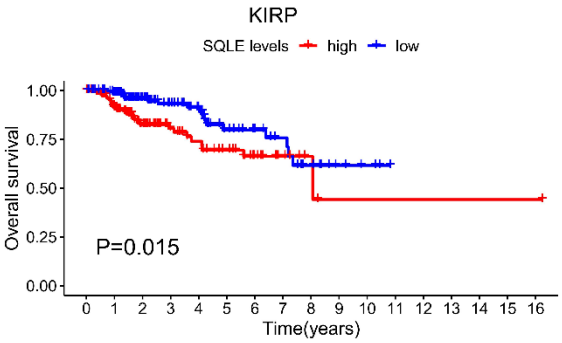
KIRP
SQLE levels high low
Overall survival
1.00
0.75
0.50
0.25
0.00
P=0.015
0 1 2 3 4 5 6 7 8 9 10 11 12 13 14 15 16
Time(years)

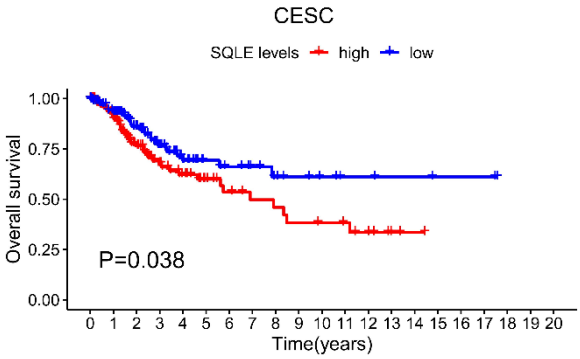
CESC
SQLE levels high low
Overall survival
1.00
0.75
0.50
0.25
0.00
P=0.038
0 1 2 3 4 5 6 7 8 9 10 11 12 13 14 15 16 17 18 19 20
Time(years)

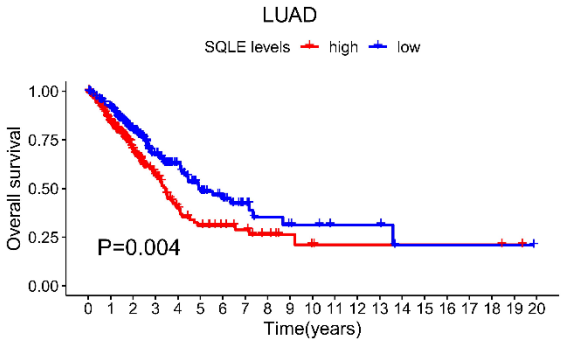
LUAD
SQLE levels high low
Overall survival
1.00
0.75
0.50
0.25
0.00
P=0.004
0 1 2 3 4 5 6 7 8 9 10 11 12 13 14 15 16 17 18 19 20
Time(years)

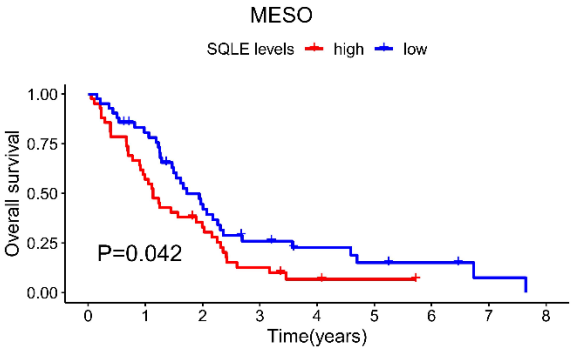
MESO
SQLE levels high low
Overall survival
1.00
0.75
0.50
0.25
0.00
P=0.042
0 1 2 3 4 5 6 7 8
Time(years)

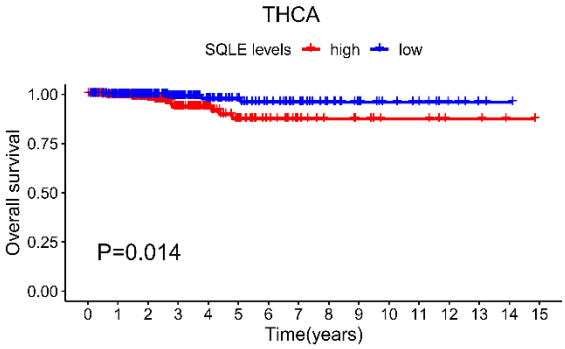
THCA
SQLE levels high low
Overall survival
1.00
0.75
0.50
0.25
0.00
P=0.014
0 1 2 3 4 5 6 7 8 9 10 11 12 13 14 15
Time(years)

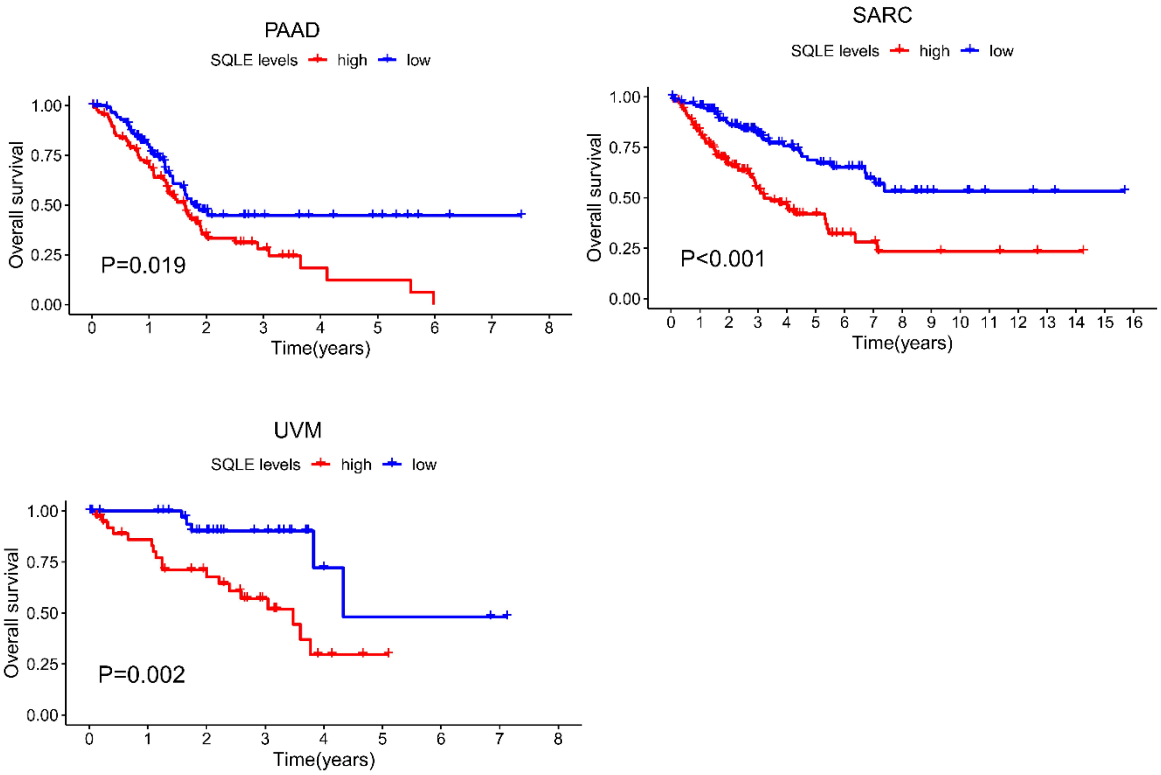

Figure 6. Adrenocortical carcinoma (ACC), BRCA, cervical squamous cell carcinoma and endocervical adenocarcinoma (CESC), kidney renal papillary cell carcinoma (KIRP), LIHC, lung adenocarcinoma (LUAD), mesothelioma (MESO), pancreatic adenocarcinoma (PAAD), sarcoma (SARC), thyroid carcinoma (THCA), and uveal melanoma (UVM) patients with high SQLE expression had a worse long-term overall survival rate than those patients with low SQLE expression.

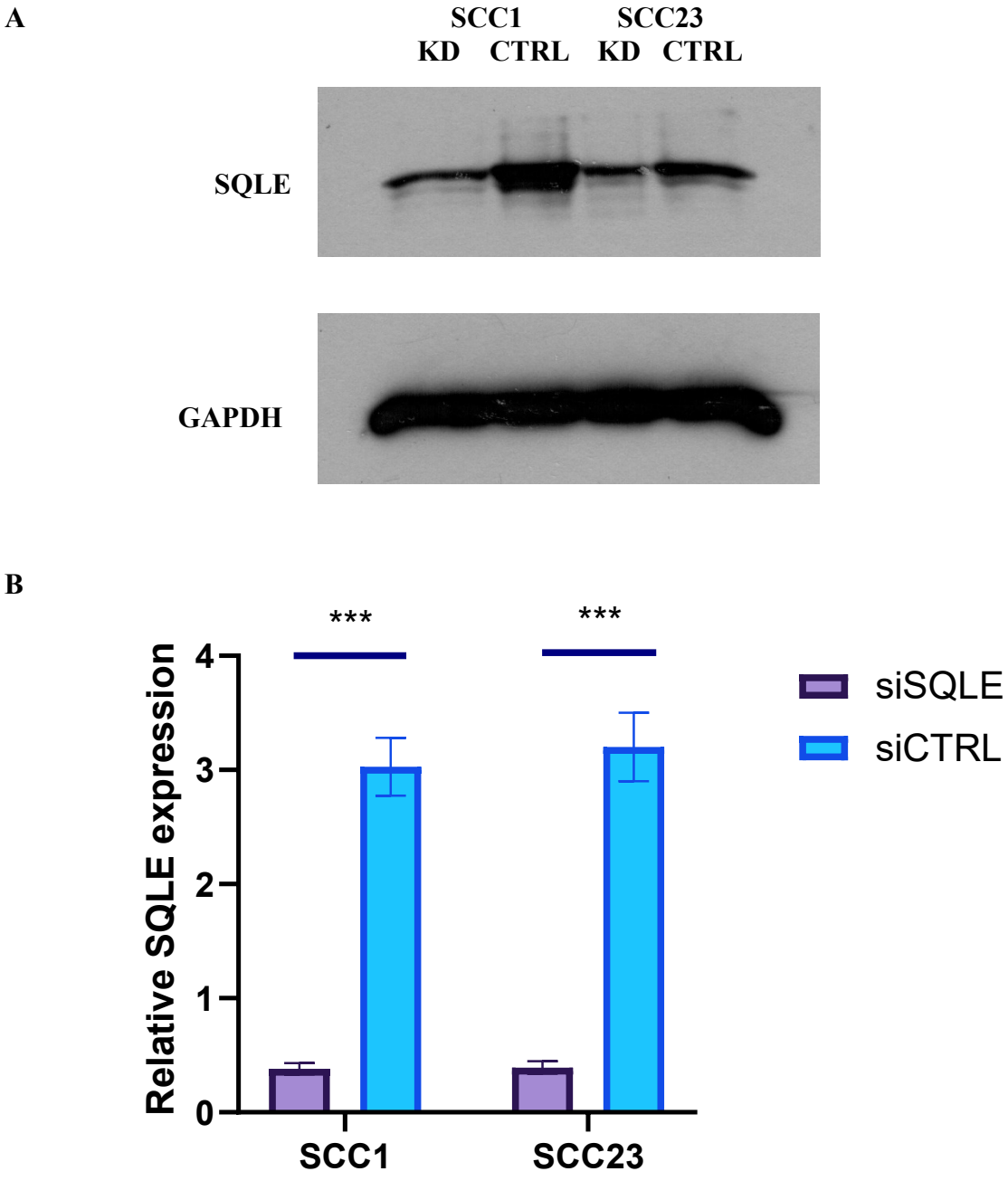

Figure 7. siRNA knockdown of SQLE in UMSCC1 and UMSCC23 cells. **(A)** Western blot analysis showing knockdown of SQLE with siSQLE vs siControl. **(B)** Quantification of Western blot results showing significant downregulation of SQLE in both cell lines by siSQLE (***, $P < 0.001$). Each experiment was repeated in triplicate. All values are expressed as the mean ± standard deviation.

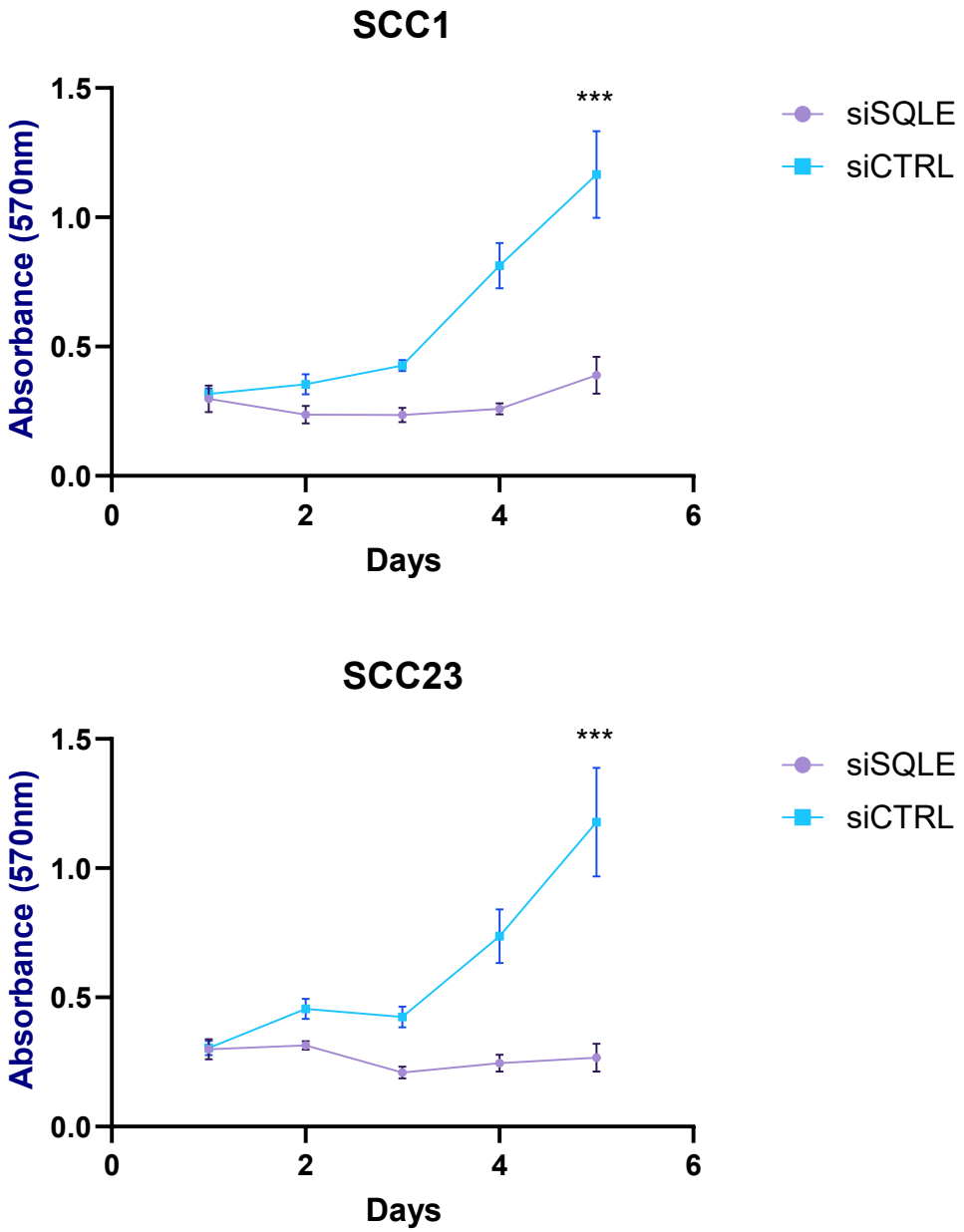

Figure 8. MTT assay of UMSCC1 and UMSCC23 cells transfected with SQLE siRNA or control siRNA. The proliferation rates of UMSCC1 cells or UMSCC23 cells transfected with siSQLE were significantly lower than the control cells at all time points except for the first day (***, $P < 0.001$). Each experiment was repeated in triplicate. All values are expressed as the mean ± standard deviation.

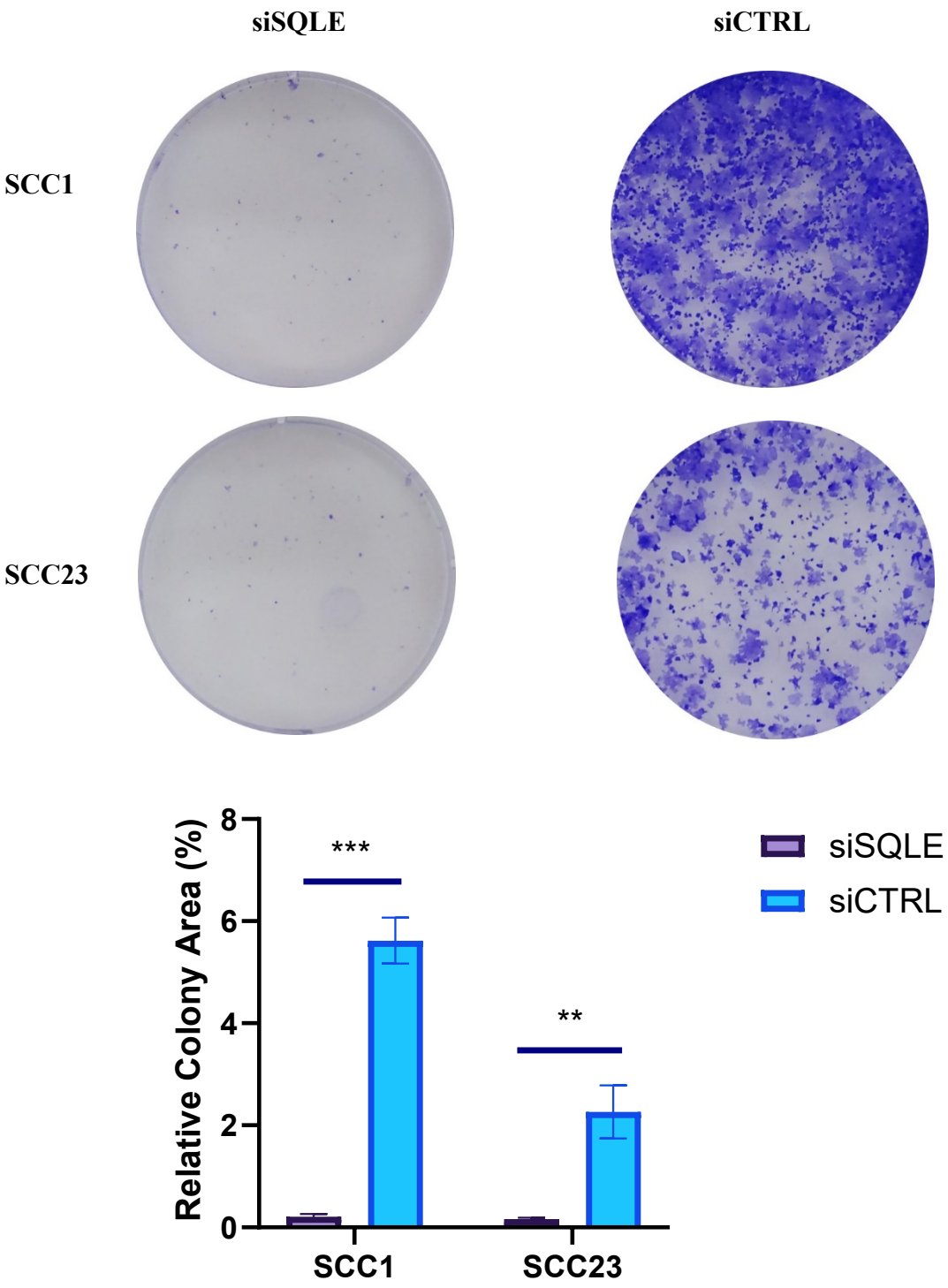

Figure 9. Colony formation assay of UMSCC1 and UMSCC23 cells transfected with SQLE siRNA or control siRNA. SQLE knockdown significantly suppressed the colony formation of both UMSCC1 and UMSCC23 cells (**, $P < 0.01$, ***, $P < 0.001$). Each experiment was repeated in triplicate. All values are expressed as the mean ± standard deviation.

A

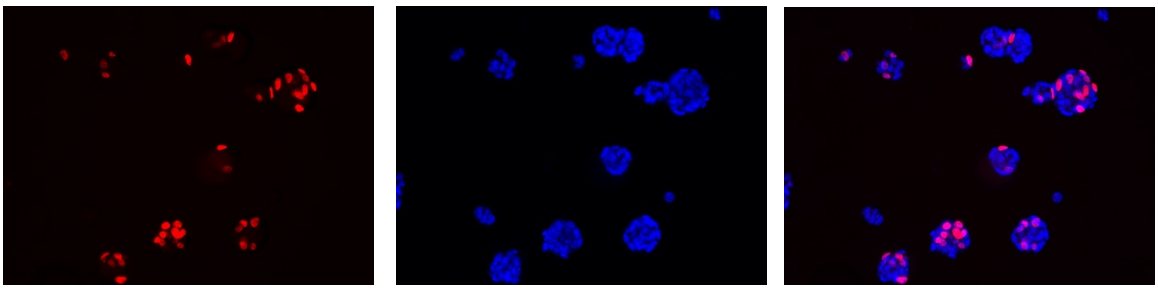

B

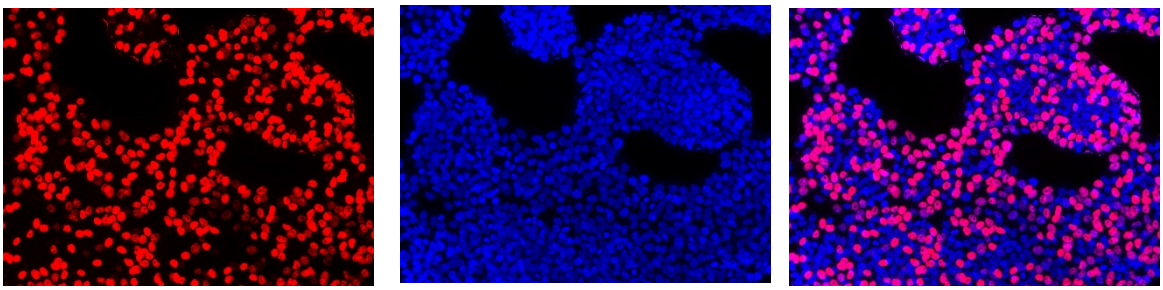

C

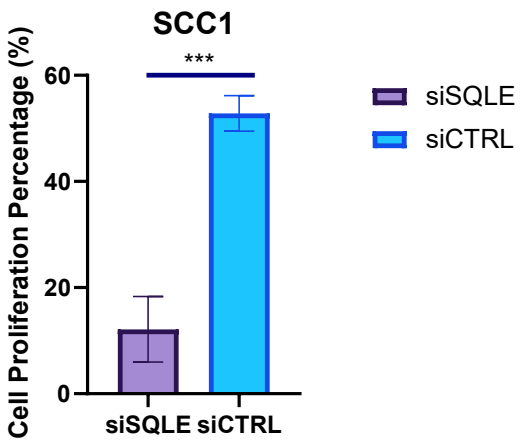

Figure 10. EdU cell proliferation assay. UMSCC1 cells were treated with SQLE siRNA **(A)** or control siRNA **(B)**. The left image shows proliferating cells labeled with EdU. The middle one shows a total population of cells, in which nucleic acid were stained with Hoechst 33342. The right one represents the overlapping images showing the proliferating cells. **C** presents the percentage of proliferating cells out of total cell population. The figures show significantly reduction in the proliferation rate in UMSCC1 cells treated with SQLE siRNA (***, $P < 0.001$). Each experiment was repeated in triplicate. All values are expressed as the mean ± standard deviation.

A

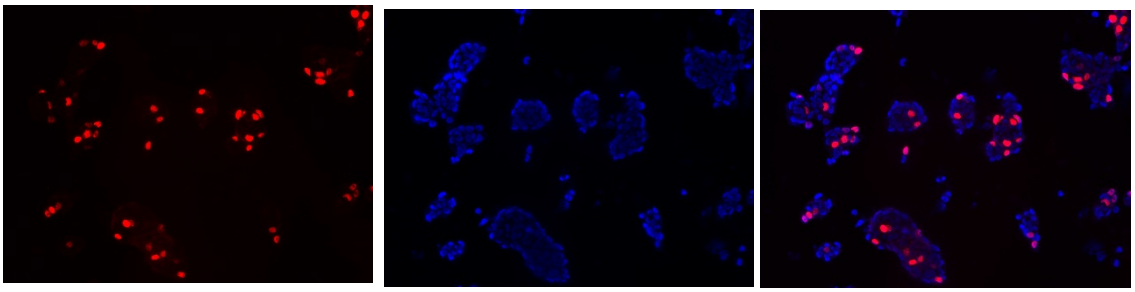

B

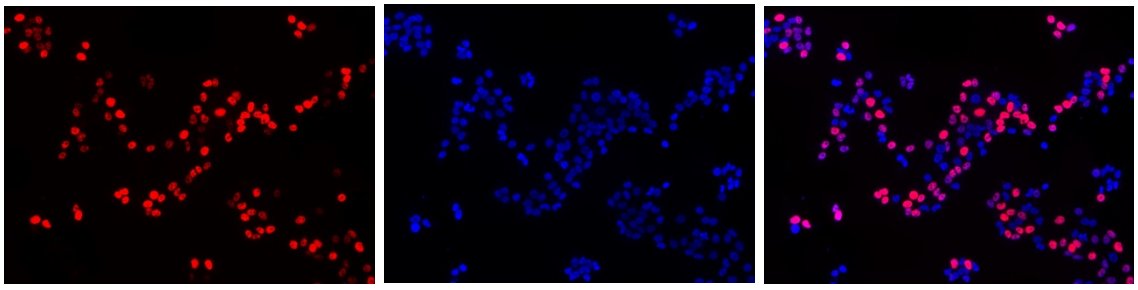

C

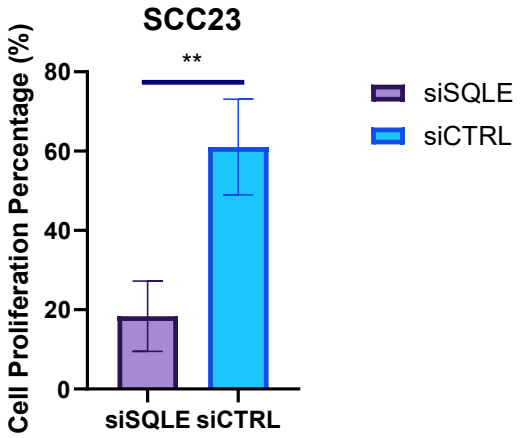

Figure 11. EdU cell proliferation assay. UMSCC23 cells were treated with SQLE siRNA **(A)** or control siRNA **(B)**. The left image shows proliferating cells labeled with EdU. The middle one shows a total population of cells, in which nucleic acid were stained with Hoechst 33342. The right one represents the overlapping images showing the the proliferating cells. **C** presents the percentage of proliferating cells out of total cell population. The figures show significantly reduction in the proliferation rate in UMSCC23 cells treated with SQLE siRNA (**, $P < 0.01$). Each experiment was repeated in triplicate. All values are expressed as the mean ± standard deviation.

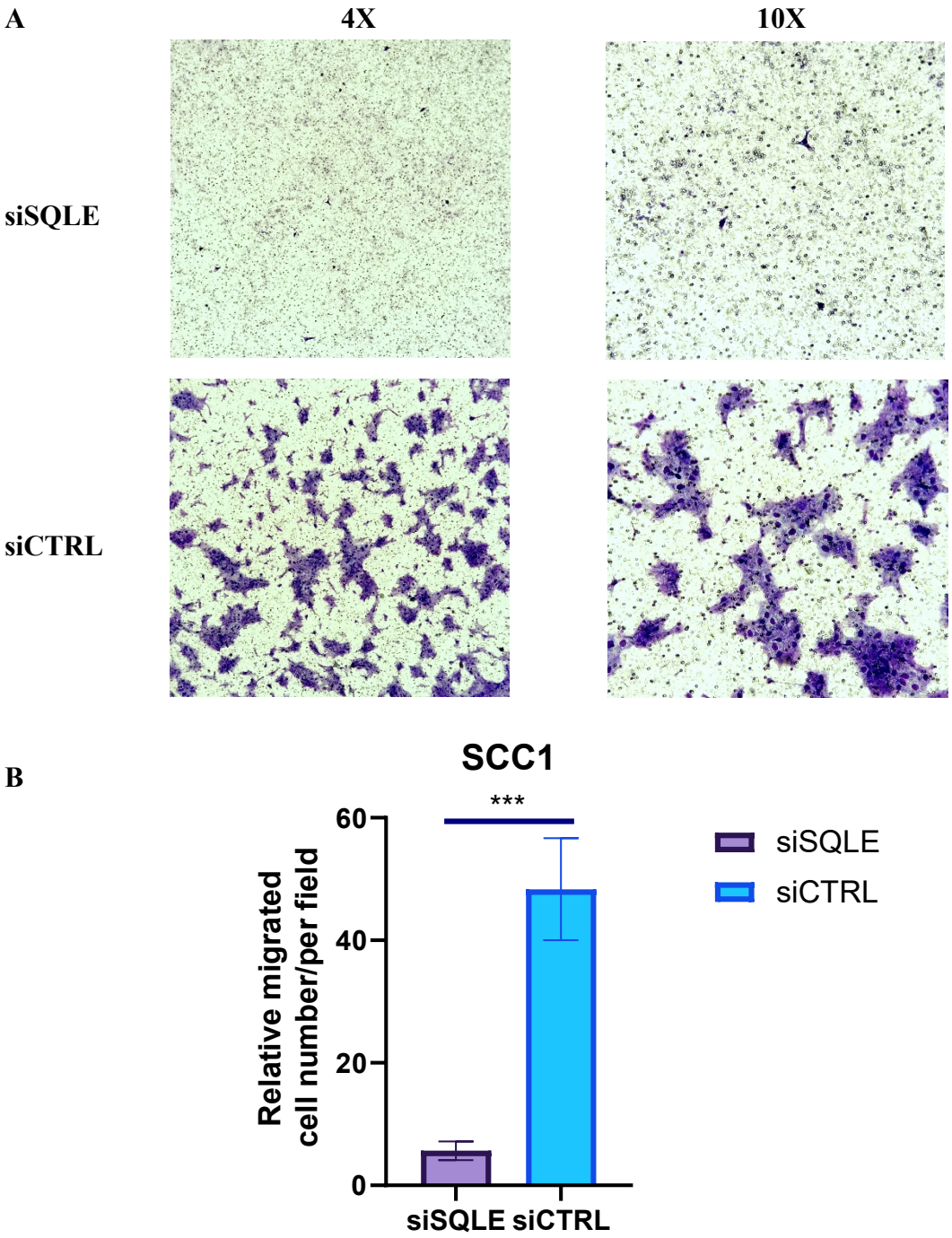

Figure 12. Migration Assay for UMSCC1 cells. **(A)** Visualization of migration of UMSCC1 cells through Transwells (4x and 10x). **(B)** Quantification of the relative migrated cell number per field, showing a significant reduction of migration in the cells with SQLE knockdown (***, $P < 0.001$). Each experiment was repeated in triplicate. All values are expressed as the mean ± standard deviation.

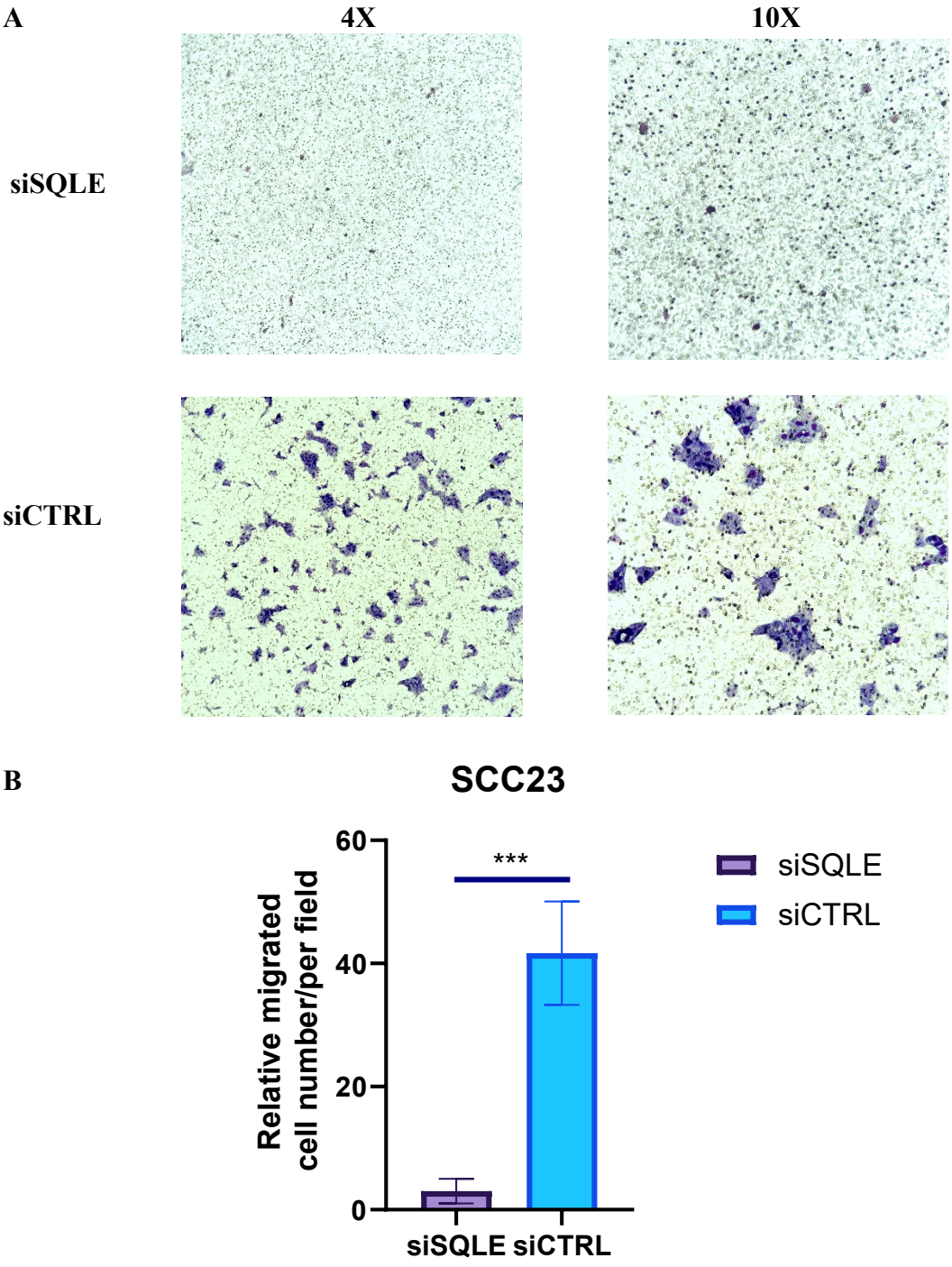

Figure 13. Migration Assay for UMSCC23 cells. **(A)** Visualization of migration of UMSCC23 cells through Transwells (4x and 10x). **(B)** Quantification of the relative migrated cell number per field, showing a significant reduction of migration in the cells with SQLE knockdown (***, $P < 0.001$). Each experiment was repeated in triplicate. All values are expressed as the mean ± standard deviation.

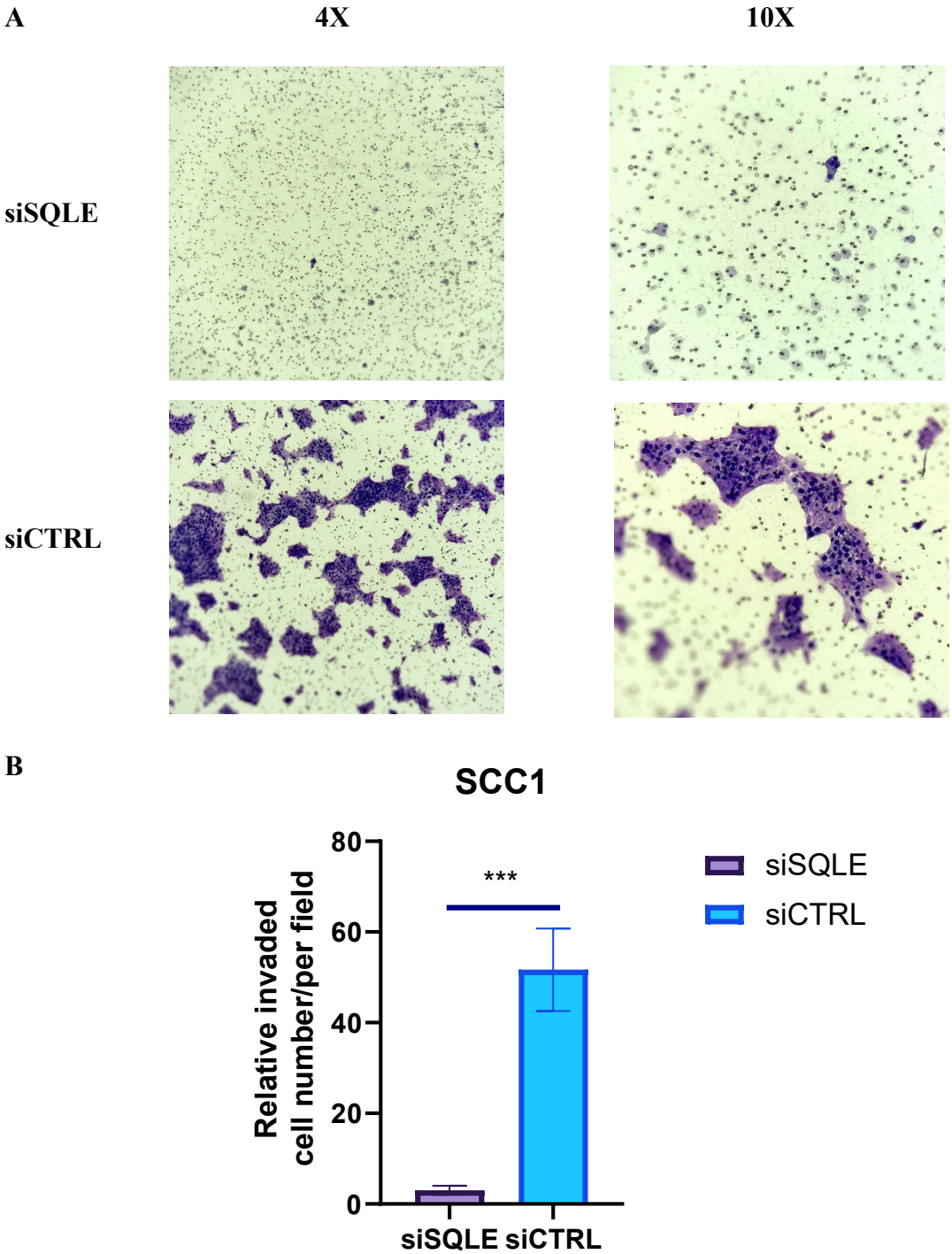

Figure 14. Invasion Assay for UMSCC1 cells. **(A)** Visualization of invasion of UMSCC1 cells through Matrigel chambers (4x and 10x). **(B)** Quantification of the relative invaded cell number per field, showing a significant reduction of invasion in the cells with SQLE knockdown (***, $P < 0.001$). Each experiment was repeated in triplicate. All values are expressed as the mean ± standard deviation.

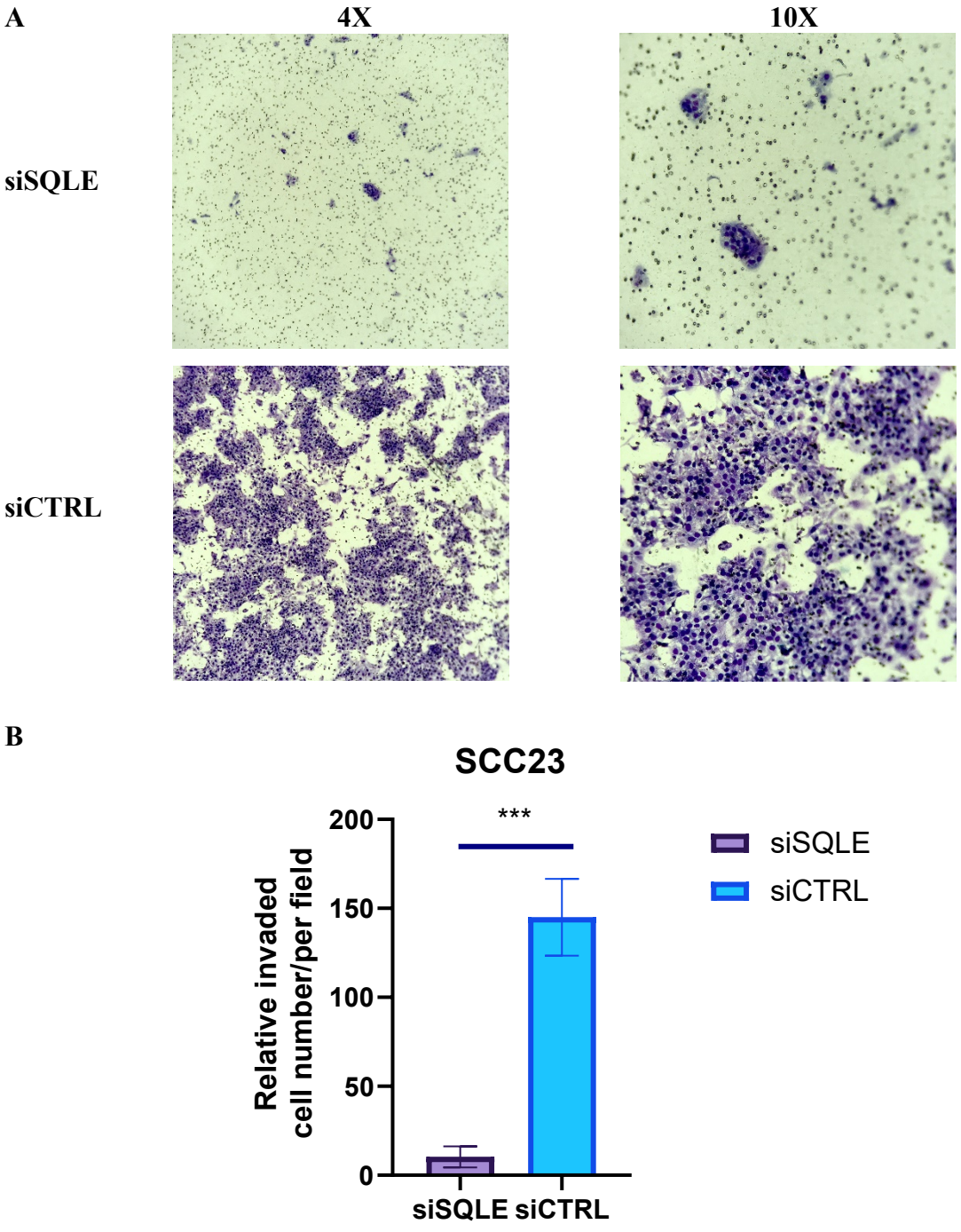

Figure 15. Invasion Assay for UMSCC23 cells. **(A)** Visualization of invasion of UMSCC23 cells through Matrigel chambers (4x and 10x). **(B)** Quantification of the relative invaded cell number per field, showing a significant reduction of invasion in the cells with SQLE knockdown (***, $P < 0.001$). Each experiment was repeated in triplicate. All values are expressed as the mean ± standard deviation.

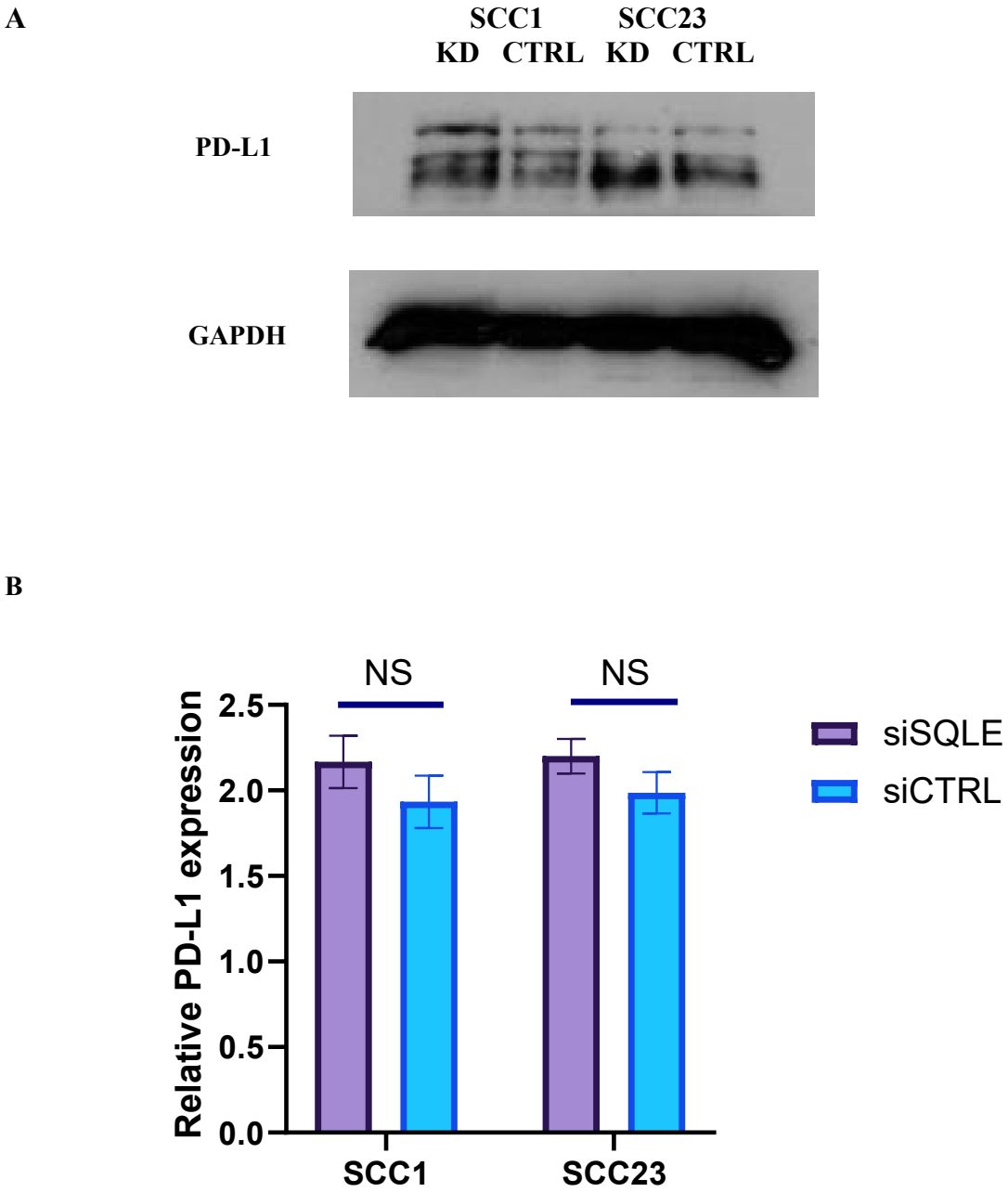

Figure 16. The expression level of PD-L1 after siRNA knockdown of SQLE in UMSCC1 and UMSCC23 cells. **(A)** Western blot analysis showing PD-L1 expression level with siSQLE vs siControl. **(B)** Quantification of Western blot results showing no significantly alteration of PD-L1 expression in both cell lines after siSQLE. Each experiment was repeated in triplicate. All values are expressed as the mean ± standard deviation.

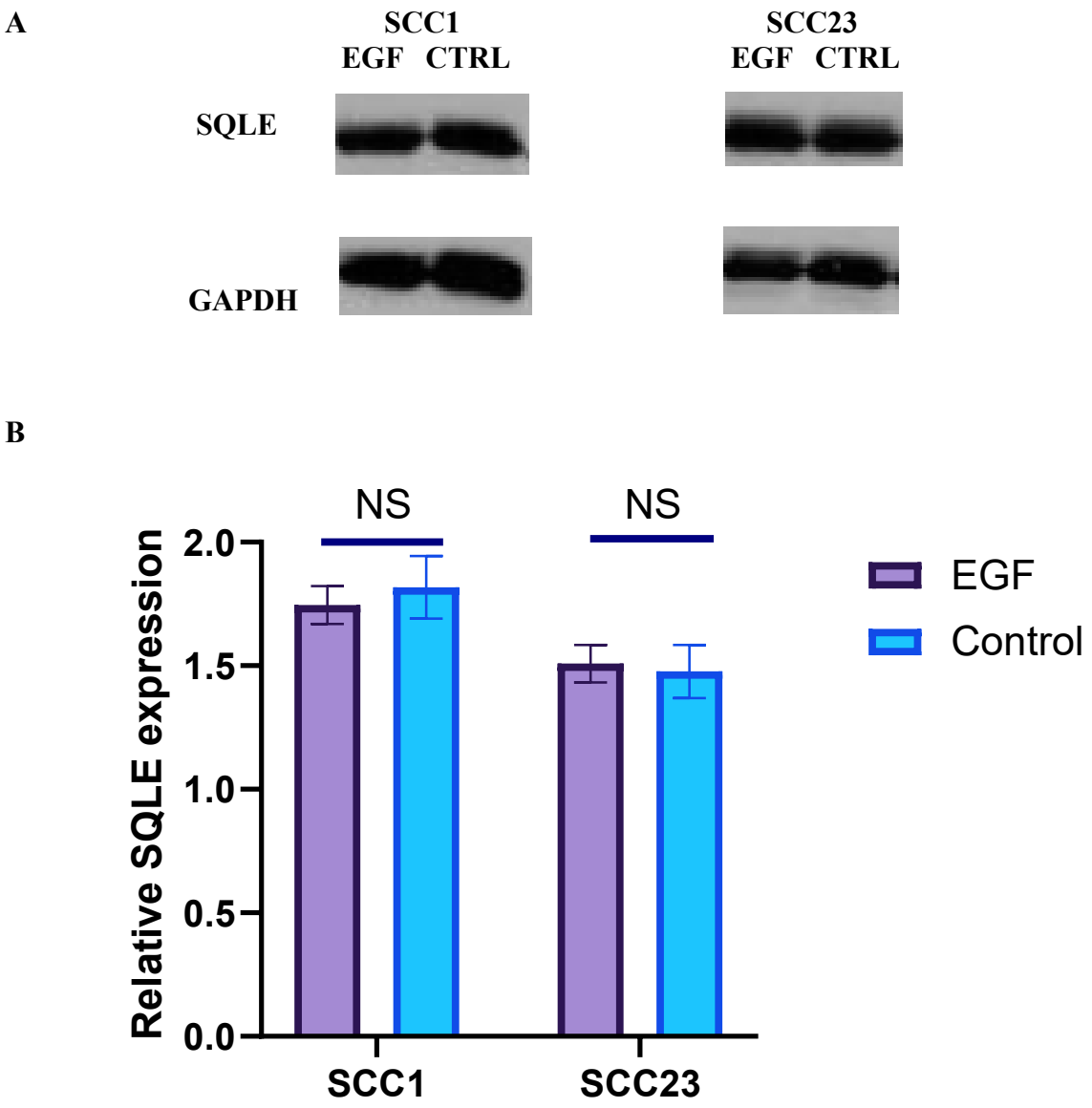

Figure 17. Western blot analysis of SQLE in UMSCC1 and UMSCC23 cells after treated with EGF. **(A)** Protein expression levels of SQLE when treated with EGF. **(B)** Quantification of protein expression showing no significant alteration in the expression level of SQLE in EGF-treated UMSCC1 and UMSCC23 cells compared to the corresponding control cells. Each experiment was repeated in triplicate. All values are expressed as the mean ± standard deviation.

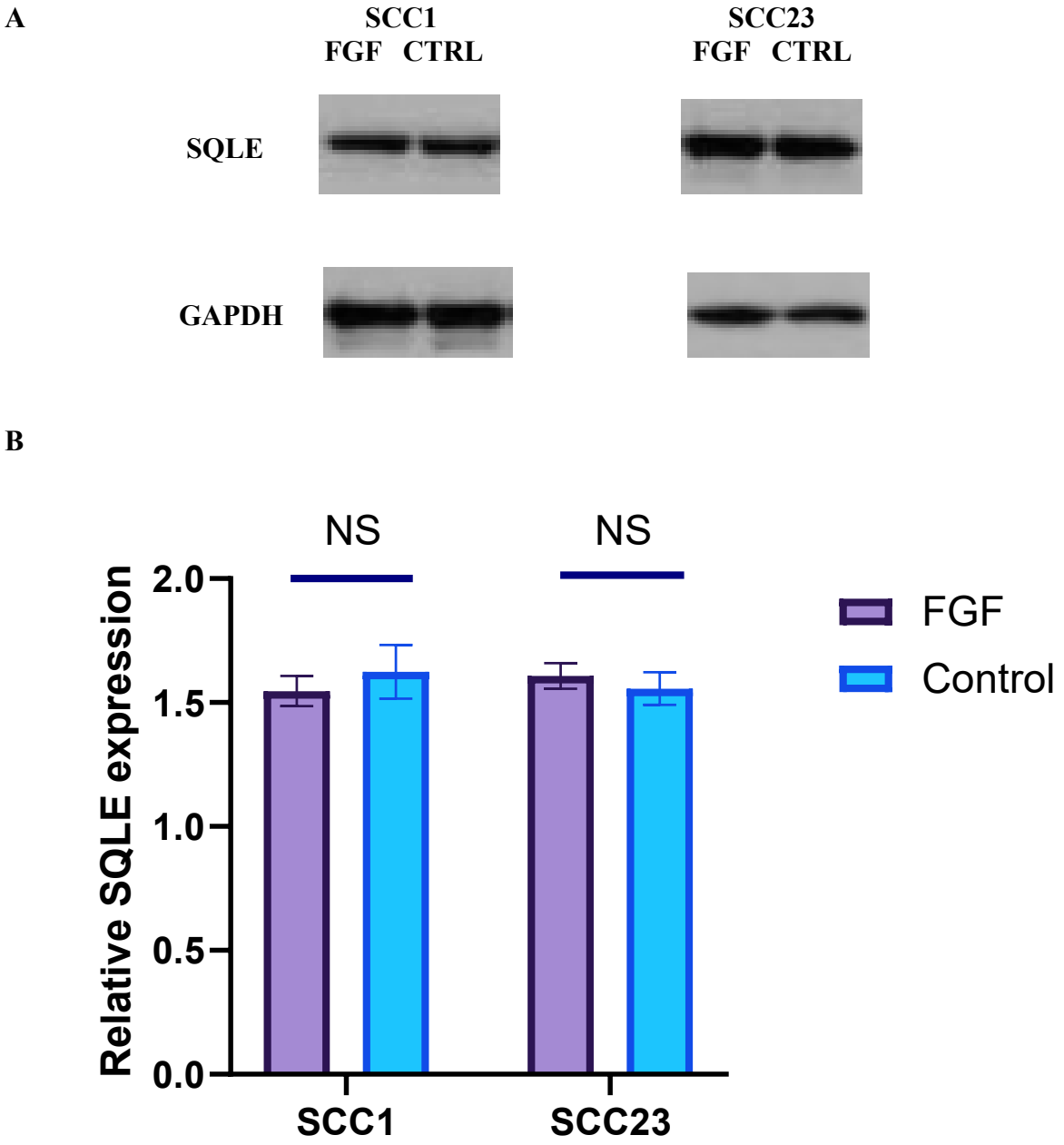

Figure 18. Western blot analysis of SQLE in UMSCC1 and UMSCC23 cells after treated with FGF. **(A)** Protein expression level of SQLE when treated with FGF. **(B)** Quantification of protein expression showing no significant alteration in the expression level of SQLE in FGF-treated UMSCC1 and UMSCC23 cells compared to the corresponding control cells. Each experiment was repeated in triplicate. All values are expressed as the mean ± standard deviation.

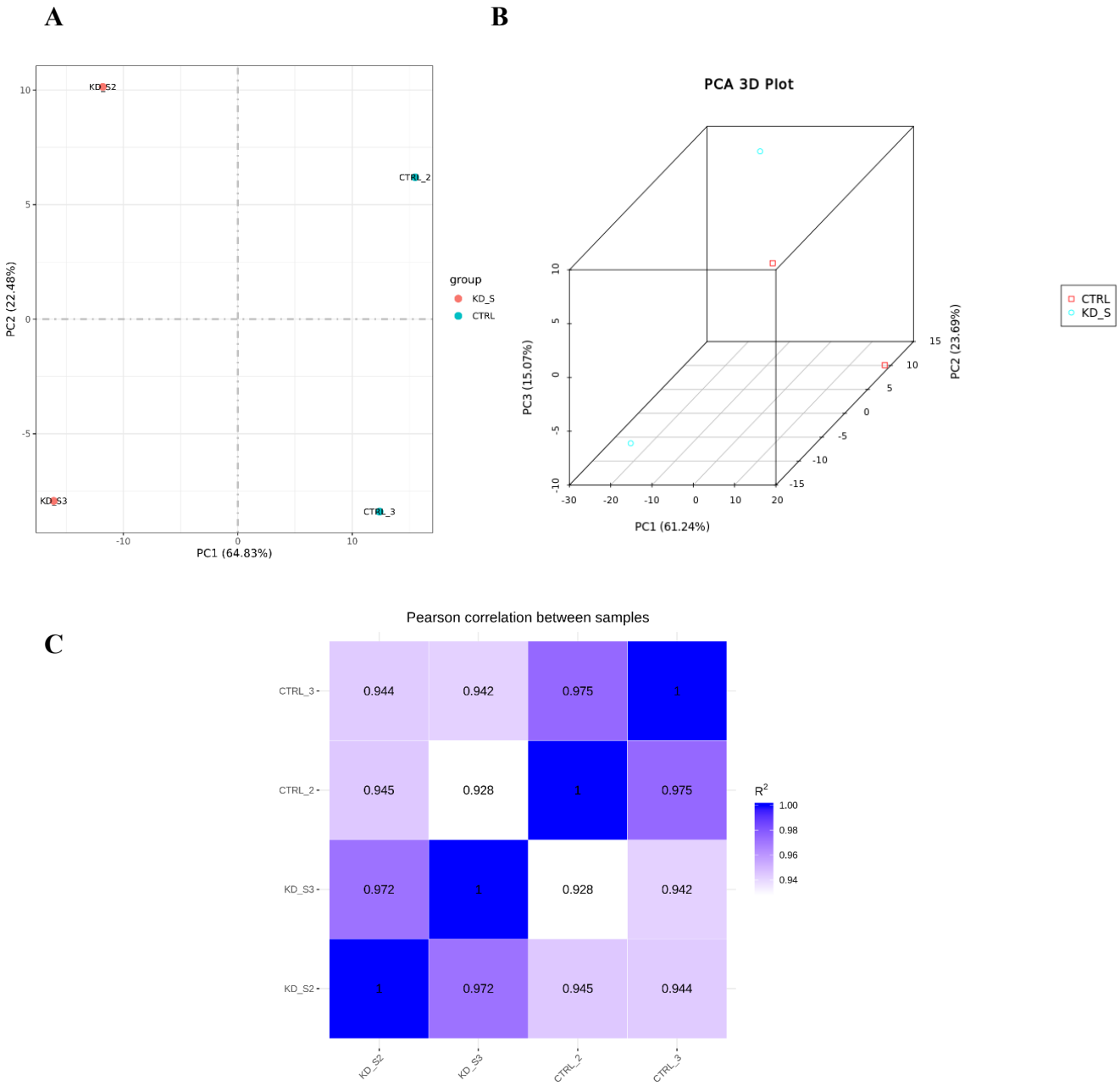

Figure 19. Assessing intra- and intergroup variability. Principal component (PC) analysis plot displaying all 4 samples along PC1 and PC2 (**A**), or PC1, PC2 and PC3 (**B**). PC analysis was applied to normalized (reads per kilobases of transcript per 1 million mapped reads) and log-transformed count data. (**C**) Pearson's correlation plot visualizing the correlation (r) values between samples. According to all gene expression level (RPKM or FPKM) of each sample, correlation coefficient of sample between groups is calculated and drawn as heat maps. Scale bar represents the range of the correlation coefficients (r) displayed. The closer correlation coefficient is to 1, the higher similarity the samples have.

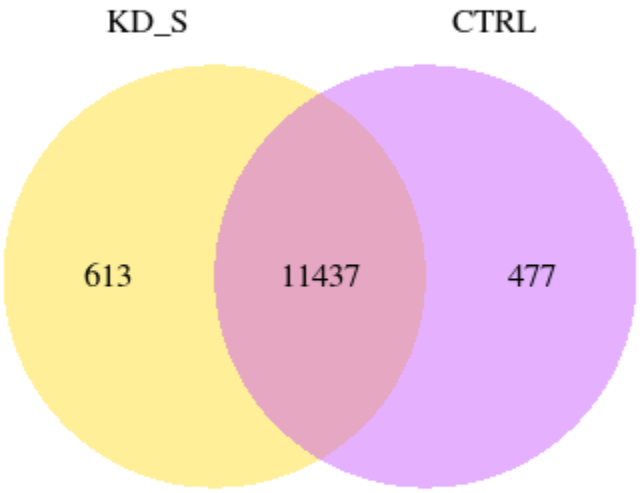

Figure 20. A Venn diagram was generated from the number of genes that were uniquely expressed in SQLE knockdown group (yellow circle) and control group (purple circle), with 11437 overlapped genes.

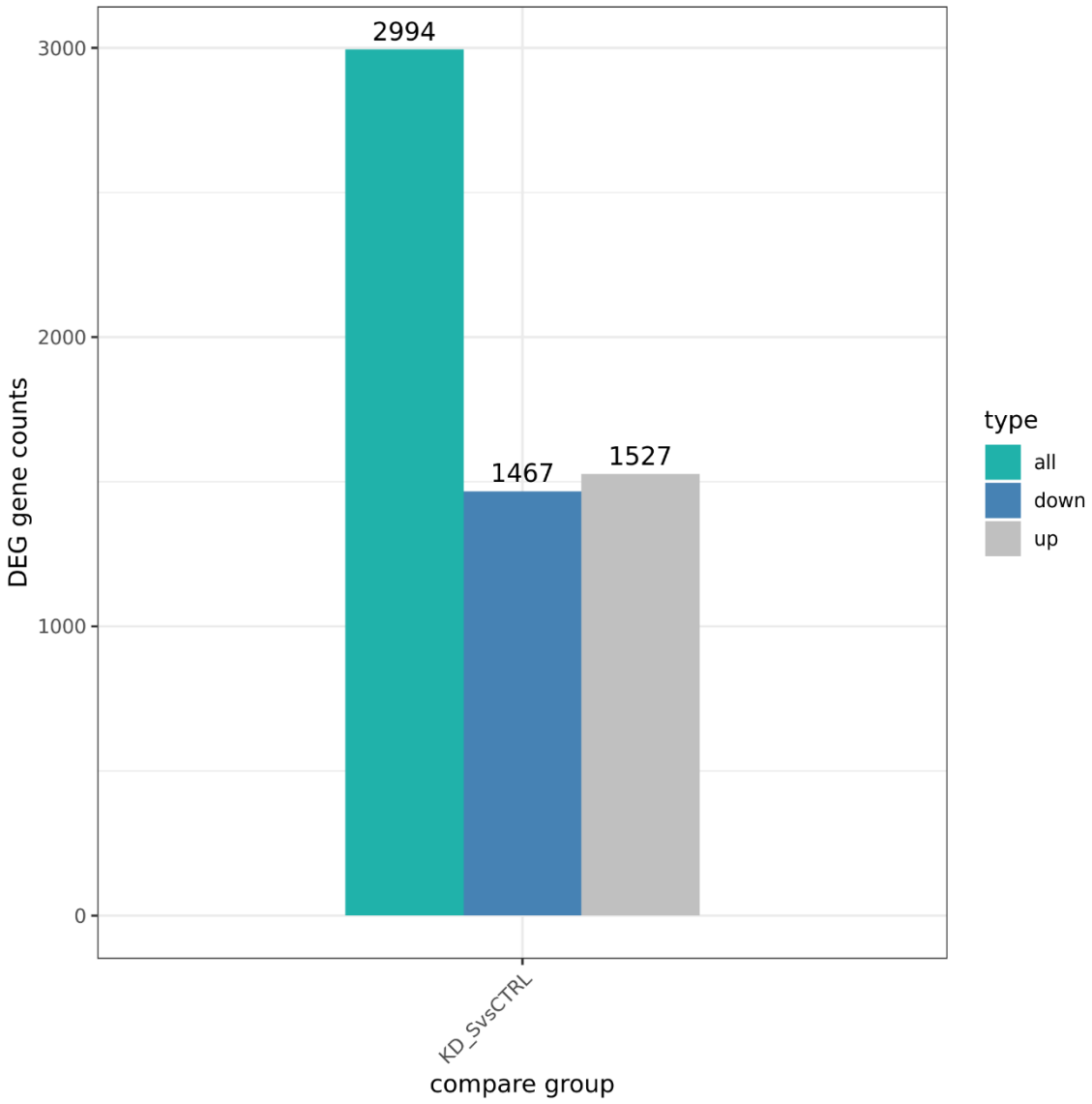

Figure 21. Differentially expressed genes (DEGs) counts. In a total number of 2994 DEGs, 1467 genes are downregulated and 1527 genes are upregulated.

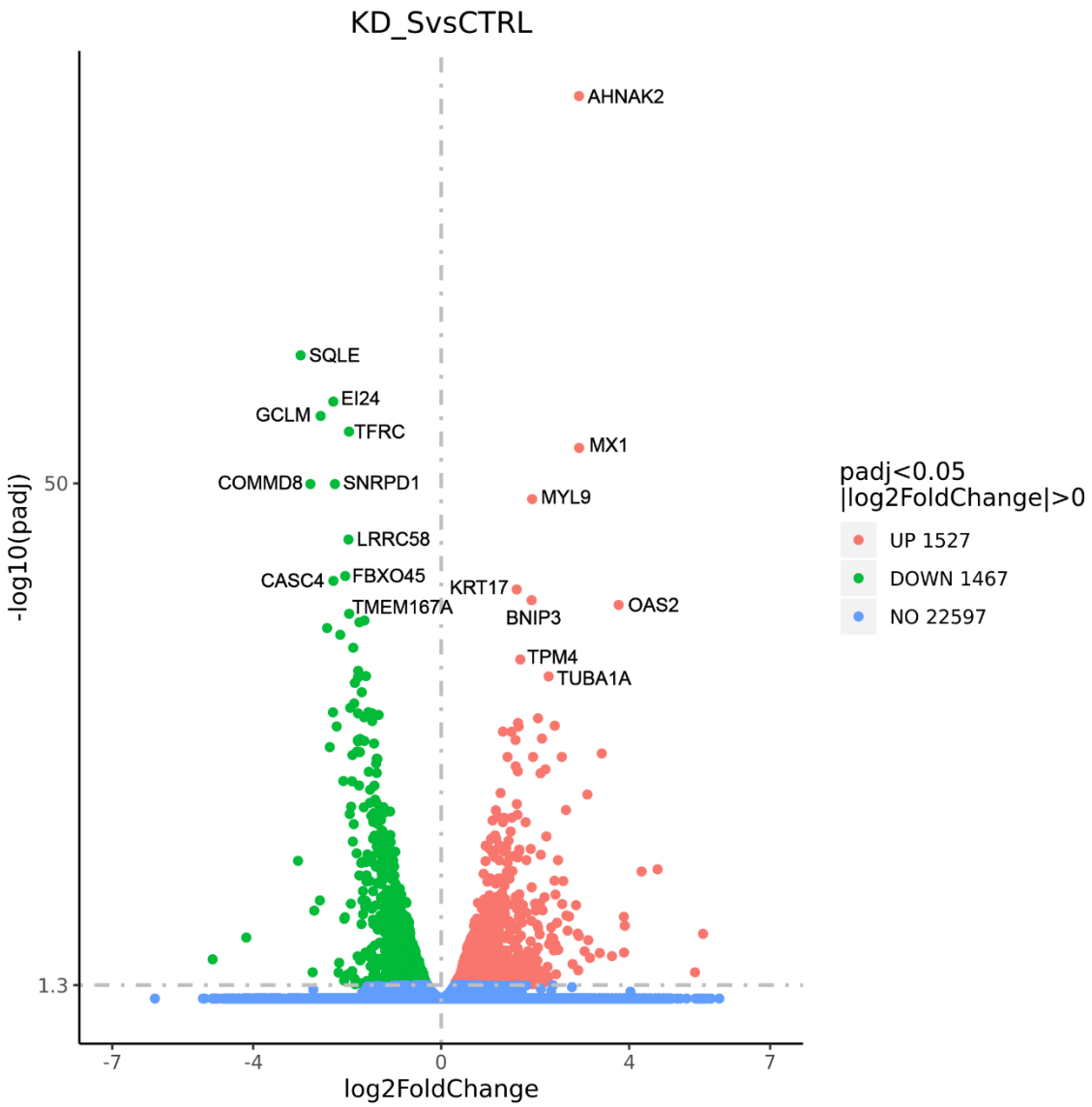

Figure 22. Volcano plot highlights significant genes, labeled with top significant genes. Horizontal axis represents the fold change of genes. Vertical axis represents statistically significant degree of changes in gene expression levels, the smaller the corrected pvalue, the bigger -log10(corrected pvalue), the more significant the difference. The points represent genes, blue dots indicate no significant difference in genes, red dots indicate upregulated differential expression genes, green dots indicate downregulated differential expression genes. Corrected pvalue<0.05, |log2Fold Change|>0.

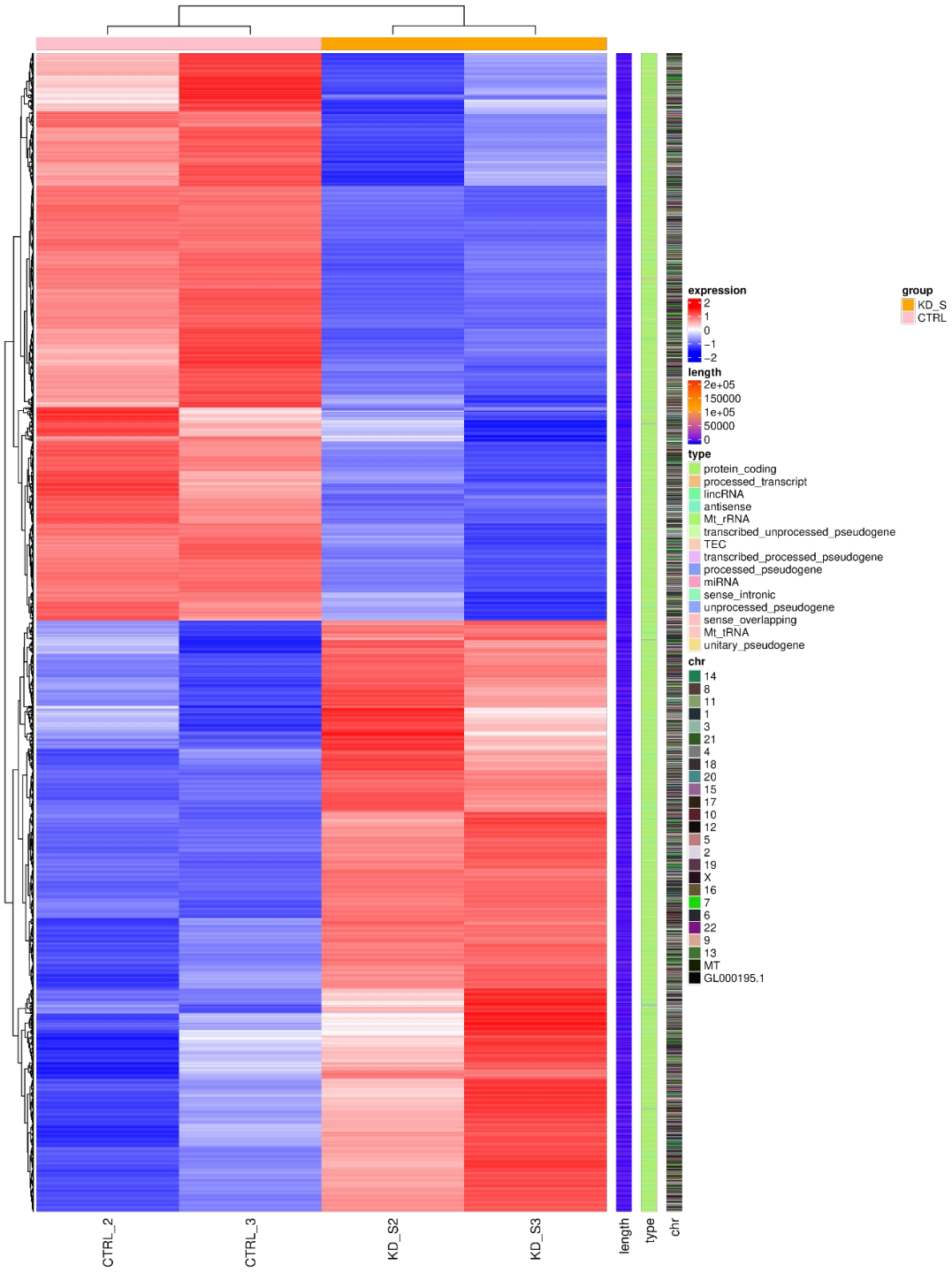

Figure 23. Hierarchical clustering heatmap. The overall results of FPKM cluster analysis, clustered using the log2(FPKM+1) value. Red color indicates genes with high expression levels, and blue color indicates genes with low expression levels. The color ranging from red to blue indicates that log2(FPKM+1) values where from large to small.

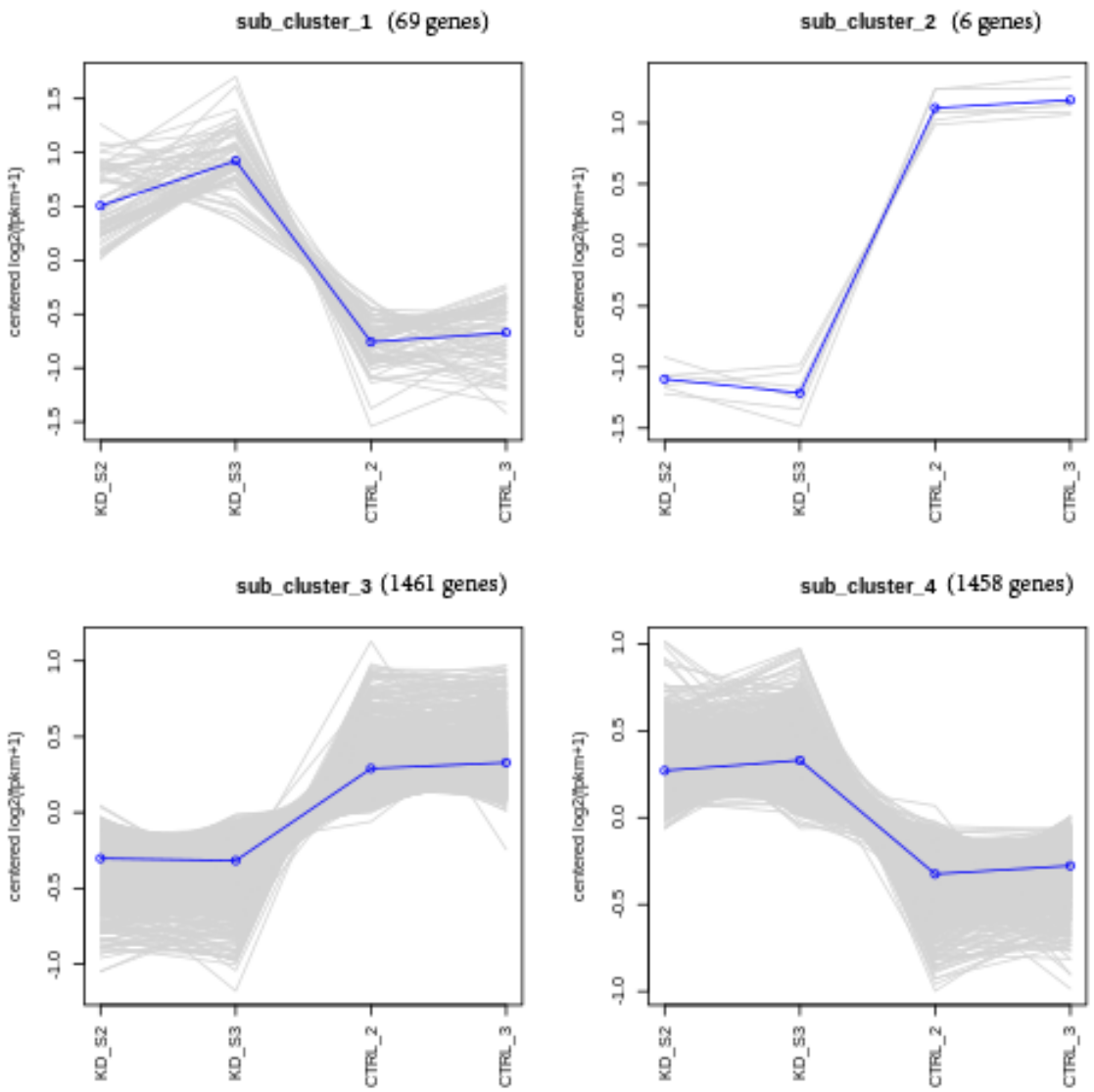

Figure 24. Genes grouped into four clusters (I, II, III, and IV) on the basis of the similarity of expression. The number of the expressed genes in each cluster are indicated. The blue line on each plot represents the mean expression profile for the cluster.

A

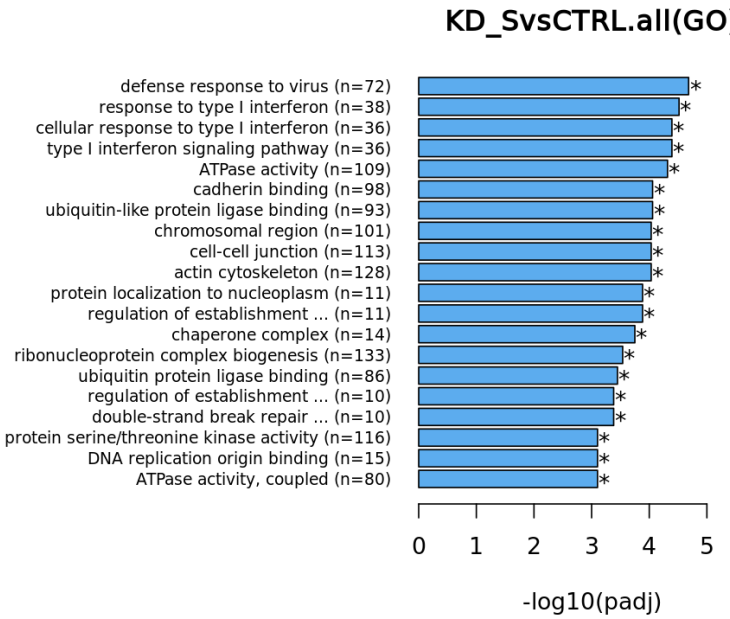

B

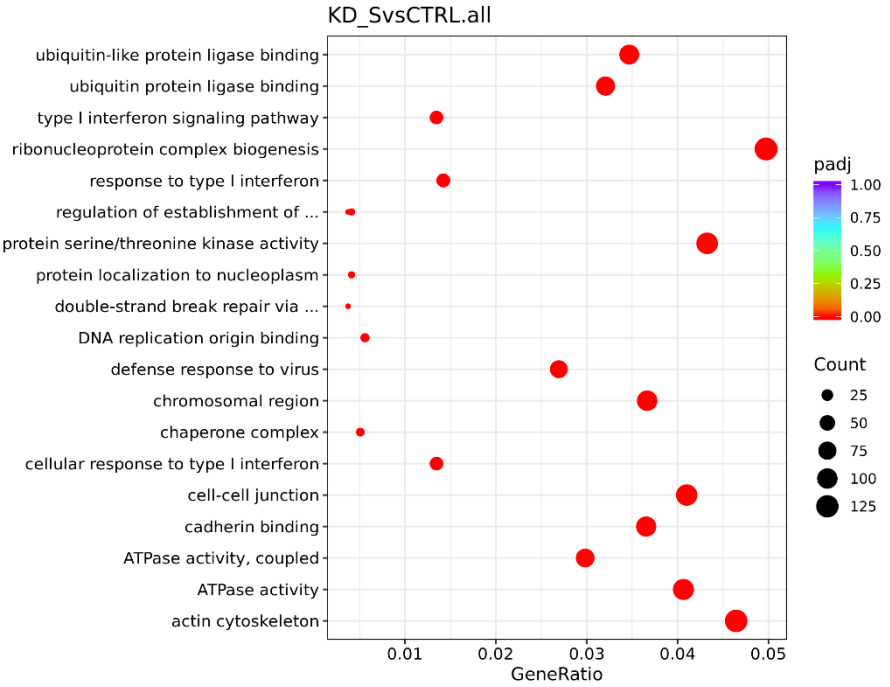

Figure 25. GO (Gene Ontology) enrichment analysis for all DEGs. (**A**) Histogram: the horizontal axis is customized as -log10 (padj) of significantly enriched term and the vertical axis is customized as the number of significantly enriched term. Top 20 significantly enriched terms in the GO enrichment analysis are displayed. (**B**) Scatter plot: the horizontal axis is customized as GeneRatio and the vertical axis is customized as the term's description. The size of every spot represents the number of the differential expression genes and the color of every spot represents the range of padj.

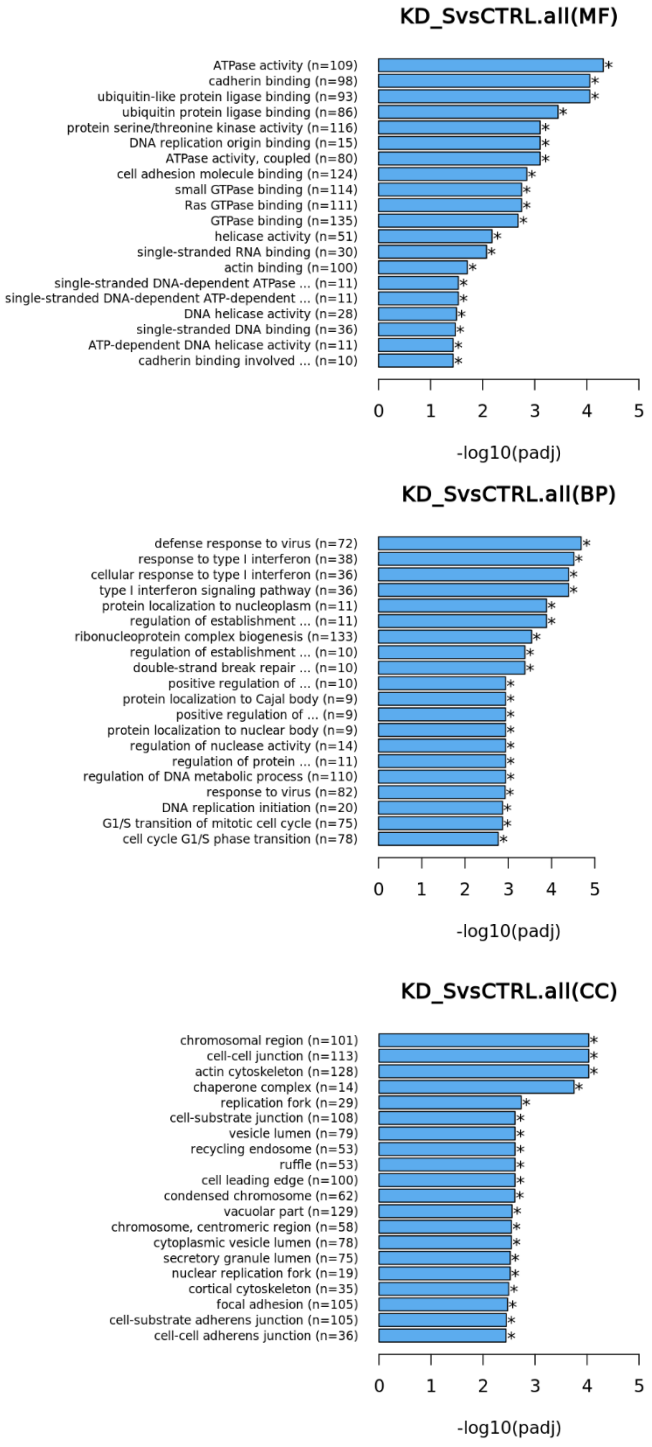

Figure 26. GO classifcation of all assembled unigenes. 2,994 unigenes in total were divided into three main categories: molecular function, biological process, and cellular component.

A

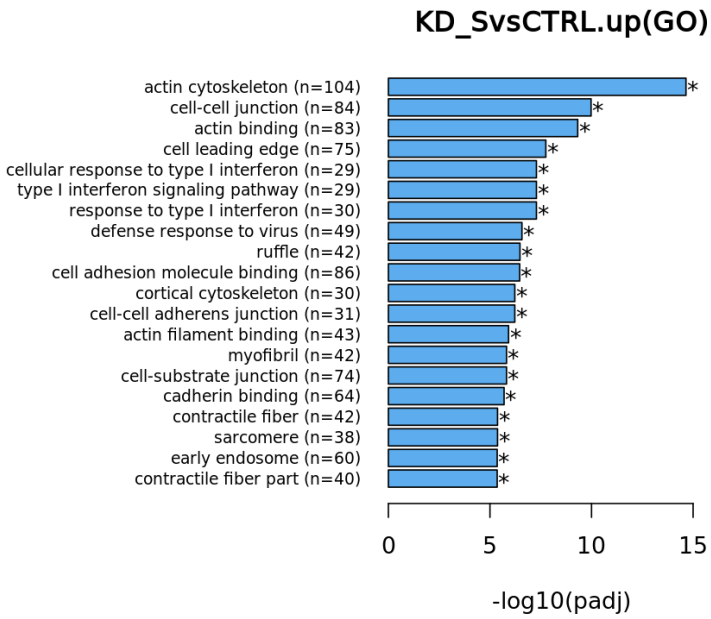

B

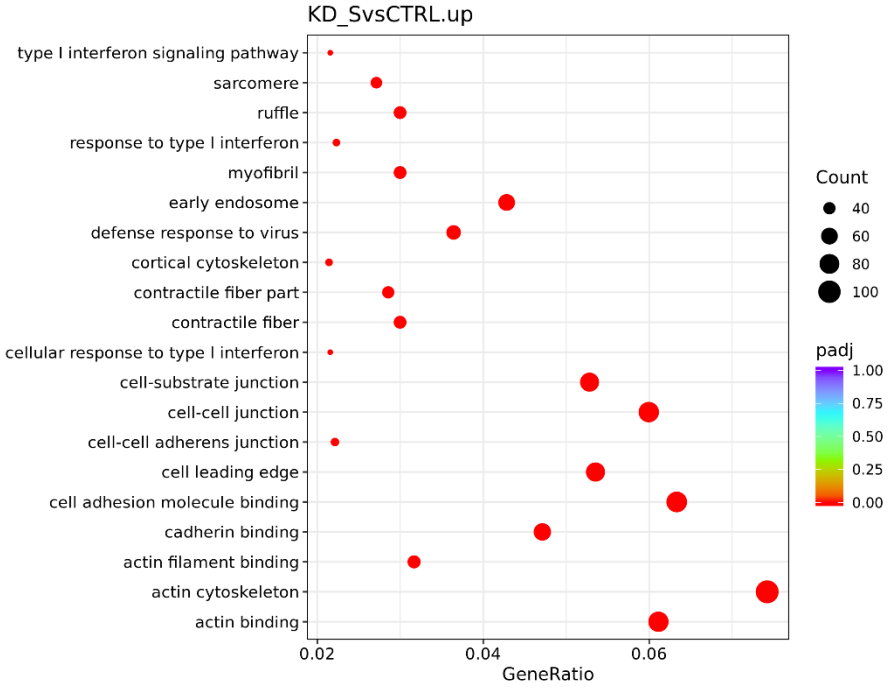

Figure 27. GO enrichment analysis for upregulated DEGs. (**A**) Histogram: the horizontal axis is customized as -log10 (padj) of significantly enriched term and the vertical axis is customized as the number of significantly enriched term. Top 20 significantly enriched terms in the GO enrichment analysis are displayed. (**B**) Scatter plot: the horizontal axis is customized as GeneRatio and the vertical axis is customized as the term's description. The size of every spot represents the number of the differential expression genes and the color of every spot represents the range of padj.

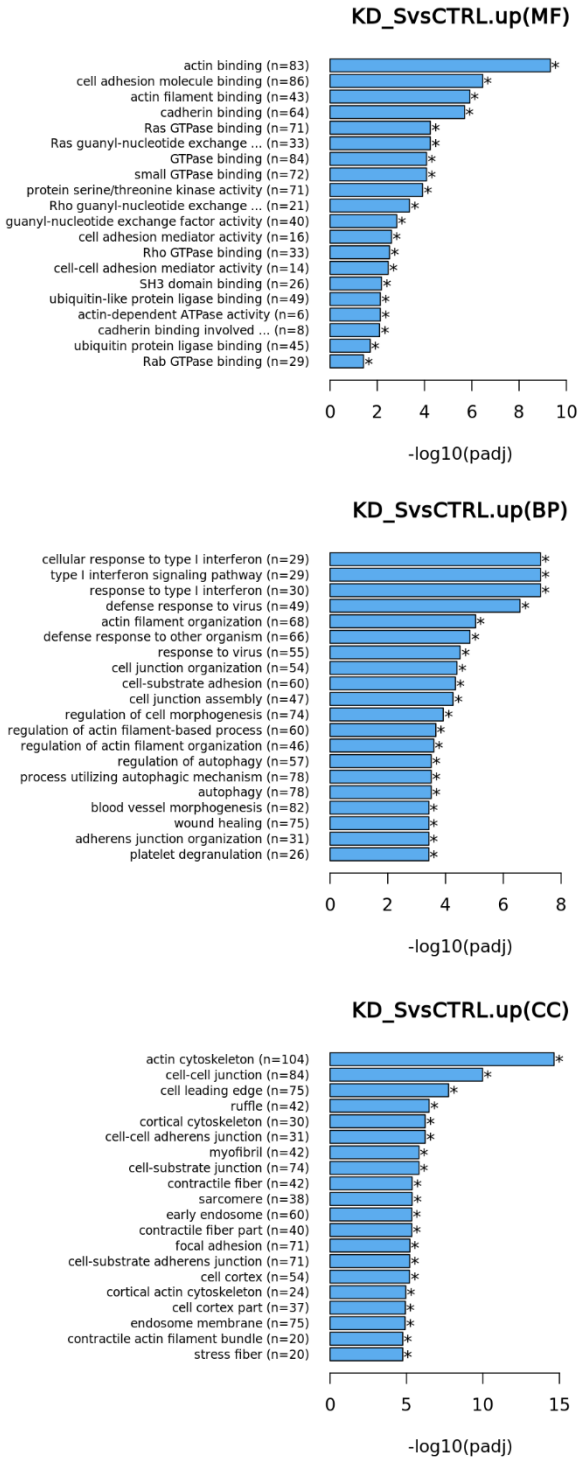

Figure 28. GO classifcation of upregulated unigenes. 1,527 unigenes in total were divided into three main categories: molecular function, biological process, and cellular component.

A

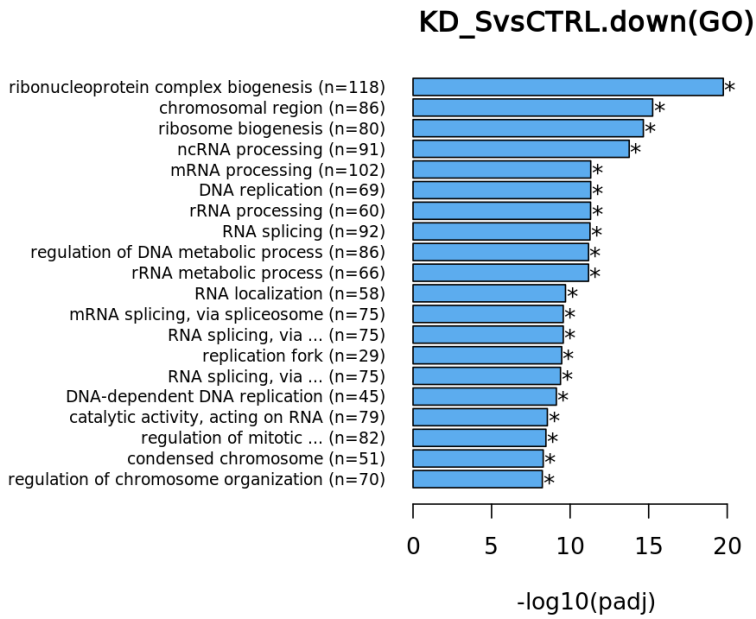

B

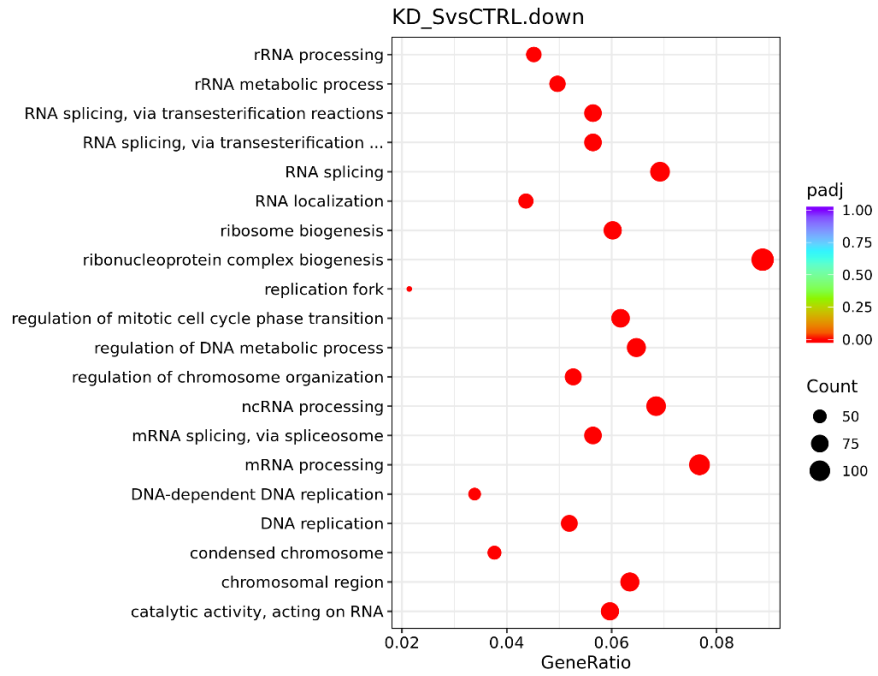

Figure 29. GO enrichment analysis for downregulated DEGs. (**A**) Histogram: the horizontal axis is customized as -log10 (padj) of significantly enriched term and the vertical axis is customized as the number of significantly enriched term. Top 20 significantly enriched terms in the GO enrichment analysis are displayed. (**B**) Scatter plot: the horizontal axis is customized as GeneRatio and the vertical axis is customized as the term's description. The size of every spot represents the number of the differential expression genes and the color of every spot represents the range of padj.

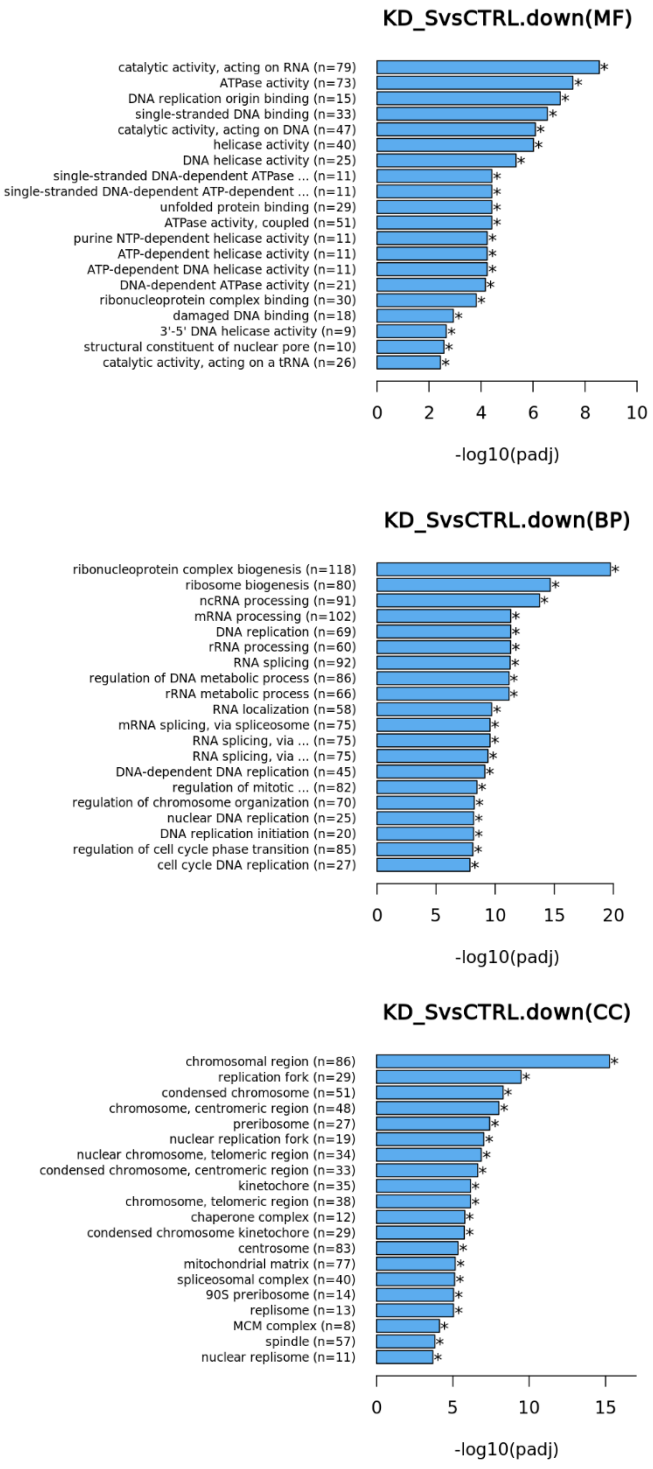

Figure 30. GO classifcation of downregulated unigenes. 1,467 unigenes in total were divided into three main categories: molecular function, biological process, and cellular component.

A

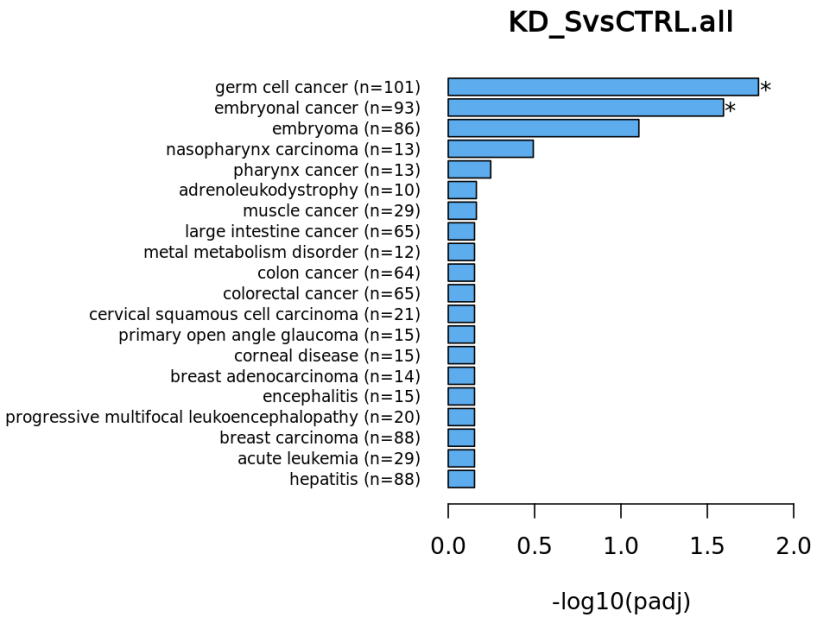

B

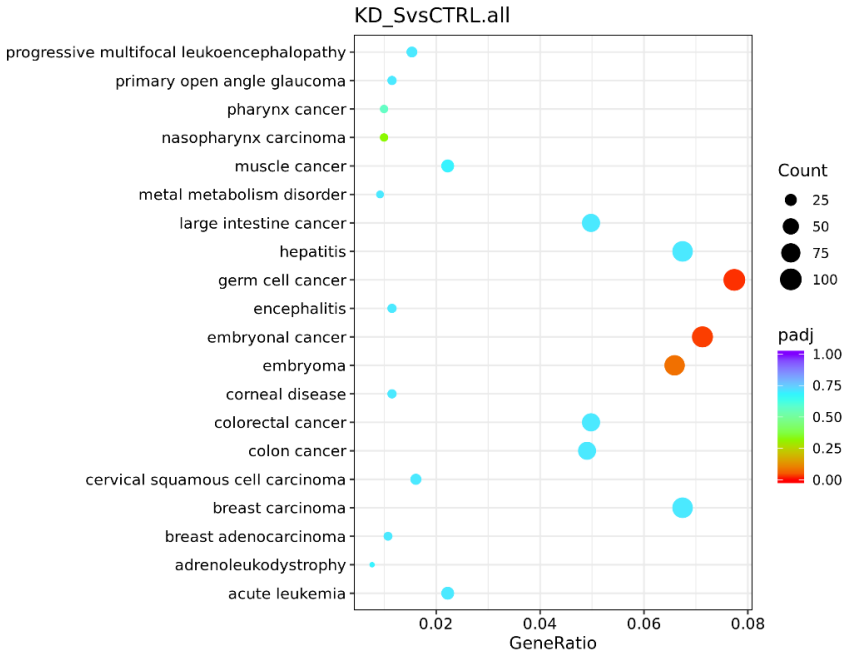

Figure 31. DO (Disease Ontology) enrichment analysis for all DEGs. (**A**) Histogram: the horizontal axis is customized as -log10 (padj) of significantly enriched term and the vertical axis is customized as the number of significantly enriched term. Top 20 significantly enriched terms in the DO enrichment analysis are displayed. (**B**) Scatter plot: the horizontal axis is customized as GeneRatio and the vertical axis is customized as the term's description. The size of every spot represents the number of the differential expression genes and the color of every spot represents the range of padj.

A

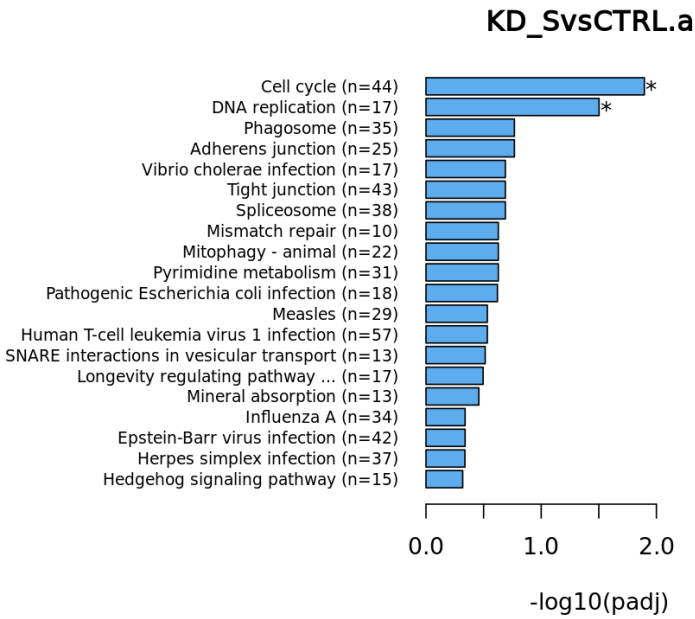

B

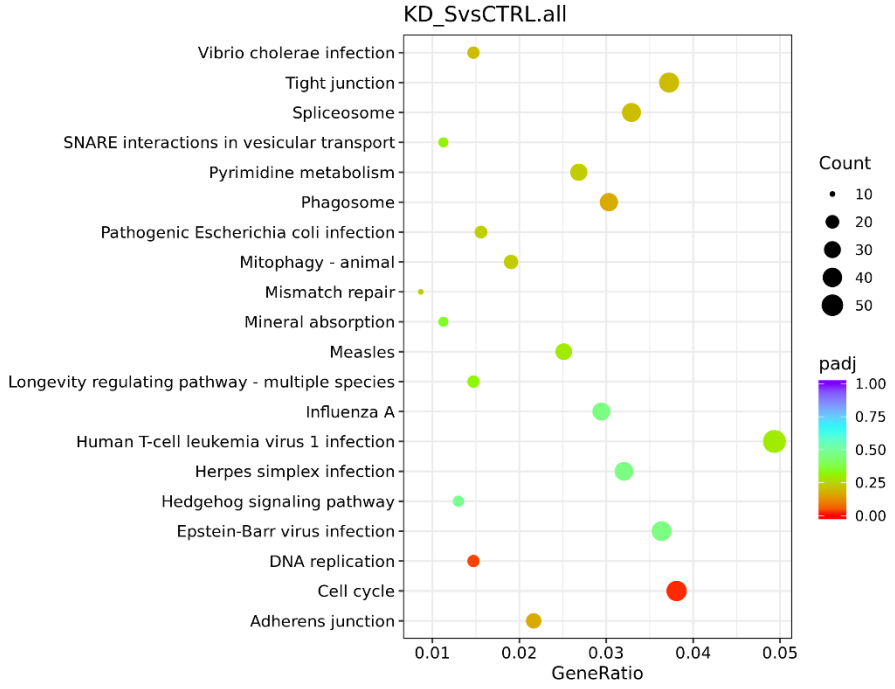

Figure 32. KEGG (Kyoto Encyclopedia of Genes and Genomes) enrichment analysis for all DEGs. (**A**) Histogram: the horizontal axis is customized as -log10 (padj) of significantly enriched term and the vertical axis is customized as the number of significantly enriched term. Top 20 significantly enriched terms in the KEGG enrichment analysis are displayed. (**B**) Scatter plot: the horizontal axis is customized as GeneRatio and the vertical axis is customized as the term's description. The size of every spot represents the number of the differential expression genes and the color of every spot represents the range of padj.

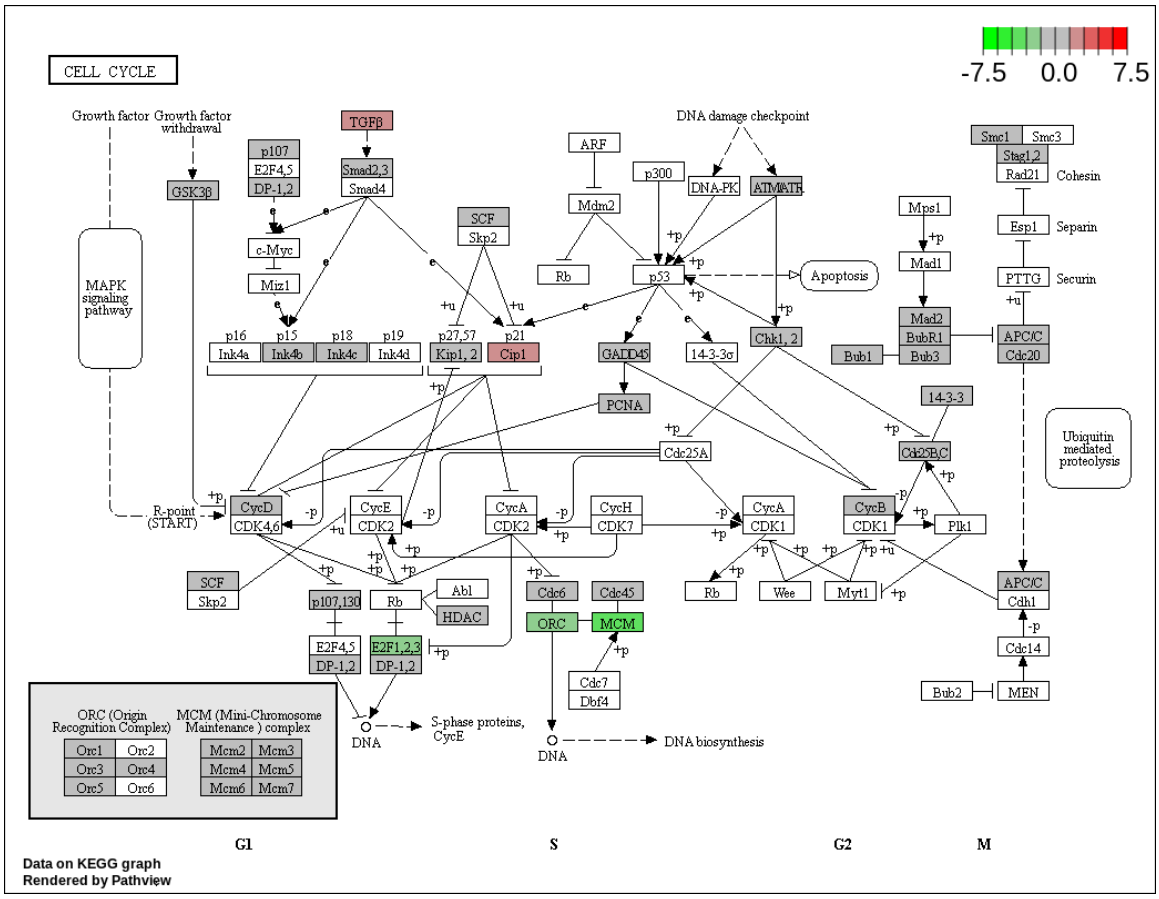

Figure 33. Cell cycle KEGG pathway.

A

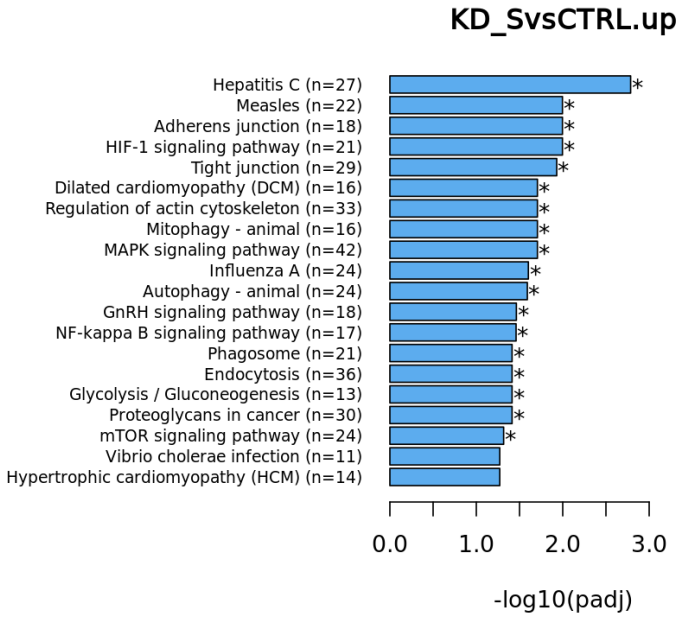

B

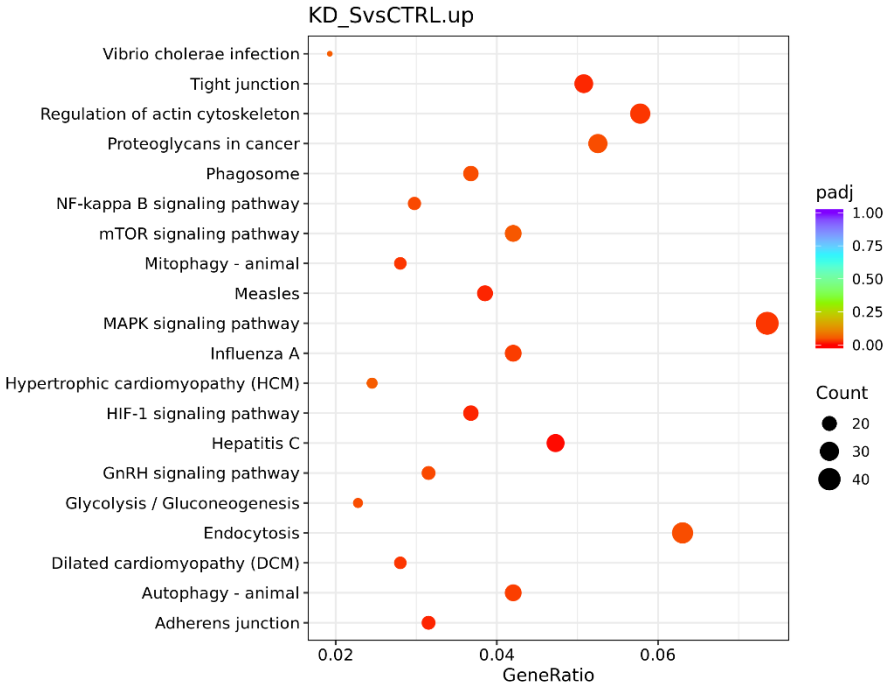

Figure 34. KEGG enrichment analysis for upregulated DEGs. (**A**) Histogram: the horizontal axis is customized as -log10 (padj) of significantly enriched term and the Vertical axis is customized as the number of significantly enriched term. Top 20 significantly enriched terms in the KEGG enrichment analysis are displayed. (**B**) Scatter plot: the horizontal axis is customized as GeneRatio and the vertical axis is customized as the term's description. The size of every spot represents the number of the differential expression genes and the color of every spot represents the range of padj.

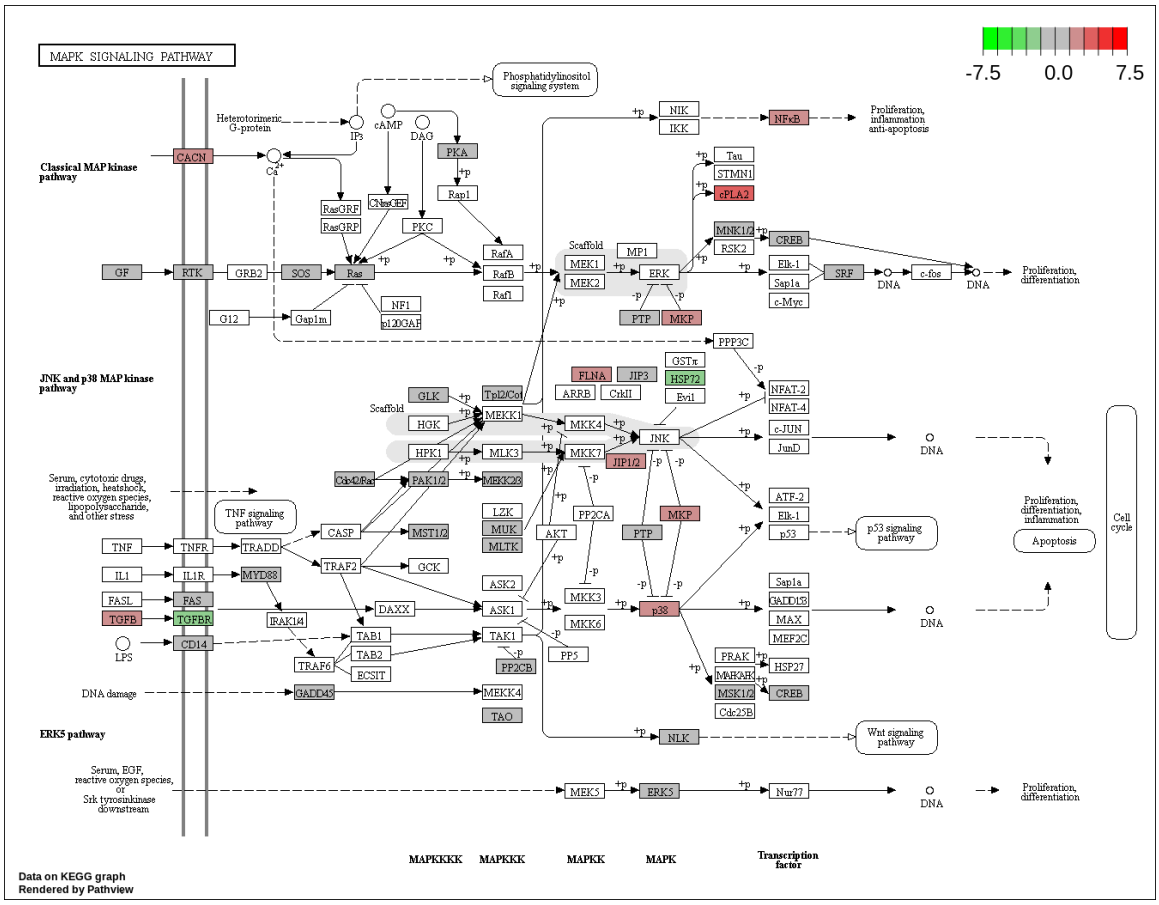

Figure 35. MAPK signaling pathway with upregulated genes.

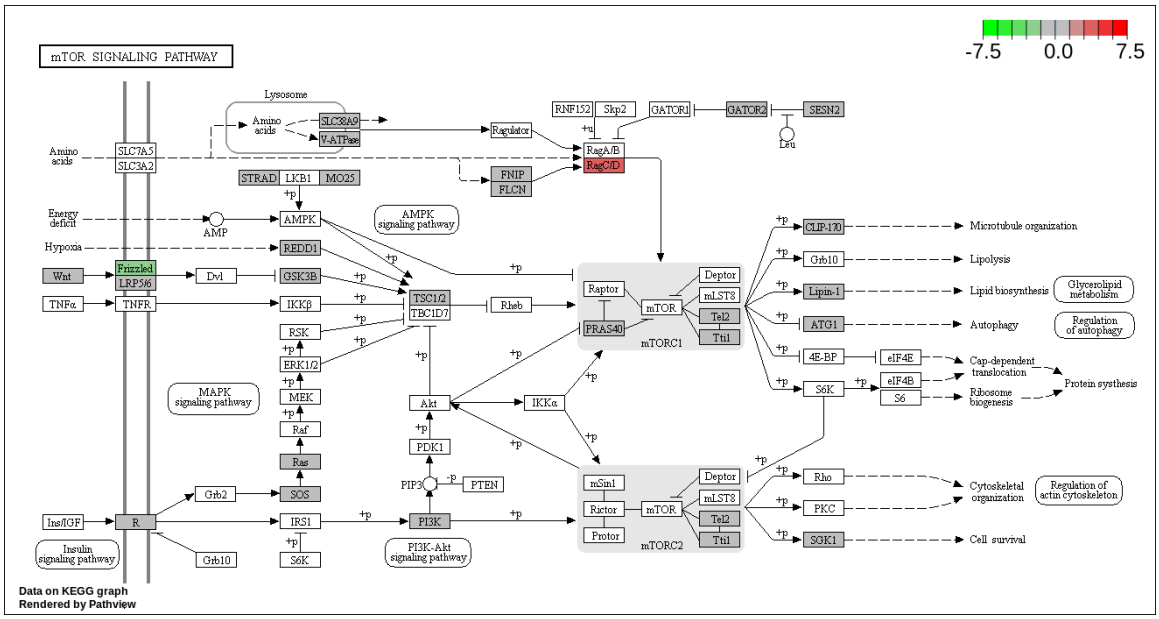

Figure 36. mTOR signaling pathway with upregulated genes.

A

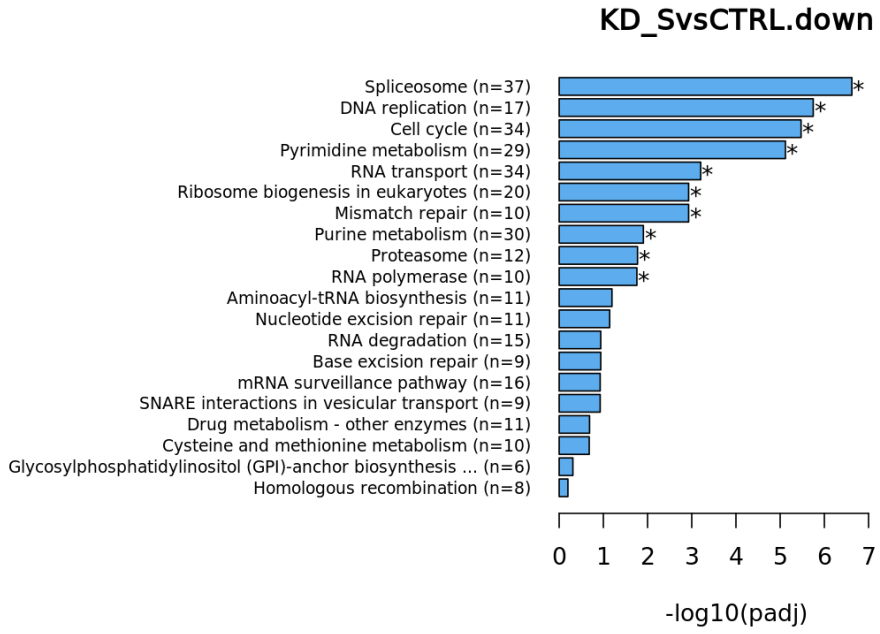

B

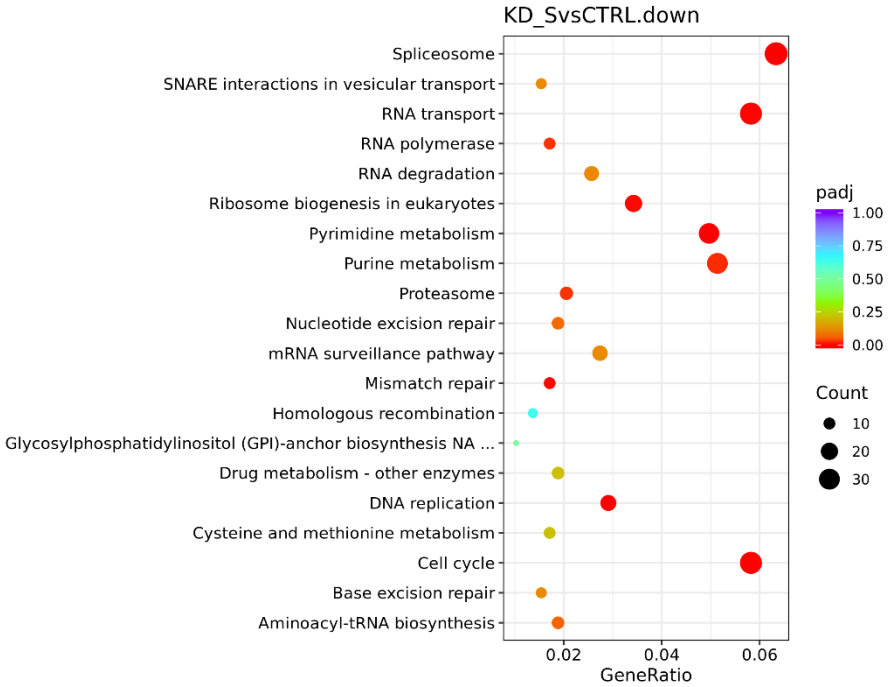

Figure 37. KEGG enrichment analysis for downregulated DEGs. (**A**) Histogram: the horizontal axis is customized as -log10 (padj) of significantly enriched term and the vertical axis is customized as the number of significantly enriched term. Top 20 significantly enriched terms in the KEGG enrichment analysis are displayed. (**B**) Scatter plot: the horizontal axis is customized as GeneRatio and the vertical axis is customized as the term's description. The size of every spot represents the number of the differential expression genes and the color of every spot represents the range of padj.

A

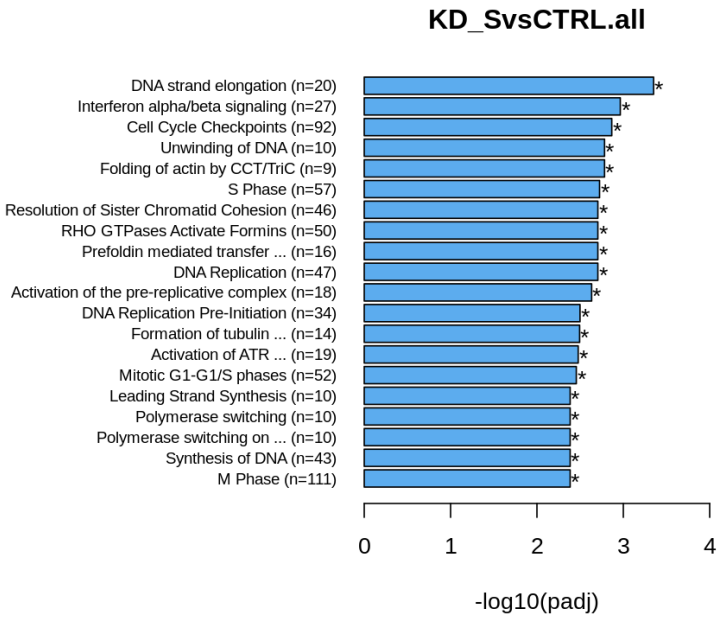

B

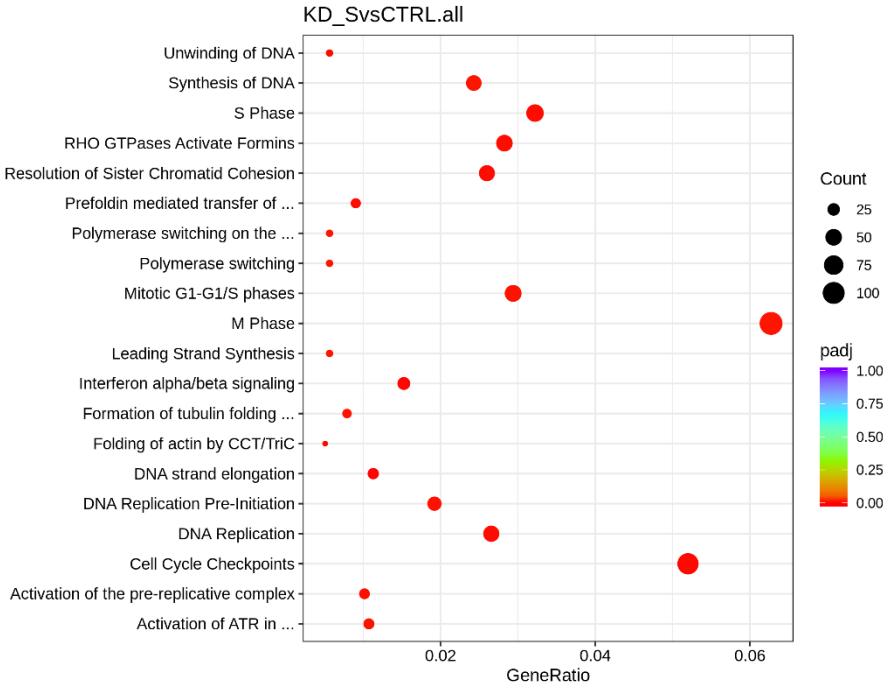

Figure 38. Reactome enrichment analysis for all DEGs. (**A**) Histogram: the horizontal axis is customized as -log10 (padj) of significantly enriched term and the vertical axis is customized as the number of significantly enriched term. Top 20 significantly enriched terms in the Reactome enrichment analysis are displayed. (**B**) Scatter plot: the horizontal axis is customized as GeneRatio and the vertical axis is customized as the term's description. The size of every spot represents the number of the differential expression genes and the color of every spot represents the range of padj.

A

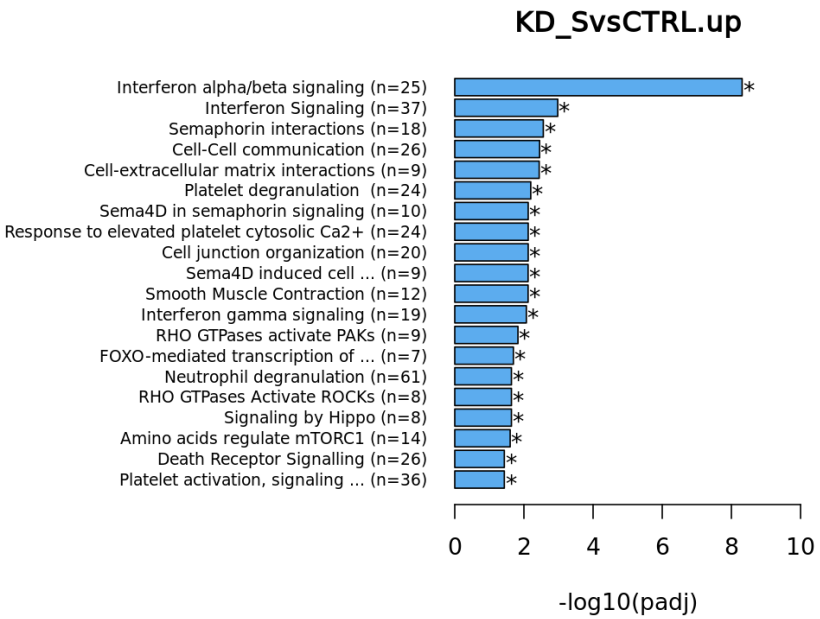

B

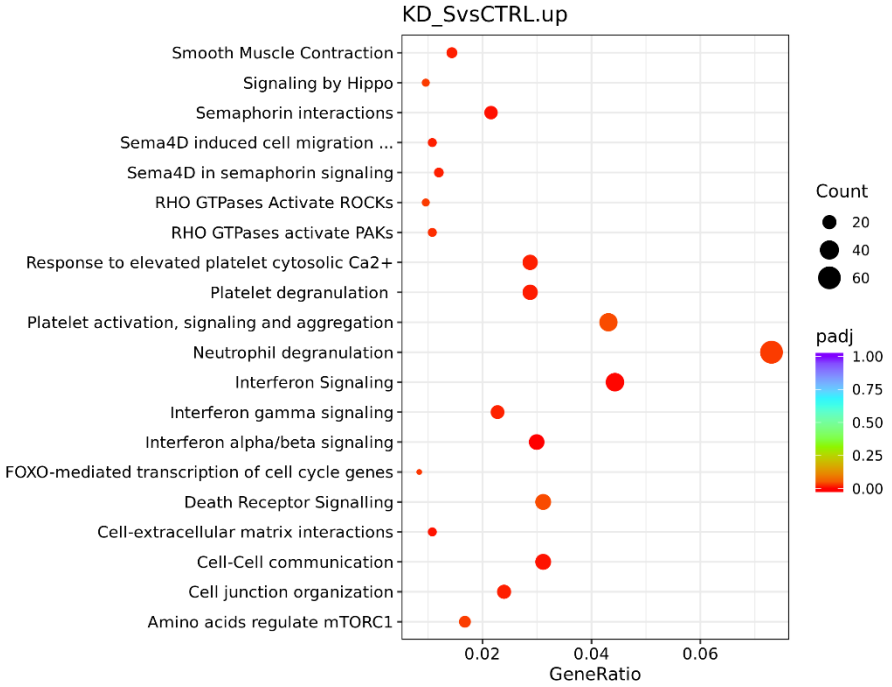

Figure 39. Reactome enrichment analysis for upregulated DEGs. (**A**) Histogram: the horizontal axis is customized as -log10 (padj) of significantly enriched term and the vertical axis is customized as the number of significantly enriched term. Top 20 significantly enriched terms in the Reactome enrichment analysis are displayed. (**B**) Scatter plot: the horizontal axis is customized as GeneRatio and the vertical axis is customized as the term's description. The size of every spot represents the number of the differential expression genes and the color of every spot represents the range of padj.

A

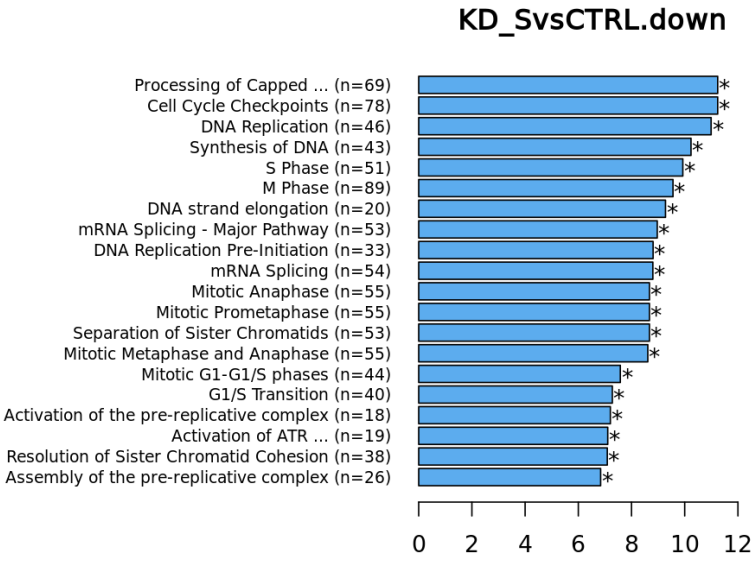

B

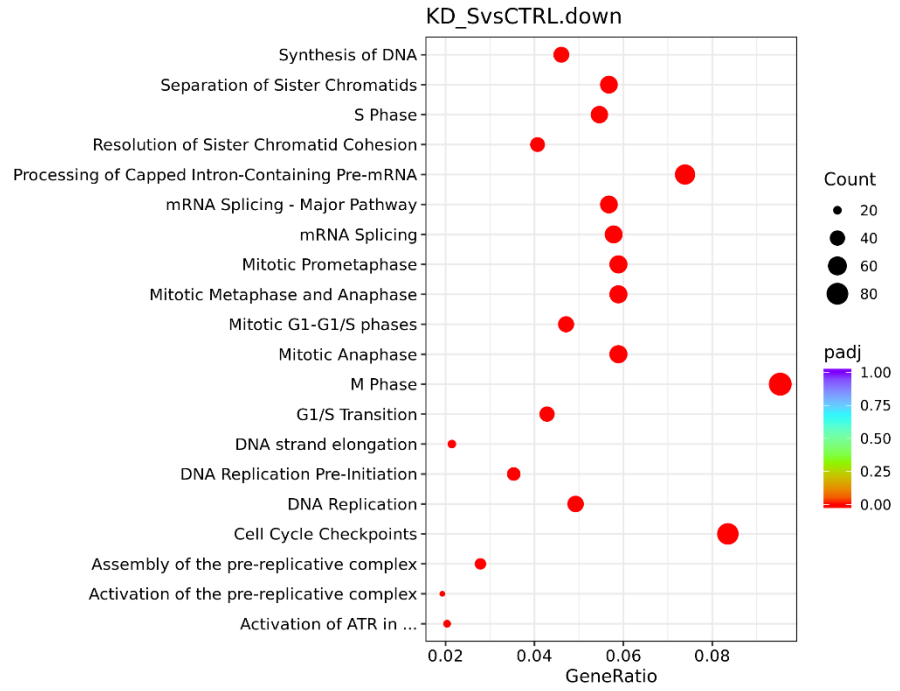

Figure 40. Reactome enrichment analysis for downregulated DEGs. (**A**) Histogram: the horizontal axis is customized as -log10 (padj) of significantly enriched term and the vertical axis is customized as the number of significantly enriched term. Top 20 significantly enriched terms in the Reactome enrichment analysis are displayed. (**B**) Scatter plot: the horizontal axis is customized as GeneRatio and the vertical axis is customized as the term's description. The size of every spot represents the number of the differential expression genes and the color of every spot represents the range of padj.

gene_id	tumour_type	KD_S2	KD_S3	CTRL_2	CTRL_3
ENSG00000072274	NHL	2099.71749329201	1921.15696696177	7859.7699593491	7813.88354026355
ENSG00000167460	ALCL	26255.5547764672	31999.4808925272	8462.30769047467	9667.21912244221
ENSG00000163513	head and neck;colorectal,colorectal	1011.03627529088	1293.47441066154	3867.3995853356	4351.72328176859
ENSG00000136826	meningioma	526.994398395083	690.450811930251	152.866054007784	171.252774533963

log2FoldChange	pvalue	padj	gene_name	gene_chr	gene_start	gene_end	gene_strand
-1.96210235016371	3.55701331841777e-59	9.38126692599504e-56	TFRC	3	196027183	196082189	-
1.68385613112426	2.07393100591533e-36	1.24313309886388e-33	TPM4	19	16067021	16103005	+
-1.83669862105785	4.7843034074916e-34	2.3366892235034e-31	TGFBR2	3	30606502	30694142	+
1.90558805976611	2.99864528666046e-17	3.01855995383141e-15	KLF4	9	107484852	107490482	-

gene_length	gene_biotype	gene_description	tf_family
7887	protein_coding	transferrin receptor [Source:HGNC Symbol;Acc:HGNC:11763]	-
8632	protein_coding	tropomyosin 4 [Source:HGNC Symbol;Acc:HGNC:12013]	-
4704	protein_coding	transforming growth factor beta receptor 2 [Source:HGNC Symbol;Acc:HGNC:11773]	-
3659	protein_coding	Kruppel like factor 4 [Source:HGNC Symbol;Acc:HGNC:6348]	zf-C2H2

Figure 41. Function Annotation of Oncogene. Top 4 most significant oncogenes are displayed.

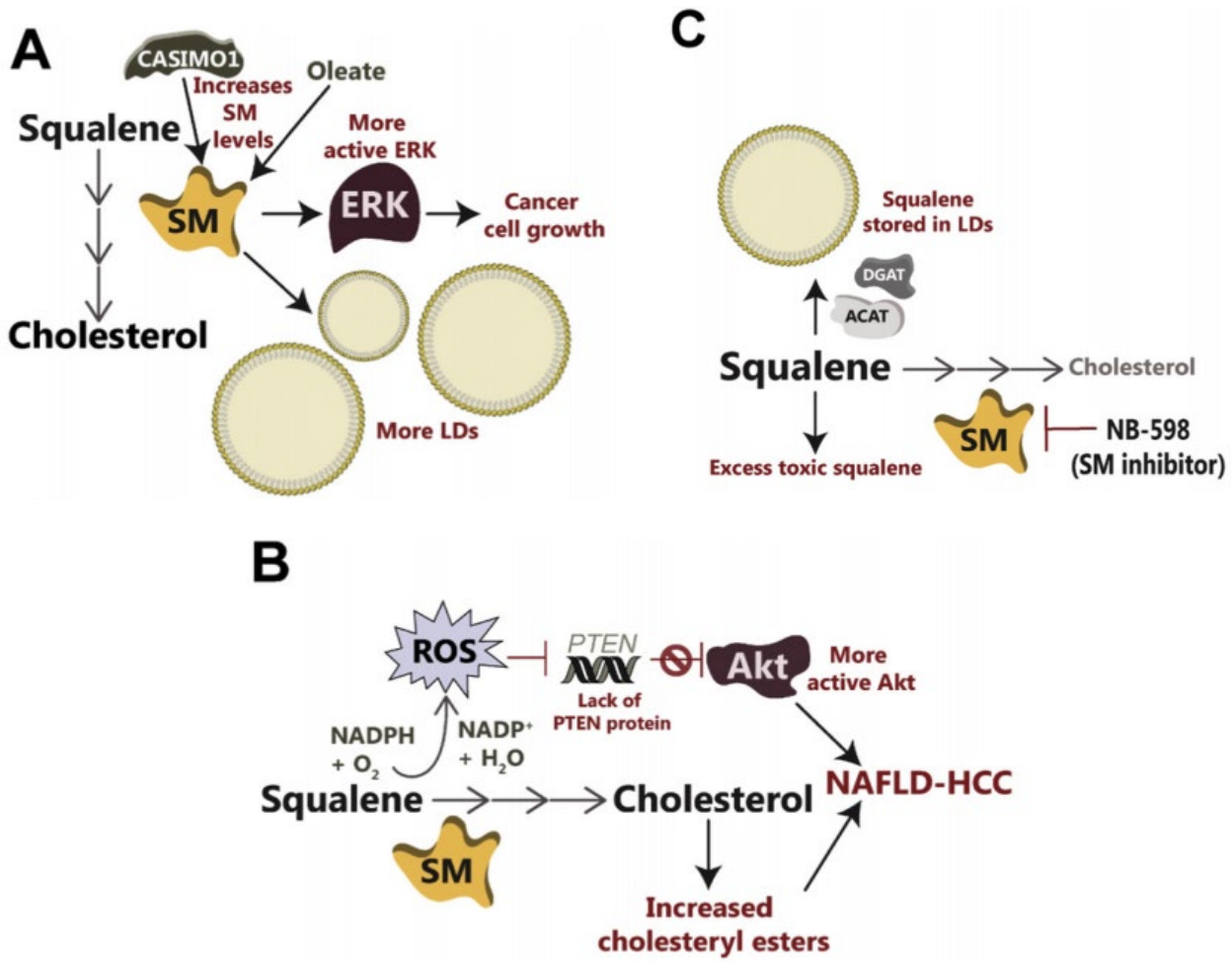

Figure 42. (A) Both oleate and CASIMO1 microprotein can increase SM (SQLE) levels. In breast cancer cell lines, this leads to more lipid droplets (LD), enhanced ERK signaling, and cancer cell phenotype [13]. **(B)** In non-alcoholic fatty liver disease-related hepatocellular carcinoma (NAFLD-HCC), increased SM protein levels elevate reactive oxygen species (ROS), which epigenetically silence the PTEN promoter and enhance oncogenic Akt signaling [13]. **(C)** LDs formed by DGAT and ACAT enzymes serve as protective storage depots for toxic squalene. Some neuroendocrine cancer cells are sensitive to squalene accumulation upon SM inhibition by NB-598 as they lack the capacity to sequester squalene in LDs [13].

REFERENCES

1. Horton, J.D., et al., *Immune evasion by head and neck cancer: foundations for combination therapy.* Trends in cancer, 2019. **5**(4): p. 208-232.
2. Shah, J.P. and Z. Gil, *Current concepts in management of oral cancer–surgery.* Oral oncology, 2009. **45**(4-5): p. 394-401.
3. Argiris, A., et al., *Head and neck cancer.* The Lancet, 2008. **371**(9625): p. 1695-1709.
4. Marur, S. and A.A. Forastiere. *Head and neck cancer: changing epidemiology, diagnosis, and treatment*. in *Mayo Clinic Proceedings*. 2008. Elsevier.
5. Qin, Y., et al., *SQLE induces epithelial-to-mesenchymal transition by regulating of miR-133b in esophageal squamous cell carcinoma.* Acta biochimica et biophysica Sinica, 2017. **49**(2): p. 138-148.
6. Zhang, H.Y., et al., *Expression and significance of squalene epoxidase in squamous lung cancerous tissues and pericarcinoma tissues.* Thoracic cancer, 2014. **5**(4): p. 275-280.
7. Qin, Y., et al., *A Novel Long Non-Coding RNA lnc030 Maintains Breast Cancer Stem Cell Stemness by Stabilizing SQLE mRNA and Increasing Cholesterol Synthesis.* Advanced Science, 2021. **8**(2): p. 2002232.
8. Stäubert, C., et al., *Increased lanosterol turnover: a metabolic burden for daunorubicin-resistant leukemia cells.* Medical Oncology, 2016. **33**(1): p. 6.
9. Li, L., et al., *Squalene epoxidase-induced cholesteryl ester accumulation promotes nasopharyngeal carcinoma development by activating PI3K/AKT signaling.* Cancer science, 2020. **111**(7): p. 2275.

10. Marur, S. and A.A. Forastiere. *Head and neck squamous cell carcinoma: update on epidemiology, diagnosis, and treatment*. in *Mayo Clinic Proceedings*. 2016. Elsevier.

11. Hashim, D., et al., *Head and neck cancer prevention: from primary prevention to impact of clinicians on reducing burden.* Annals of Oncology, 2019. **30**(5): p. 744-756.

12. Kaidar-Person, O., Z. Gil, and S. Billan, *Precision medicine in head and neck cancer.* Drug Resistance Updates, 2018. **40**: p. 13-16.

13. Chua, N.K., H.W. Coates, and A.J. Brown, *Squalene monooxygenase: a journey to the heart of cholesterol synthesis.* Progress in lipid research, 2020: p. 101033.

14. Yamamoto, S., K. Lin, and K. Bloch, *Some properties of the microsomal 2, 3-oxidosqualene sterol cyclase.* Proceedings of the National Academy of Sciences, 1969. **63**(1): p. 110-117.

15. Astruc, M., et al., *Squalene epoxidase and oxidosqualene lanosterol-cyclase activities in cholesterogenic and non-cholesterogenic tissues.* Biochimica et Biophysica Acta (BBA)-Lipids and Lipid Metabolism, 1977. **487**(1): p. 204-211.

16. Brown, A.J., N.K. Chua, and N. Yan, *The shape of human squalene epoxidase expands the arsenal against cancer.* Nature communications, 2019. **10**(1): p. 1-4.

17. Van Berkel, W., N. Kamerbeek, and M. Fraaije, *Flavoprotein monooxygenases, a diverse class of oxidative biocatalysts.* Journal of biotechnology, 2006. **124**(4): p. 670-689.

18. Solomon, K.R. and M.R. Freeman, *Do the cholesterol-lowering properties of statins affect cancer risk?* Trends in Endocrinology & Metabolism, 2008. **19**(4): p. 113-121.

19. Gill, S., et al., *Cholesterol-dependent degradation of squalene monooxygenase, a control point in cholesterol synthesis beyond HMG-CoA reductase.* Cell metabolism, 2011. **13**(3): p. 260-273.

20. Iyer, V.R., et al., *The transcriptional program in the response of human fibroblasts to serum.* science, 1999. **283**(5398): p. 83-87.

21. Padyana, A.K., et al., *Structure and inhibition mechanism of the catalytic domain of human squalene epoxidase.* Nature communications, 2019. **10**(1): p. 1-10.

22. Micera, M., et al., *Squalene: More than a Step toward Sterols.* Antioxidants, 2020. **9**(8): p. 688.

23. Miettinen, T.A. and H. Vanhanen, *Serum concentration and metabolism of cholesterol during rapeseed oil and squalene feeding.* The American journal of clinical nutrition, 1994. **59**(2): p. 356-363.

24. Desmaële, D., R. Gref, and P. Couvreur, *Squalenoylation: a generic platform for nanoparticular drug delivery.* Journal of controlled release, 2012. **161**(2): p. 609-618.

25. O'Hagan, D.T., *MF59 is a safe and potent vaccine adjuvant that enhances protection against influenza virus infection.* Expert review of vaccines, 2007. **6**(5): p. 699-710.

26. Toews, A.D., et al., *Tellurium causes dose-dependent coordinate down-regulation of myelin gene expression.* Molecular brain research, 1997. **49**(1-2): p. 113-119.

27. Matthan, N.R., et al., *Sex-Specific Differences in the Predictive Value of Cholesterol Homeostasis Markers and 10-Year Cardiovascular Disease Event Rate in F ramingham O ffspring S tudy Participants.* Journal of the American Heart Association, 2013. **2**(1): p. e005066.

28. Cirmena, G., et al., *Squalene epoxidase as a promising metabolic target in cancer treatment.* Cancer letters, 2018. **425**: p. 13-20.

29. Tabacik, C., et al., *Squalene epoxidase, oxido-squalene cyclase and cholesterol biosynthesis in normal and tumoral mucosa of the human gastro-intestinal tract: Evidence of post-HMG CoA regulation.* Biochimica et Biophysica Acta (BBA)-Lipids and Lipid Metabolism, 1981. **666**(3): p. 433-441.

30. Polycarpou-Schwarz, M., et al., *The cancer-associated microprotein CASIMO1 controls cell proliferation and interacts with squalene epoxidase modulating lipid droplet formation.* Oncogene, 2018. **37**(34): p. 4750-4768.

31. Sui, Z., et al., *Squalene epoxidase (SQLE) promotes the growth and migration of the hepatocellular carcinoma cells.* Tumor Biology, 2015. **36**(8): p. 6173-6179.

32. Ge, H., et al., *Squalene epoxidase promotes the proliferation and metastasis of lung squamous cell carcinoma cells though extracellular signal-regulated kinase signaling.* Thoracic cancer, 2019. **10**(3): p. 428-436.

33. Liu, D., et al., *Squalene epoxidase drives NAFLD-induced hepatocellular carcinoma and is a pharmaceutical target.* Science translational medicine, 2018. **10**(437).

34. Stopsack, K.H., et al., *Cholesterol metabolism and prostate cancer lethality.* Cancer research, 2016. **76**(16): p. 4785-4790.

35. Yuen, H.-F., et al., *TAZ expression as a prognostic indicator in colorectal cancer.* PloS one, 2013. **8**(1): p. e54211.

36. Brown, D.N., et al., *Squalene epoxidase is a bona fide oncogene by amplification with clinical relevance in breast cancer.* Scientific reports, 2016. **6**(1): p. 1-13.

37. Chen, G., et al., *Restructured GEO: restructuring Gene Expression Omnibus metadata for genome dynamics analysis.* Database, 2019. **2019**.

38. Tomczak, K., P. Czerwińska, and M. Wiznerowicz, *The Cancer Genome Atlas (TCGA): an immeasurable source of knowledge.* Contemporary oncology, 2015. **19**(1A): p. A68.

39. Castellone, R.D., et al., *Inhibition of tumor cell migration and metastasis by the proton-sensing GPR4 receptor.* Cancer letters, 2011. **312**(2): p. 197-208.

40. Albini, A., *Tumor and endothelial cell invasion of basement membranes.* Pathology & Oncology Research, 1998. **4**(3): p. 230-241.

41. Fidler, I.J. *Critical determinants of metastasis*. in *Seminars in cancer biology*. 2002. Elsevier.

42. Steeg, P.S., *Tumor metastasis: mechanistic insights and clinical challenges.* Nature medicine, 2006. **12**(8): p. 895-904.

43. Justus, C.R., et al., *In vitro cell migration and invasion assays.* Journal of visualized experiments: JoVE, 2014(88).

44. Sun, C., R. Mezzadra, and T.N. Schumacher, *Regulation and function of the PD-L1 checkpoint.* Immunity, 2018. **48**(3): p. 434-452.

45. Qiao, X.-w., et al., *Evolving Landscape of PD-1/PD-L1 Pathway in Head and Neck Cancer.* Frontiers in Immunology, 2020. **11**: p. 1721.

46. Burtness, B., *The role of cetuximab in the treatment of squamous cell cancer of the head and neck.* Expert opinion on biological therapy, 2005. **5**(8): p. 1085-1093.

47. Concu, R. and M. Cordeiro, *Cetuximab and the head and neck squamous cell cancer.* Current topics in medicinal chemistry, 2018. **18**(3): p. 192-198.

48. Ornitz, D.M. and N. Itoh, *The fibroblast growth factor signaling pathway.* Wiley Interdisciplinary Reviews: Developmental Biology, 2015. **4**(3): p. 215-266.

49. Ghedini, G.C., et al., *Future applications of FGF/FGFR inhibitors in cancer.* Expert review of anticancer therapy, 2018. **18**(9): p. 861-872.

50. Dietrich, D., *FGFR-targeted therapy in head and neck carcinomas.* Hno, 2020: p. 1-13.

51. Yu, G., et al., *clusterProfiler: an R package for comparing biological themes among gene clusters.* Omics: a journal of integrative biology, 2012. **16**(5): p. 284-287.

52. Kanehisa, M. and S. Goto, *KEGG: kyoto encyclopedia of genes and genomes.* Nucleic acids research, 2000. **28**(1): p. 27-30.

53. Wang, X., et al., *HSP72 and gp96 in gastroenterological cancers.* Clinica Chimica Acta, 2013. **417**: p. 73-79.

54. Nusse, R., *Wnt signaling in disease and in development.* Cell research, 2005. **15**(1): p. 28-32.

55. Williams, H., *Molecular pathogenesis of oral squamous carcinoma.* Molecular Pathology, 2000. **53**(4): p. 165.

56. Jun, S.Y., et al., *Reduction of squalene epoxidase by cholesterol accumulation accelerates colorectal cancer progression and metastasis.* Gastroenterology, 2021. **160**(4): p. 1194-1207. e28.

57. Malkoski, S.P. and X.-J. Wang, *Two sides of the story? Smad4 loss in pancreatic cancer versus head-and-neck cancer.* FEBS letters, 2012. **586**(14): p. 1984-1992.

58. Honjo, Y., et al., *TGFβ Receptor I Conditional Knockout Mice Develop Spontaneous Squamous Cell Carcinoma.* Cell Cycle, 2007. **6**(11): p. 1360-1366.

59. C Connolly, E. and R. J Akhurst, *The complexities of TGF-β action during mammary and squamous cell carcinogenesis.* Current pharmaceutical biotechnology, 2011. **12**(12): p. 2138-2149.

60. Pring, M., et al., *Dysregulated TGF-β1-induced Smad signalling occurs as a result of defects in multiple components of the TGF-β signalling pathway in human head and neck carcinoma cell lines.* International journal of oncology, 2006. **28**(5): p. 1279-1285.

61. Pang, X., Y.L. Tang, and X.H. Liang, *Transforming growth factor-β signaling in head and neck squamous cell carcinoma: Insights into cellular responses.* Oncology letters, 2018. **16**(4): p. 4799-4806.

62. White, R., S. Malkoski, and X. Wang, *TGFβ signaling in head and neck squamous cell carcinoma.* Oncogene, 2010. **29**(40): p. 5437-5446.

63. Ueno, K., et al., *Frizzled homolog proteins, microRNAs and Wnt signaling in cancer.* International journal of cancer, 2013. **132**(8): p. 1731-1740.

64. Fukukawa, C., et al., *Radioimmunotherapy of human synovial sarcoma using a monoclonal antibody against FZD10.* Cancer science, 2008. **99**(2): p. 432-440.

65. Mahoney, C.E., et al., *A chemical biology screen identifies a vulnerability of neuroendocrine cancer cells to SQLE inhibition.* Nature communications, 2019. **10**(1): p. 1-14.

66. Cruz, A.L., et al., *Lipid droplets: platforms with multiple functions in cancer hallmarks.* Cell death & disease, 2020. **11**(2): p. 1-16.

67. Lee, W.S., et al., *In vitro and in vivo studies of the anticancer action of terbinafine in human cancer cell lines: G0/G1 p53-associated cell cycle arrest.* International journal of cancer, 2003. **106**(1): p. 125-137.

68. Ho, P.Y., et al., *Inhibition of human vascular endothelial cells proliferation by terbinafine.* International journal of cancer, 2004. **111**(1): p. 51-59.

69. Chien, M.H., et al., *Terbinafine inhibits oral squamous cell carcinoma growth through anti-cancer cell proliferation and anti-angiogenesis.* Molecular carcinogenesis, 2012. **51**(5): p. 389-399.

70. Pickup, M., S. Novitskiy, and H.L. Moses, *The roles of TGFβ in the tumour microenvironment.* Nature Reviews Cancer, 2013. **13**(11): p. 788-799.

71. Drabsch, Y. and P. Ten Dijke, *TGF-β signalling and its role in cancer progression and metastasis.* Cancer and Metastasis Reviews, 2012. **31**(3): p. 553-568.